Aerodynamic Characteristics of a Four Bladed Savonius Rotor
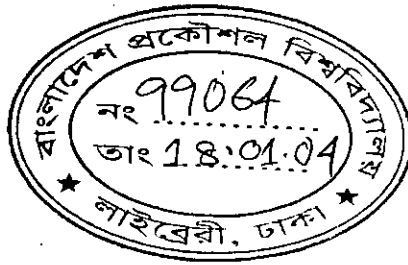
by

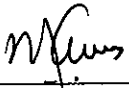Md. Humayun Kabir Bhuiyan

MASTER OF SCIENCE IN MECHANICAL ENGINEERING

BANGLADESH UNIVERSITY OF ENGINEERING AND TECHNOLOGY

November, 2003

The thesis titled **"AERODYNAMIC CHARACTERISTICS OF A FOUR BLADED SAVONIUS ROTOR"**, submitted by **Md. Humayun Kabir Bhuiyan,** Roll No: 100110033F, Session: October 2001 has been accepted as satisfactory in partial fulfillment of the requirement for the degree of Master of Science in Mechanical Engineering on 18 November 2003.

BOARD OF EXAMINARS

1.   Dr. Md. Quamrul Islam   Chairman
    Professor
    Department of Mechanical Engineering
    BUET, Dhaka-1000.

2.   Dr. Mohammad Ali   Member
    Associate Professor
    Department of Mechanical Engineering
    BUET, Dhaka-1000.

3.   Dr. Maglub Al Nur   Member
    Professor and Head   (Ex- officio)
    Department of Mechanical Engineering
    BUET, Dhaka-1000.

4.   Dr. Md.Reaz Hasan Khondakar   Member
    Professor   (External)
    Department of Naval Architecture
    BUET, Dhaka-1000.

CANDIDATE'S DECLARATION

It is hereby declared that this thesis or any part of it has not been submitted elsewhere for the award of any degree or diploma.

MD. HUMAYUN KABIR BHUIYAN

TABLE OF CONTENTS

Chapter-1

INTRODUCTION

Chapter-2

REVIEW OF THE LITERATURE

Chapter-3

EXPERIMENTAL SET-UP AND PROCEDURE

Chapter-4

DETAILS OF NON-DIMENSIONAL PARAMETERS

Chapter-5

RESULTS AND DISCUSSIONS

Chapter-6

CONCLUSIONS AND RECOMMENDATIONS

REFERENCES

APPENDICES

LIST OF FIGURES

LIST OF SYBOLS

a	Overlap distance
C_P	Power coefficient, $2\,(P-P_a)\,/\,\rho U_0^3$
C_{pe}	Pressure coefficient for concave surface of the blade
C_{px}	Pressure coefficient for convex surface of the blade
C_p	Pressure coefficient
C_t	Drag coefficient in the transverse direction of the chord
C_q	Static torque coefficient for a single blade
C_Q	Total static torque coefficient
d	Diameter of the blade
D	Diameter of the rotor
F_n	Normal force acting on the blade
F_t	Tangential force acting on the blade
H	Height of the rotor
P	Pressure on blade
P_a	Atmospheric
R_e	Reynolds number, $U_0 D\,/\,v$
S	Ratio of overlap distance to diameter of blade
T	Static torque on the blade
U_0	Free stream velocity
V_r	Relative velocity
V_w	Component of relative velocity along U_0

Greek Symbols

α Rotor angle

ϕ Angle of the pressure tapping

λ Tip speed ratio, $D\omega / 2U_0$

ω Angular speed of the rotor

ν Kinematics viscosity of air

Δp Difference of pressure between concave and convex surfaces of a blade

ACKNOWLEDGEMENT

ABSTRACT

Drag and torque coefficients of a stationary four bladed Savonius rotor are investigated by measuring the pressure distribution on the blade surfaces for various rotor angles. The experiments are carried out at a Reynolds number of 1.89×10^5 in a uniform flow jet produced by an open circuit wind tunnel.

To calculate the drag forces and torque in non–dimensional form, Fortran programmes are developed. Data inputs are pressure on 17 tapping points on each blades of the four bladed Savonius rotor for every 10^0 interval of the angle of rotation and different fluid properties. The outputs of these programmes are subsequently plotted and analyzed. The effects of the individual blade and also the combined effects of four blades on different aerodynamic characteristics are analyzed in the present research work.

The total static torque coefficient increases with the rotor angle and reaches its maximum value at a rotor angle of $\alpha=20^0$ and then decreases at $\alpha=30^0$ and remains constant from $\alpha=50^0$ to 80^0. Total static torque coefficient at different rotor angles curve repeats from $\alpha=90^0$ to 170^0, $\alpha=180^0$ to 260^0 and $\alpha=270^0$ to 350^0 angle of rotation. A quasi-steady approach is applied for the prediction of dynamic performance of the rotor using the static drag and torque coefficients.

CHAPTER 1
INTRODUCTION

Chapter-1
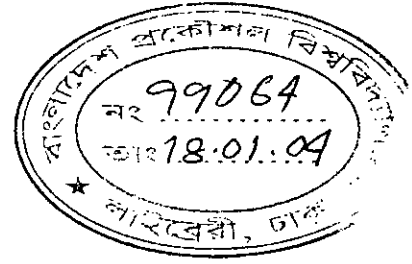
INTRODUCTION

1.1   General

Energy is one of the basic inputs in everyday life of human being. Various types of energy sources, like oil, hydro, coal, natural gas, nuclear etc., are used for different activities all around the world. Among these conventional fuels, only hydro is renewable in nature and other sources are major causes of air pollution and greenhouse effect. Conventional fuels may be replaced with renewable energy sources like wind energy, solar thermal systems, biomass energy (wood and other plant fuels), geothermal energy, fuel cell, municipal waste etc. Costs of many of these technologies have come down considerably in recent years, particularly wind energy, which is now competitive with conventional power sources in regions with strong winds.

For the past few centuries, people are extracting energy from the wind in various ways. One means for converting wind energy to a more useful form is through the use of windmills. Recently, due to the fuel crisis, this form of energy is gaining more popularity. According to a projection by American Wind Energy Association (AWEA)- wind turbine installation in the world through the end of 2006 will be about 6,950 MW. The emerging forecast of incremental wind power is shown in the following table.

Year	1990	1995	2000	2005	2010
Incremental World Capacity Additions (MW/Yr)	300	727	1761	3861	8465

Source: D.P. Kothari, "Importance of Renewable Energy Sources."-Proceeding on NSREPA '97

1

There are various types of windmills. The most common one having blades of airfoil shape is the horizontal axis turbine. Another type is the vertical-axis wind turbine. The primary attraction of the vertical axis wind turbine is the simplicity of its manufacturing compared to that of the horizontal axis wind turbine. Among the different vertical axis wind turbines, the Savonius rotor is a slow running wind machine and has a relatively lower efficiency. Still it is being used in developing countries because of its simple design, easy and cheap technology for construction and having a good starting torque at low wind speed [2,3]. Rigorous studies on the performance characteristics of Savonius rotor are found in the literature and these enable the identification of an optimum geometrical configuration for practical design [4,5,6,7,8].

1.2   Wind as a Source of Energy

For a long time people are extracting energy from fossil fuels in almost all the countries. In some of the countries, they are also utilizing uranium fuel, which is a source of nuclear energy. With the rising demand of the energy and for many other reasons, the prices of the fuels are increasing day by day. So the people are trying to find alternative sources of energy to exploit them at the cheapest cost. Wind energy is a kind of energy source, which will never be diminished. It is available almost all the time, at all places and in large quantities all over the world. Again fossil and uranium fuels will be finished some day. These are not available in all countries. Besides these, people are interested to be self-dependent; they do not like to rely on imported fuel, which require huge amount of foreign currency. As a result, in different parts of the world, people are taking keen interest to develop efficient and economic devices to collect energy from the wind. Recently, the utilization of wind power is increasing in many developed as well as under developed countries.

1.3 Global Wind Energy Utilization Scenario

In 1997, wind turbines installed all around the world generated about 13 trillion watt-hour of energy; the installed capacity was 7500 MW. According to AWEA, Europe will continue to dominate worldwide installations over the next 10 years, erecting 14,310 MW of additional wind capacity, or nearly half of the 30,000MW projected for the world. European countries, in particular, Germany, Spain, and the United Kingdom have very strong and consistent domestic market supports in place for at least several years. While these supports are being reduced in many markets, the European wind industry now has enough momentum and investment that rapid growth is expected to continue into the indefinite future. Green Peace and European Wind Energy Association had jointly studied and forecasted the various important features regarding the growth and contribution of wind energy as shown in the following table.

Year	Annual growth rate %	Annual capacity (MW)	Cumulative capacity by end of the year (MW)	Annual wind electricity production (TWH)	World electricity demand (TWH)	Wind power penetration of world electricity (%)
1999	20	3120	13273	29.1	14919	.19
2000	20	3744	17017	37.3	15381	.24
2001	20	4493	21510	47.1	15858	.30
2002	20	5391	26901	59.9	16350	.36
2003	20	6470	33371	73.1	16857	.43
2004	30	8411	41781	91.5	17379	.53
2005	30	10934	52715	115.4	17918	.64
2010	30	40596	181252	444.6	20873	2.13
2015	20	101016	537059	1333.8	23894	5.58
2020	10	150000	1209466	2966.6	27351	10.85

Source: Page 74, Renewable Energy World / November-December 2001.

1.4 Wind Energy Extraction in Bangladesh

Though Bangladesh has a 723 km long coastal line and a vast hilly region, which shows a great potential of wind energy, we are much lagging behind. In fact, there is no commercial use of wind energy except those used in sailing boats. Now with the help of BUET, different non-government organizations, different energy and environmental bodies are collecting wind data. Besides that, few pilot projects have been established in Patenga, St Martins, Teknaf and Kutubdia. 2.5 kW, 1.2 kW and 600 W turbines are going to be installed at St Martins island and Teknaf by Institute of Fuel Research and Development (IFRD). Bangladesh Power Development Board (BPDB) is going to establish a 1.8 MW Demonstration Wind Park at Patenga. Ministry of Non–Conventional Energy Sources, India will provide technical assistance for this purpose. Local Government Engineering Department (LGED) has established some wind power driven pumps that can pump 20000 liters per day at different corners of the country. Bangladesh Rural Advancement Committee (BRAC) has installed 3 stand-alone wind generators of a total of 0.9 kW and a wind-solar hybrid system (4.32 kW) in coastal areas of Bangladesh. Grameen Shakti has installed four wind diesel hybrid generators at four cyclone shelters at Cox's Bazar, Barguna and Patuakhali districts. Bangladesh Centre for Advanced Studies (BCAS) has Wind Energy Study Project (WEST), which set up a wind pump at Patenga with an installation cost of Tk 3,25,000 [28]. So Bangladesh has just started its journey to extract wind energy. Government, non-government, environmental bodies and technical institutes like BUET must have strong initiative to keep pace with other parts of the world. If we compare with Tamilnadu, an Indian coastal state, it had a 919 MW capacity wind farm in September 1999 [29]. It is the right time to be serious regarding wind energy extraction process in Bangladesh. There is a vast scope of utilities in the fields of

agriculture, fish farming and salt processing besides electricity generation and water lifting.

To exploit wind energy, sufficient information has to be gathered about wind speed, direction, and duration. If we have enough information then we shall be able to exploit wind energy efficiently, in the form of pumping water, producing electricity etc.

1.5   Aim of The Present Work

The present research work consists of finding static drag coefficients at the normal and tangential direction of the chord, static torque coefficient for individual blade C_q, total static torque coefficient C_Q at different Reynolds number of a four-bladed Savonius rotor at different angles of rotation ranging from $\alpha=0^0$ to 360^0 by measuring the surface pressure on blades. The quasi-steady approach applied to the analysis of a Darricus rotor may finally be considered for predicting the performance of the four bladed Savonius rotor.

1.6   Objectives:

The study has the following objectives:

a.   To study the effects of four blades of the Savonius rotor on aerodynamic characteristics i.e. torque coefficient, drag coefficient etc. Determination of the location of separation point with the increase of rotor angle at various Reynolds number is also included.

b.   To determine the drag coefficient and torque coefficient from the measurement of the pressure difference between the convex and concave surfaces of the blades.

c.   Finally, a comparison is made between the present dynamic prediction (for four-bladed Savonius rotor) with the previous works (for two-bladed and three-bladed Savonius rotors) in terms of power coefficient for different tip speed ratios.

1.7   Scope of the Thesis

The study covers only the experimental investigation of a four bladed Savonius rotor. Some important computer programmings have been made for useful purposes.

The prime objective of the investigation is to observe the effects of the four semi-cylindrical blades in the Savonius rotor in place of two semi-cylindrical blades and S-shaped Savonius rotors, on the aerodynamic characteristics of a vertical axis wind turbine.

The present research programme covers only the experimental investigation of pressure distribution over the blade surfaces of the Savonius rotor both on the convex and concave surfaces for different angles of rotation, α ranging from 0^0 to 360^0 for every 10^0 interval. Several phases of the entire investigation are described

in this thesis. Chapter 2 provides a brief description of findings of several researches in the field of flow over different types of Savonius rotors, Darrius rotors and S-shaped rotors with different conditions. Notable contributions were made by M. Rahman [1], H.G. Bos, E.H. Cordes [2], J..Park [3], E.H. Lysen [2,6], T. Ogawa , H. Yoshida [8], M.D. Huda, M.A. Salim, M.Q. Islam, A.K.M.S. Islam, A.C. Mandal, M.M. Razzaque [9,10,12], J. Gavalda, J. Massons, F. Diaz [11], T.K. Aldoss, K.M. Obeidat [25] and R.D. Littler [26]. Beside these, findings of several other researchers are also included in this chapter.

In Chapter 3 mainly an account of the experimental arrangement and procedure adopted for the investigation are presented. It includes the description of the wind tunnel, the constructional details of the test section and four semi-cylindrical bladed Savonius rotor used for the study. The experiment is conducted in the wind tunnel for only two-dimensional uniform cross flow keeping the velocity and turbulence intensity constant.

Chapter 4 presents the derivation technique of different non-dimensional parameters both for static and dynamic aerodynamic characteristics.

Chapter 5 presents the analysis concerning the results and discussions of the present experimental results, which are presented in graphical form. In few cases

the existing experimental results of different researchers are correlated with the present one.

Finally, the conclusions, which are drawn from the present investigation, are given in Chapter 6. This chapter also includes an outline regarding further research in the field.

CHAPTER 2
REVIEW OF THE LITERATURE

Chapter-2

REVIEW OF THE LITERATURE

2.1   Introduction

From the ancient period people have been working on various types of wind turbine to extract energy. However, expected developments have not been achieved in wind driven machines to cope with the characteristics of wind turbines. Conventional machines are being used now a days even though they are not always suitable from the operational point of view. Wind turbines in ancient period were of drag types only and their efficiencies were not up to the mark. Arising from the increasing practical importance of wind turbine aerodynamics, there have been, over the past few decades, an enormous increase in research works concerning laboratory simulations, full scale measurements and more recently, numerical calculations and theoretical predictions of flows over a wide variety of Savonius rotors. Researchers in different countries have been contributing greatly to the knowledge of analytical prediction methods of wind turbines, but the major part of the reported works have been of fundamental nature involving the flow over horizontal axis wind turbine and vertical axis Darrieus rotor. The primary attraction of the vertical axis wind turbine is the simplicity of its manufacture compared to the horizontal axis wind turbine. Most of the researchers have conducted research works on either two semi cylindrical bladed Savonius rotor or S-shaped rotor with various flow parameters. A brief description of some of the papers related to the present work is given in this chapter.

2.2 Historical Background

The history of wind power utilization is very long. However, its practical use has so far been almost neglected, mainly because of the instability of power supply for energy intensive modern society. Because of its small energy density and extreme fluctuation, wind can not produce a constant power supply unless it has appropriate strength with proper controlling devices.

From the ancient period people have been working on various classes of wind machines. Works on windmills probably started in 2000 B.C. In the ancient period, in 644 A.D., the Persian vertical-axis windmill circa (figure 2.1) was constructed which was used to grind grain. That kind of windmill was working up to about 12th century, when simultaneously in France and England, Dutch type of windmills (figure 2.2, figure 2.3) were made whose purpose were to grind grains and pump water. These windmills were of horizontal-axis types. Up to the end of 19th century people were working with these classes of windmills only.

At the end of 19th century, the first modern windmill of horizontal-axis type with multi-blade was built in Denmark to produce electricity. It was the beginning of the modern development period. Starting from that time, people in different countries, especially in rural America, have been constructing a large number of multi-bladed wind turbines for pumping water and generating electricity (figure 2.4). Afterwards, as a consequence of development works for several years, two or three-blade propeller type of windmills with aerofoil-shaped blades were built in about 1925. In 1931, 100-kW Russian horizontal-axis wind turbine was constructed while in 1934, the large 1250-kW Smith-Putnam horizontal axis wind turbine was built.

Modern development period really began with the development of horizontal-axis wind turbines. In 1924, Finnish Engineer S.J. Savonius constructed the first Savonius rotor of vertical-axis type and he conceived the idea from the Flettner's Rotor (figure 2.5). In 1925, G.J.M. Darrieus of France, submitted a proposal for a US patent for a new type of wind turbine designed for the generation of power. The patent issued in 1931 as Number 1,835,018 was for a "turbine having its rotating shaft transverse to the flow of the current". The straight-bladed configuration was also covered in the original Darrius patent. This kind of wind machine is called Darrieus turbine (figure 2.6) after the name of G.J.M. Darrieus.
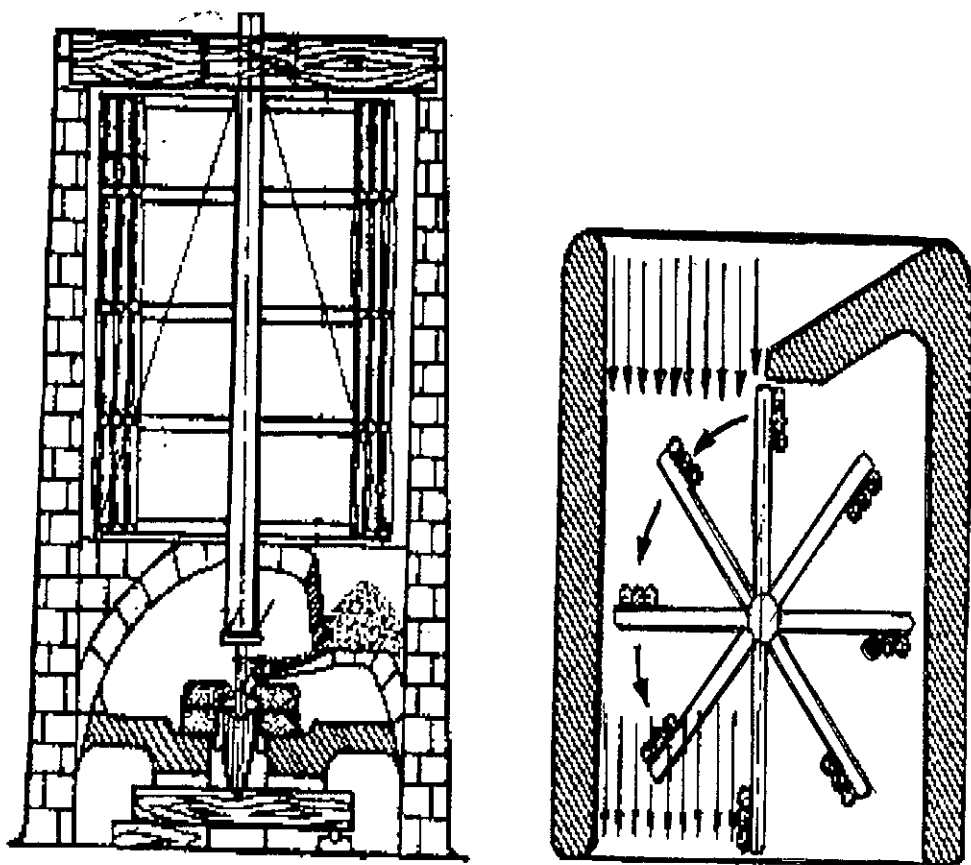
View on Vertical Section   View on Horizontal Section

Figure 2.1 : Persian windmill of vertical-axis type [29]
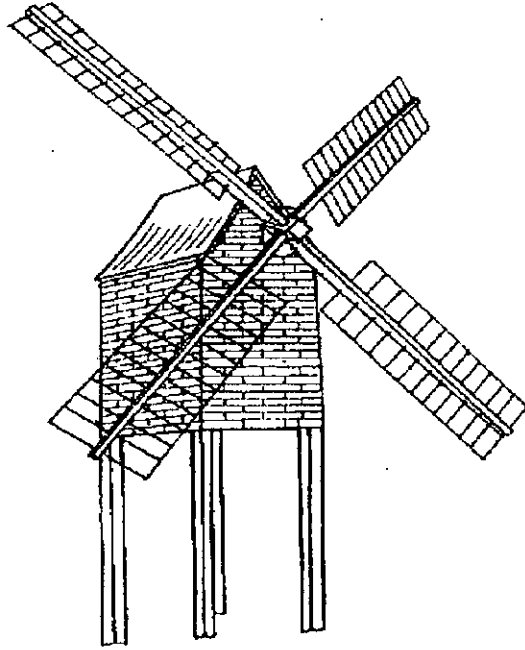
Figure 2.2   : Dutch Windmill [29]
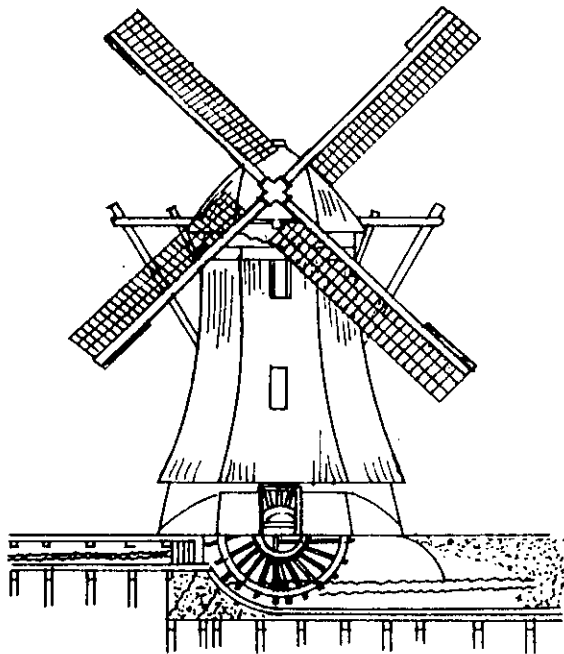
Figure 2.3 : Dezwan Dutch Windmill [29]
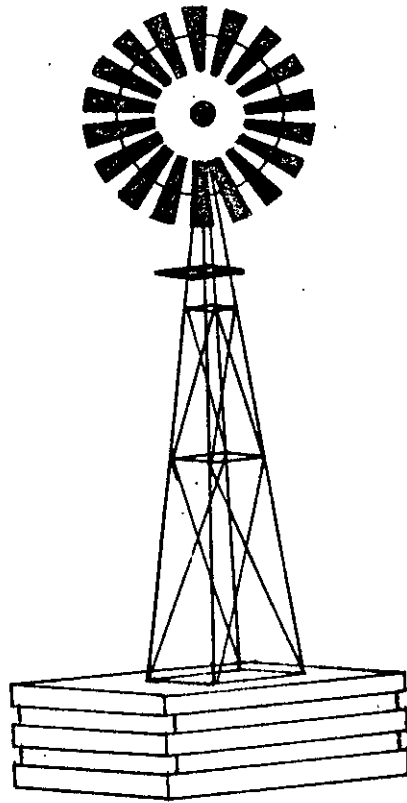
Figure 2.4   : Multi-bladed American Windmill [29]
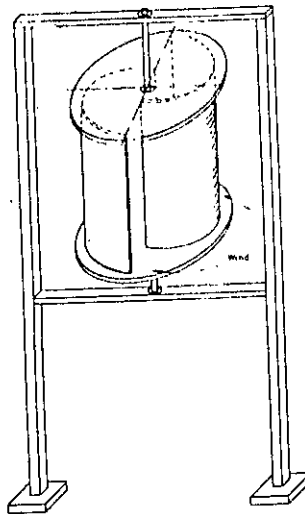
Figure 2.5 Savonius Rotor [29]
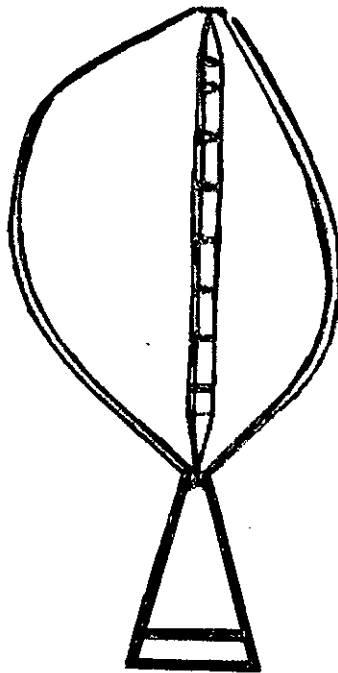
Figure 2.6 : Darrieus Wind Turbine [29]

2.3 Literature Concerning S-Shaped Savonius Rotor

Islam et al. [9] investigated the aerodynamic forces acting on a stationary S-shaped rotor and made an attempt to predict the dynamic performance from these forces. The work was done by measuring the pressure distribution over the surfaces of the blades. The measurements were carried out in a uniform flow jet produced by an open circuit wind tunnel and at a constant wind speed of 8.9 m/s, which corresponds to a Reynolds number ($R_e = U_o D/v$) of $1.13 10^5$. The results indicate that flow separates over the front and back surfaces of the blades and the point of separation depends on the rotor angle. The pressure difference was observed between the convex and concave surfaces of each blade, which in turn, gave drag coefficients. The drag and hence, the torque of each blade varies with

14

rotor angle and was found to be maximum at $\alpha=45^\circ$ for the advancing blade and at $\alpha=105^\circ$ for the returning blade. The maximum net torque was obtained at $\alpha=45^\circ$ and became negative in the range of rotor angle between 135° to 165°.

Islam et al. [10] analyzed the performance of S-shaped rotor by placing a flat plate in front of the returning blade. They found that the power coefficient of the S-rotor was dependent on the Reynolds number. The value of C_P (power coefficient) increased with Reynolds number in the range of the Reynolds number studied and a maximum of 20% of power coefficient was increased by using the deflecting plate which occured at a deflecting angle of 35^0 for b = 0.5D, where b = distance between plate and rotor center and D= diameter of the rotor.

Bowden, G. J. and McAleese, S.A [13] made some measurements on the Queensland optimum S-shaped rotor to examine the properties of isolated and coupled S-shaped rotor. In particular it was shown that the efficiency of the turbine was 18%, which was lower than the figure of 23% given in earlier works. In the experimental setup, the UNSW open jet air-stream, diameter 0.76m, was used to produce wind speeds in the range 0 to 30 m/s. The turbulence ($\sqrt{\overline{u^2}}/V_\alpha$) in the jet stream was low. Wind flow measurements were investigated using 'tell-tales' (light pieces of cotton attached to a probe) and a stroboscope. In this way it was possible to detect the direction of the air-flow relative to the angular position of the rotor blades. Many photographs were taken and later used to construct a visual air-flow pattern around the rotor. The liberalized hot-wire anemometer, on the other hand, enabled measurements to be made of velocity magnitudes and fluctuations to an upper frequency limit of 5 kHz. It did not however, measure the direction. The hot-wire anemometer lineariser was based on a design due to the Institute of Sound and Vibration Research (ISVR), Southampton University, U.K. In general, a storage oscilloscope was used to record the data, particularly from the

15

more structured turbulent regions. However, measurements of turbulence intensity were also made by connecting an rms voltmeter to the output of the hot-wire linearizer. The results of this research were subsequently used to suggest that some form of active coupling between Savonius rotors might be possible. In particular, it has been shown that if two counter-rotating rotors are placed side by side, a natural phase locking occurs between the two turbines.

2.4   Literature Concerning Vertical Axis Darrieus Wind Turbine

The simplest prediction method for the calculation of performance characteristics of a Darrieus wind turbine is the single stream tube mode. It has been introduced first by Templin [14] in 1974. In this method, the whole turbine is assumed to be enclosed within the single stream tube. Templin first incorporated the concept of the windmill actuator disc theories into the analytical model of a Darrieus wind turbine. In the actuator disc theory the induced velocity (rotor axial flow velocity) is assumed to be constant through the disc and is obtained by equating the stream-wise drag with the change in axial momentum. In the assumption of Templin, the actuator disc is considered as the surface of the imaginary body of revolution. It is assumed that the flow velocity is constant. This theory presented by Templin was the first approach to permit the numerical design calculation for a vertical-axis Darrieus wind turbine.

An analytical method using single stream tube model was presented by Noll and Ham [15] for the performance prediction of a vertical-axis wind turbine with straight blades, which were cyclically pitched. They added the effect of strut drag, turbulence wake state and dynamic stall to their analytical method.

An improvement to the above method was the multiple stream tube model introduced by Wilson and Lissaman [16]. In this model, the swept volume of the turbine was divided into a series of adjacent, aerodynamically independent stream tubes. Blade element and momentum theories were then employed for each stream tube. In their method they considered the flow as inviscid and incompressible for the calculation of induced velocity through the stream tube. As a result, there appeared only the lift force in the calculation of induced velocity through the stream tube. Wilson et al considered the theoretical lift for their calculation. This induced velocity was varied over the frontal disc area both in the vertical and the horizontal directions. Atmospheric wind shear was included in the multiple stream tube model. Multiple stream tube model was inadequate in its description of the flow field. Wilson's model could be applied only for a fast running lightly loaded wind turbine.

Strickland [17] in his paper presented a multiple stream tube model for a vertical axis Darrieus turbine. He found the induced velocity by equating the blade element forces (including the airfoil drag) and the changes of momentum along each stream tube. The basic difference between the Wilson's and Strickland's models was that Wilson used the lift force (theoretical) only in the calculation of theoretical velocity while Stickland added the effect of drag force as well for the similar calculation. Wilson's model gave fast convergence while Stickland's model gave slow convergence.

An improved version of multiple stream tube method was presented by Read and Sharpe [18] for vertical-axis Darrieus wind turbines. In their model the parallel stream tube concept was dispensed with and the expansion of the stream tube was included. It was strictly applicable to low solidity lightly loaded wind turbines with large aspect ratio. It could predict instantaneous aerodynamic blade forces and the induced velocities better than that by the conventional multiple streamtube

17

model. Prediction of overall power coefficients was also made with reasonable accuracy. It gave lower power than that obtained experimentally.

In the paper presented by Paraschivoiu and Delelaux [19], improvements were made in the double multiple stream tube model. They considered the induced velocity variation as a function of the azimuth angle for each stream-tube. They added a new formulation for an approximate Troposkien shape by considering the effect of gravitational field and a semi-empirical dynamic stall model.

Paraschivoiu, Fraunie and Beguier [20] introduced in their paper the expansion effects of the stream tubes through the rotor and these were included with the double multiple stream tube model. With the measured and predicted data they observed that streamtube expansion effects were relatively significant at high tip speed ratio.

Fanacci and Walters [21] presented a two dimensional vortex model applicable to a straight-bladed wind turbine. In their analysis they considered a very small angle of attack thereby eliminating the stall effect.

Holme [22] presented a vortex model for a fast running vertical-axis wind turbine having a large number of straight, very narrow blades and a high height-diameter ratio (in order to make two dimensional flow assumption). The analysis was valid for a lightly loaded wind turbine only.

Wilson [23] also introduced a two-dimensional vortex analysis to predict the performance of a giromill. In his method he did not take into account the stall effect, because the angle of attack was assumed to be small.

2.5   Literature Concerning Two Semi-cylindrical Bladed Savonius Rotor

Diaz et al [11] analyzed the drag and lift coefficients of Savonius wind machine, in order to obtain quantitative information about the aerodynamic performance of the Savonius rotor. The experiments were carried out in a low turbulence open jet of 300 x 500 mm section outlet, which provides an air speed adjustable between 0 and 30 m/s. The results of this work showed that for e/d=1/6, at which the rotor generated the optimum power, the drag and lift coefficients were little dependent on the operating conditions (Reynolds number, tip speed rotation λ) if λ was near the optimum value $\lambda=1$. There were three findings of this work: (a) the maximum efficiency of the Savonius rotor, in terms of power coefficient, took place for $\lambda\approx1$, and that C_D decreased sharply when λ increased or decreased from the value, (b) for a given Reynolds number, as the tip speed ratio increased from zero, the drag values were maintained practically constant, $C_D \approx 1.5$ in the interval ranging from $\lambda= 0$ to $\lambda= 1.25$. The most interesting zone for power extraction was located near $\lambda\approx1$, where C_D showed minimal values. For tip speed ratios greater that 1.25, the drag coefficient increased, (c) in a wide interval around $\lambda = 1$ (the most important region of operation of the Savonius rotor) the lift coefficient remained practically constant at $C_L =0.5$.

Sawada et al [24] experimentally studied the mechanism of rotation of Savonius rotor that had two semi cylindrical blades. The force acting on the blade was measured in a water tank for both cases, while the rotor was at rest and also when it was rotated. The flow around the rotor was observed by using aluminum powder floating on the water surface. Although the Savonius rotor is classified as a resistance type, the lift produces a torque in a pretty wide range of blade angles relative to the flow. The researchers concluded that (a) when the rotor was at rest, the rotor with overlap ratio a/d = 0.21 produced a positive torque at any attitude

angle, (b) the lift around $\alpha = 240^0 \sim 330^0$ contributed a lot to the torque occurring when the rotor was rotated. (c) When the rotor was rotated, the effect of the pressure recovery by the flow through the overlap portion of the lift was little for the rotor of a/d =0.21. For the rotor of a/d=0.51, the existence of a flow through the center of the rotor contributed to the production of a negative torque opposing the clockwise rotation.

Aldoss and Obeidat [25] analyzed the performance of two Savonius rotor running side by side at different separations using the discrete vortex method. Two configurations were considered. The torque and power coefficients were computed and compared with the available experimental results presented by Aldoss and Najjar in an earlier paper.

Littler et al [26] made comparative tests of the Savonius rotor at constant Reynolds number. They suggested that a plain S-rotor might be as good as or better than the conventional Savonius rotor with an inter vane gap. A single S-rotor gave a C_p >0.15 (0.255 uncorrected wind tunnel value); although duplex rotors had given Cp > 0.18 (0.32 uncorrected value). Comparative particle flow visualization studies within these rotors (Savonius rotor with conventional gap, S-rotor with no gap, and a rotor with separated vanes ('negative' gap)) in a water channel suggested the importance of attached flow round the convex surfaces of the vanes, the doubtful value of the conventional gap, and the importance of vane shape.

Sivasegaram and Sivapalan [27] made an experiment in improving the sectional geometry of slow running vertical axis wind rotors of the Savonius type that had resulted in considerable improvement in rotor performance. They suggested that further improvement in power output form a rotor of given overall dimensions demanded the use of power augmenting system and that of wind direction had

been investigated and the system configuration giving maximum power augmentation was determined. They showed that an eighty percent increase in power output could be achieved using a pair of vanes of moderate size.

Islam et at [12] investigated Aerodynamic characteristics of a stationary Savonius rotor of two semi cylindrical blades. The test was carried out in a uniform flow jet produced by an open circuit wind tunnel. The exit of the wind tunnel consisted of a square section nozzle with a side length of 500 mm. The rotor was placed at the jet axis and at 750 mm downstream of the nozzle exit. This study was carried out at constant wind speed of $U_0 = 13.3$ m/s i.e., at Reynolds number, $R_e = 2 \times 10^5$. The results of this work showed that flow separated over the convex surface of the blades and the separation point moved towards the leading and trailing edges of the advancing and returning blades respectively as the rotor angle increased from 0^0 to 90^0. Beyond $\alpha=90^0$, flow separated over the convex surface of the returning blade only. They also found that the difference in pressure on the convex and concave surfaces, produced drag coefficients, C_n an C_t in the normal and tangential direction of the chord. Drag coefficient C_n and C_t were a function of rotor angle and their resultant reached maximum value at $\alpha= 120^0$ and a minimum value at $\alpha = 0^0$.

CHAPTER 3
EXPERIMENTAL SET-UP AND PROCEDURE

Chapter-3

EXPERIMENTAL SET-UP AND PROCEDURE

3.1   Introduction

The objectives of the investigation of wind loading on the four semi-cylindrical bladed Savonius rotor have been realized essentially with the help of a subsonic wind tunnel, experimental set-up of the Savonius rotor and an inclined manometer. Pressure distributions of the convex and concave surfaces of each blade of the Savonius rotor placed normal to the approaching uniform flow have been measured with the help of the multi manometer. The following sections describe in detail about the experimental set-up and the techniques adopted for the investigation.

3.2   The Wind Tunnel

The open circuit subsonic wind tunnel has been 6.55m long with a test section of (490x490 mm) cross-section. Figure 3.1 depicts the wind tunnel used for the experiment. The successive sections of the wind tunnel comprise of converging mouth entry, perspex section, rectangular section, fan section (two rotary axial flow fans), butterfly section, silencer with honey comb section, an eddy breaker, diverging section, converging section, 610 mm long rectangular section, 305 mm long flow straighter section and 610 mm long rectangular exit section. The central longitudinal axis of the wind tunnel has been maintained at a constant height from the floor.

1. Converging Mouth Entry

2. Perspex Section

3. Rectangular Diverging Section

4. Fan Section

5. Butterfly Section

6. Silencer with Honeycomb Section

7. Diverging Section

8. Converging Section

9. Rectangular Section

10. Flow Straighter Section

11. Rectangular Exit Section
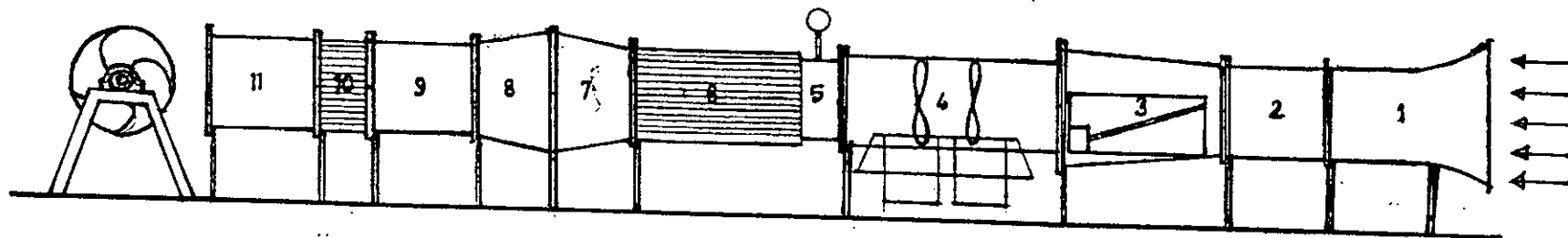
Figure 3.1   : Schematic Diagram of Wind Tunnel

VIEW –CC

VIEW –BB

VIEW – AA
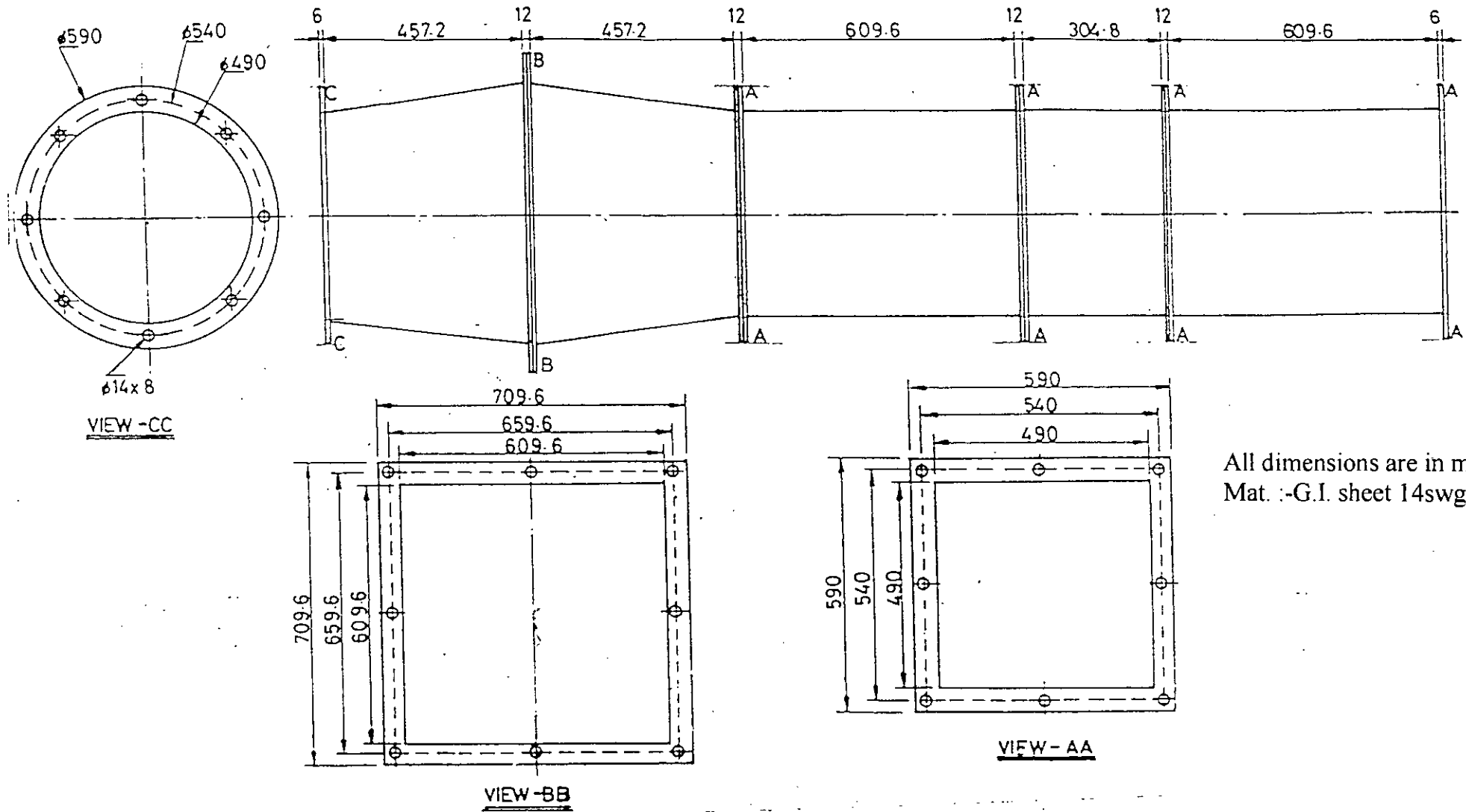
All dimensions are in mm.
Mat. :-G.I. sheet 14swg.

Figure 3.2 :Modification of part of the wind tunnel

The converging mouth entry has been incorporated into the system for the easy entry of air into the tunnel and to maintain uniform flow into the duct free from outside disturbances. The exposed surface of the mouth entry has been covered with cloth for extra protection against dust and for uniform flow.

The perspex section is (305 x 305 mm) 610 mm long that may be used for the experiment of flow around the circular cylinder. A 920 mm long rectangular diverging section has been used to make the flow uniform from rotation.

The induced flow through the wind tunnel has been produced by a two-stage rotating axial flow fan (Woods of Colchester Ltd., England, Type 38 JTE) of capacity 14.15 m^3/s at a head of 152.4 mm of water and 1475 rpm. A butterfly valve actuated by a screw thread mechanism has been placed behind the fan and used to control the flow. A silencer has been fitted at the end of the flow controlling section in order to reduce the noise of the system at the same time a flow straightner system has been used in this section. All these sections have been the existing sections of the wind tunnel. Further modification has been made to make the flow uniform (Figure 3.2). The modified parts are a diverging section, converging section, 610 mm long square section, flow straightner section and a 610 mm long square exit section. The diverging and converging section of the wind tunnel is 460 mm long and made of 16 SWG black sheets. The angle of divergence and convergence is 7^0, which has been made with a view to minimize expansion and contraction loss and to reduce the possibility of flow separation. Other three square sections have been used to make the flow straight and uniform.

3.3   The Four bladed Savonius Rotor

The constructional details of the test section are shown in figure 3.3 (a), 3.3(b) and 3.3(c). The Savonius rotor is made up of four half cylinders (blade) of diameter, d= 125 mm and height, H = 300 mm. The cylinders are made of PVC material. The overlap ratio S has been selected to be one-fifth of the cylinder diameter (i.e. S = a/d = 0.2) and the central shaft removed. The overlap distance selected have been optimum value with respect to the wind power extraction. The whole rotor is fixed on an iron frame by using two side shafts and two ball bearings.

The pressure measurements have been made at 17 pressure tapings on each blade. The tapings are made with copper tubes of 1.5 mm outer diameter and 10 mm length that have been press fitted to the taping holes. The tapings are located at the mid-plane on one side of each blade, so that pressure distribution at every 10^0 on the blade surface can be measured. The pressure tapings have been connected to a inclined multi-manometer (manometric fluid being water with an accuracy of ±0.1 mm of water column) through 2 mm PVC tubes. The pressures have been measured at every 10° interval of rotor angle (figure 3.5), so that a detailed picture of aerodynamic loading and torque characteristics can be obtained.
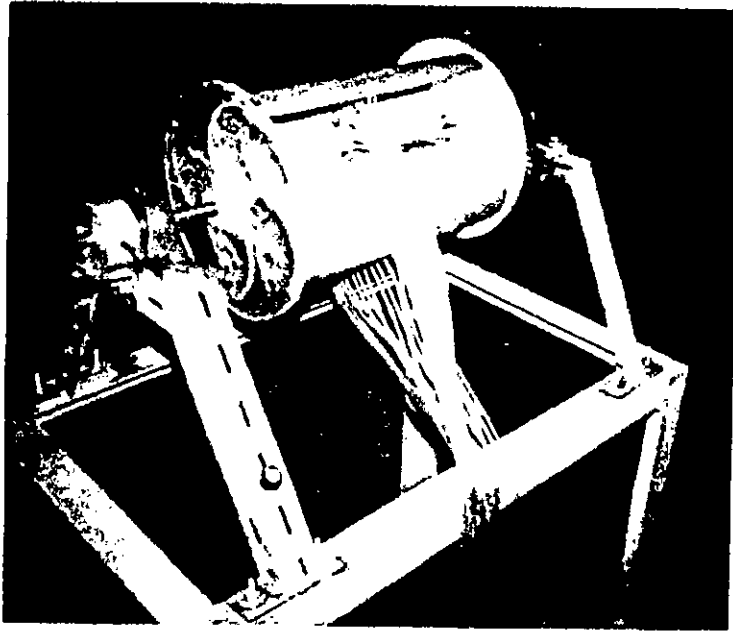
Fig 3.3 (a)   :Construction of the Four-Bladed Savonius Rotor.
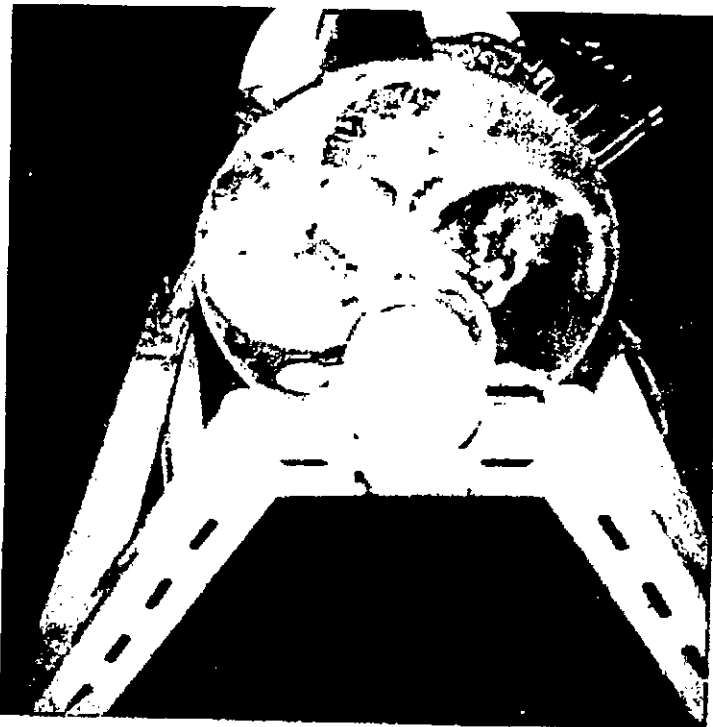
Fig 3.3 (b)   :End View of the Four-Bladed Savonius Rotor.
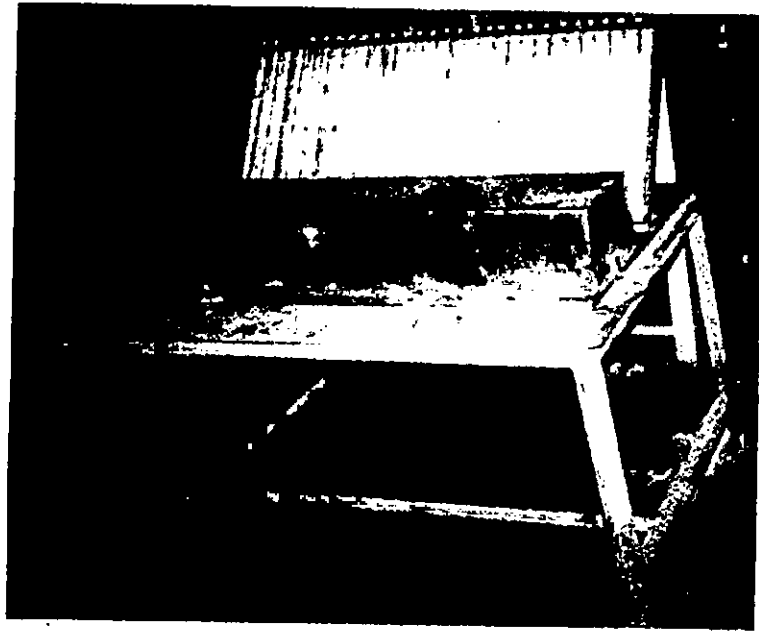
Fig 3.3 (c)   :Multimanometer.
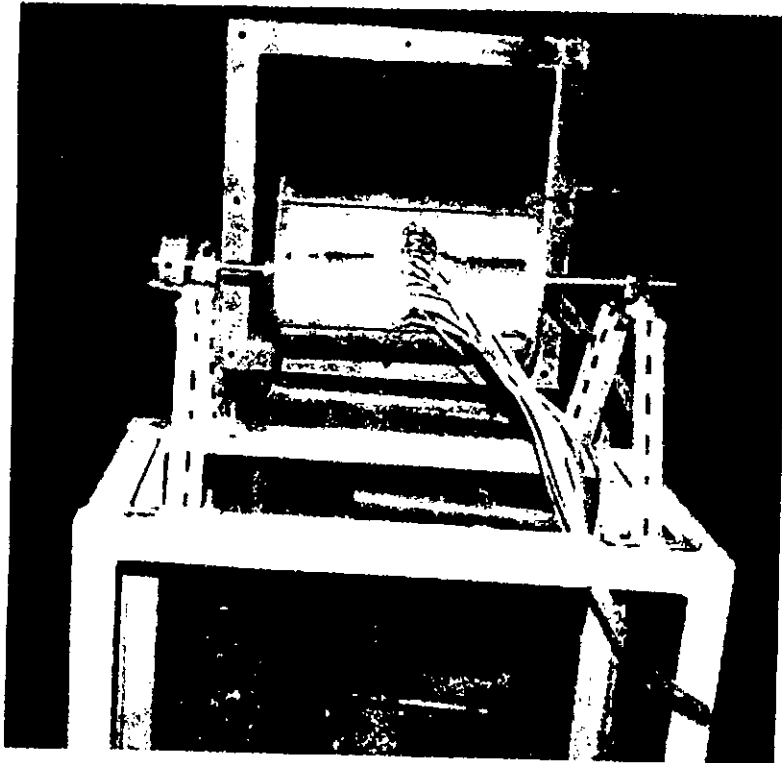
Figure 3.4   :Experimental Arrangement of the Four-Bladed Savonius Rotor.

28
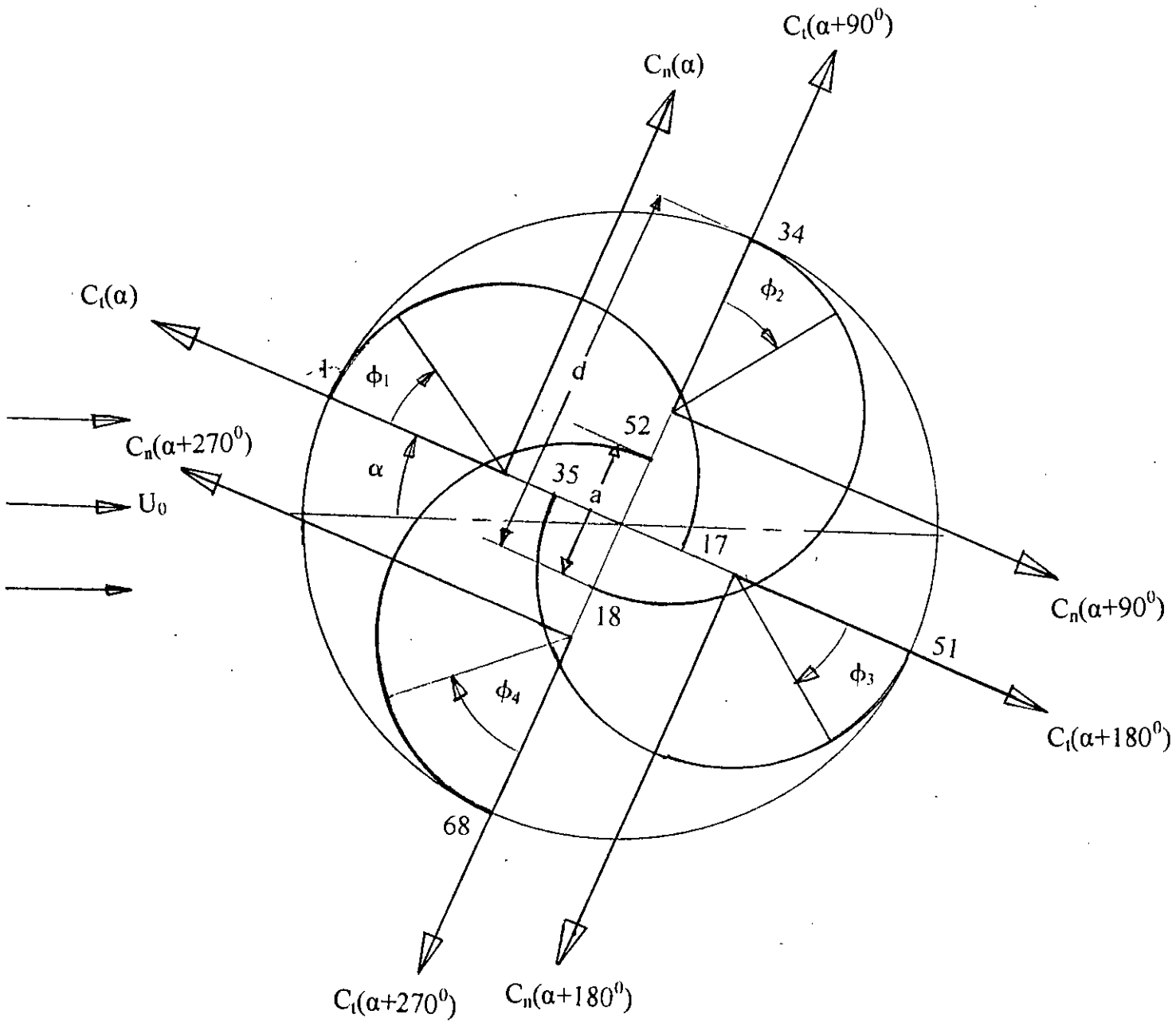
Figure 3.5   :Forces acting on the blades

3.4   Experimental procedure

The flow velocity in the test section was kept constant at 13m/s. The Reynolds number based on the rotor diameter D=225 mm was 1.89×10^5. The effect of the temperature was considered in this experiment and the experiment was carried out at atmospheric temperature i.e. at T=25°C where the kinematic viscosity of air was $v = 1.55 \times 10^{-5}$ m²/s.

Before measuring the pressure distribution the mean velocity was measured in a vertical plane 0.5 m downstream from the exit of the wind tunnel without placing the rotor by means of pitot tube connected to an inclined manometer with kerosene as manometric fluid. The measured velocity distribution was uniform as shown in figure 3.6.

The pressure distributions over the blade surfaces were measured step by step by multimanometer. At first, power was not supplied to the wind tunnel and the Savonius rotor with the frame was placed 500 mm upstream in front of the exit section of the wind tunnel. One blade of the rotor was fixed parallel to the free stream velocity i.e. parallel to the horizontal, which was called the reference plane, and from this plane, angle of rotation was measured.

Then the first blade was kept at 0^0 angle of rotation, exposing the convex surface in front of the free stream of air, and other three blades were kept at 90^0, 180^0 and 270^0 angle of rotation respectively. The rotor was made static fixing one side of the shaft of the rotor with the angle-fixing device. Pressure on the convex surfaces of blades was measured at a particular rotor angle α, keeping the rotor static. Gradually, pressure on the convex surface was measured in this process for every 10^0 interval. The same steps were repeated for the measurement of pressure on concave surfaces.

DISTANCE VERSUS VELOCITY (VELOCITY PROFILE)
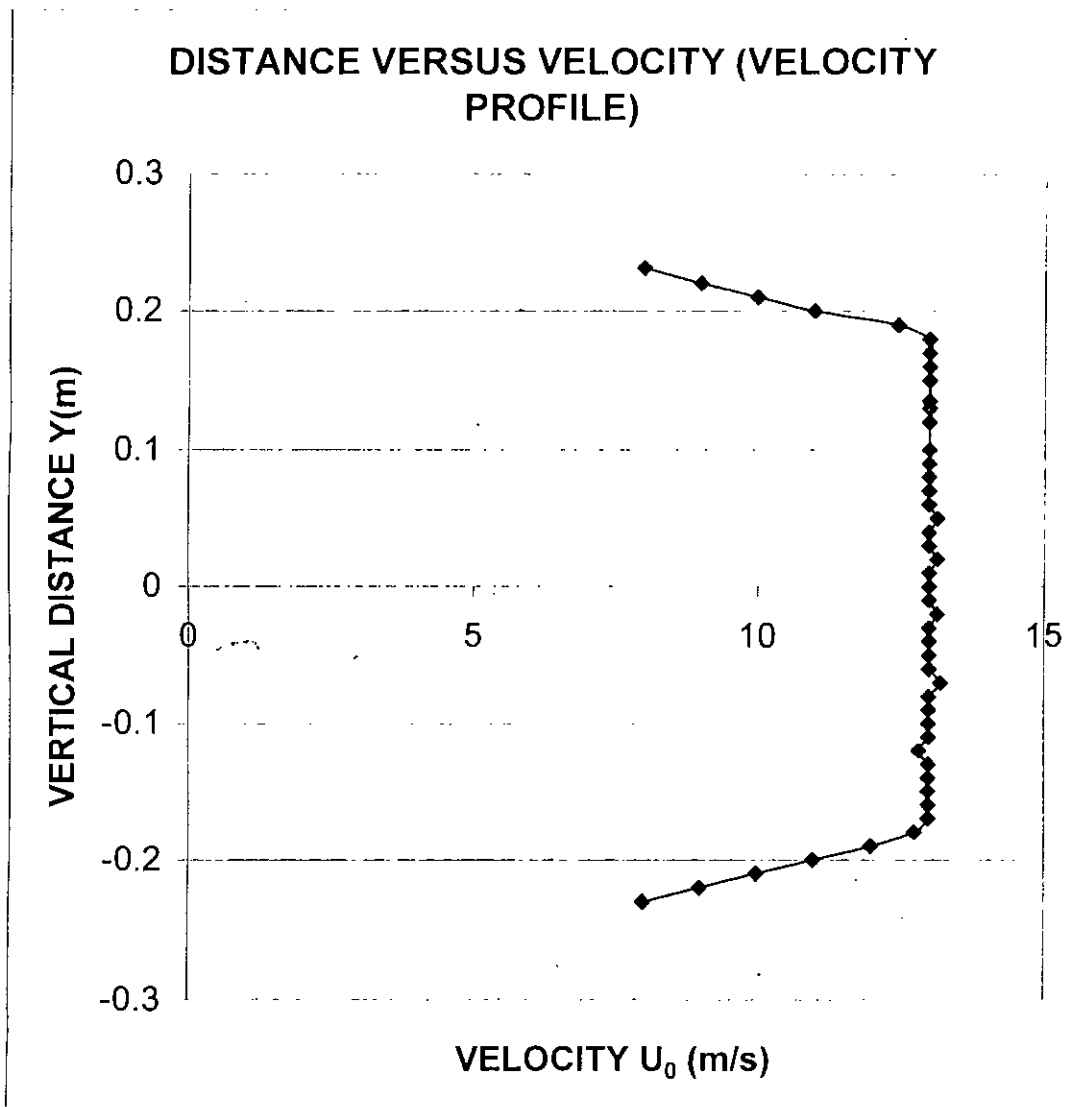
Figure 3.6   :Velocity distribution in the upstream side of the test section

At a particular rotor angle α, the rotor blades had experienced forces (per unit span of length) due to pressure difference between the concave and convex surfaces, which were resolved into normal forces, F_n and tangential forces, F_t. From figure 3.5 it can be noticed that the rotor was rotated in the direction of flow and the pressure difference was calculated by subtracting the pressure of the concave surface from the pressure on the convex surface, as most of the time the convex surface was exposed to the free stream.

31

CHAPTER 4
DETAILS OF NON-DIMENSIONAL PARAMETERS

Chapter-4

DETAILS OF NON-DIMENSIONAL PARAMETERS

4.1 Introduction

In the present experiment, the local surface pressures on the blade surfaces of the rotor were measured relative to the free upstream static pressure prevailing in the test section of the wind tunnel. The data obtained experimentally have been presented in terms of non-dimensional coefficients. The equations of coefficient of pressure, normal and tangential drag, individual torque and total static torque are derived briefly in this chapter. Derivation of equations for the prediction of power coefficient from the static drag coefficient for different tip speed ratios are also provided in this chapter.

4.2 Static Aerodynamic Characteristics

In the following three steps the procedure for calculating the static aerodynamic characteristics is mentioned:

Step 1: From the experimental data pressure coefficients both for concave and convex surfaces of blades are calculated for angle of rotation ranging from 0^0 to 80^0. After these rotational angle (α) the system would repeat.

Step 2: Considering the pressure differences between concave and convex surfaces of blades of the Savonius rotor, a Fortran programme was developed to calculate the drag coefficients in normal and tangential directions.

Step 3: From the drag coefficient in the normal direction the torque coefficient for a single blade and the total static torque coefficient produced on the rotor shaft were calculated by using a Fortran Programme.

4.2.1 Pressure Co-efficient, Cp

In the experiment, the pressure measurements were made at 17 pressure tappings on each blade for the angle of rotation (α) at every 10^0 interval ranging from 0^0 to 350^0 on both concave and convex surfaces. Using this raw data pressure coefficient on convex surfaces (C_{px}) of four blades and pressure coefficient for concave surfaces (C_{pc}) of the blades were calculated by using the following expression of pressure coefficient.

Pressure coefficient may be defined as

$$C_P = \frac{P - P_0}{\frac{1}{2}\rho U_0^2} \tag{4.1}$$

Where, $P - P_0$ = Difference between blade and atmospheric pressure

ρ = Density of air

U_0 = free stream velocity

At an angle of rotation (α) of 90^0, the fourth blade will take the position of first blade, third will take the position of the fourth, second will take the position of the third and first will take the position of the second respectively. The calculation of C_{px} and C_{pc} were plotted against pressure tapping points on the same graph for analysis.

33

4.2.2 Drag Co-efficients

For a particular rotor angle, α the rotor blades experience forces (per unit span length) due to pressure difference between the concave and convex surfaces. These forces can be resolved into two components, F_n and F_t. Since the blade surfaces are circular, F_n and F_t pass through the center of the semicircle. The positive directions of F_n and F_t are shown in figure 3.5.

The drag coefficients in normal and tangential directions can be written as follows:

$$C_n = \frac{F_n}{\frac{1}{2}\rho U_0^2 d}$$

$$C_t = \frac{F_t}{\frac{1}{2}\rho U_0^2 d}$$

To obtain the drag coefficients in normal and tangential directions of the chord, the values of F_n and F_t must be known beforehand. The values of forces F_n and F_t are obtained by integrating the pressure for a blade as follows:

$$F_n = \int_0^\pi \Delta p \frac{d}{2}\cos\phi\,d\phi = \sum_{i=1}^{17} \Delta p_i \frac{d}{2}\cos\phi_i \Delta\phi_i \qquad (4.3)$$

and similarly,

$$F_t = \sum_{i=1}^{17} \Delta p_i \frac{d}{2}\sin\phi_i \Delta\phi_i$$

Where ΔP_i is the difference in pressure on the concave and convex surfaces at a particular pressure tapping, i.

34

The normal force F_n is responsible for producing a torque on the shaft of the rotor and this torque can be expressed for a blade as,

torque on a blade,

$$
\begin{aligned}
T &= F_n x \frac{d-a}{2} \\
&= F_n x \frac{d}{2}\left(1 - \frac{a}{d}\right) \\
&= F_n x \frac{d}{2}(1 - s)
\end{aligned}
\tag{4.4}
$$

4.2.3 Torque Co-efficient

Equation (4.4) can be reduced to get the torque coefficient for a single blade at a particular rotor angle. The different parameters are shown in figure 3.5. The equation can be written as,

$$
\begin{aligned}
C_q(\alpha) &= \frac{F_n}{\frac{1}{2}\rho U_0^2 d} x \frac{(d-a)}{2} x \frac{2}{(2d-a)} \\[2mm]
&= C_n(\alpha)x\frac{d-a}{2d-a} \\[2mm]
&= C_n(\alpha)x\frac{d\left(1-\frac{a}{d}\right)}{d\left(2-\frac{a}{d}\right)} \\[2mm]
&= C_n(\alpha)x\frac{(1-s)}{(2-s)}
\end{aligned}
\tag{4.5}
$$

35

Total static torque coefficient produced on rotor shaft by the four blades can be expressed as follows:

$$C_Q = \frac{\left(F_{n1} + F_{n2} + F_{n3} + F_{n4}\right)}{\frac{1}{2}\rho U_0^2 D} \times \frac{\frac{(d-a)}{2}}{\frac{(2d-a)}{2}}$$

$$= \frac{\left(F_{n1} + F_{n2} + F_{n3} + F_{n4}\right)}{\frac{1}{2}\rho U_0^2 d} \times \frac{d-a}{(2d-a)} \times \frac{d}{D}$$

$$= \left[\frac{F_n(\alpha)}{\frac{1}{2}\rho U_0^2 d} + \frac{F_n(\alpha+90^0)}{\frac{1}{2}\rho U_0^2 d} + \frac{F_n(\alpha+180^0)}{\frac{1}{2}\rho U_0^2 d} + \frac{F_n(\alpha+270^0)}{\frac{1}{2}\rho U_0^2 d}\right] \times \frac{d(1-\frac{a}{d})}{d(2-\frac{a}{d})} \times \frac{1}{D} . d$$

$$= \left[C_n(\alpha) + C_n(\alpha+90^0) + C_n(\alpha+180^0) + C_n(\alpha+270^0)\right] x \frac{(1-s)}{(2-s)} \times \frac{1}{\frac{(2d-a)}{d}}$$

$$= \left[C_n(\alpha) + C_n(\alpha+90^0) + C_n(\alpha+180^0) + C_n(\alpha+270^0)\right] x \frac{(1-s)}{(2-s)} \times \frac{1}{(2-s)}$$

$$C_Q(\alpha) = \left[C_n(\alpha) + C_n(\alpha+90^0) + C_n(\alpha+180^0) + C_n(\alpha+270^0)\right] x \frac{(1-s)}{(2-s)^2} \qquad (4.6)$$

Where C_n (α), C_n (α+90), C_n (α+180), C_n (α+270) refer to the drag coefficients for the first, second , third and fourth blades respectively at a rotor angle α.

4.2.4 Numerical Prediction

Three computer programmes were performed using Microsoft Fortran to calculate forces experienced by the rotor blades, drag coefficients and torque coefficients by using Equations (4.2) to (4.6).

In the first programme, two components of force experienced by the individual tapping points on each blades were calculated by using equation (4.3) and also the torque T was calculated by using equation (4.4). The programme output gave 36 sets of 17 data for F_n, F_t and T.

In the second programme, integration was performed using the output of the first programme to calculate total forces F_n and F_t and total torque T acting on individual blades and shafts respectively. The programme output gave three types of 36 integrated values of forces and torques. Two types of drag coefficients and torque coefficients were calculated with the help of equation (4.2) and (4.5). The programme output gave 36 normal drag coefficients, 36 tangential drag coefficients and 36 torque coefficients ranging from 0^0 to 350^0 angle of rotation at every 10^0 interval.

From the third programme, combined effect of three blades on the normal and tangential drag coefficients were calculated. The total static torque coefficient produced on the rotor shaft was also calculated in the same programme with the help of equation (4.6).

All these programme outputs of drag coefficients and torque coefficients are plotted against angle of rotation for analysis.

4.3   Prediction of Dynamic Characteristics

This topic includes the prediction of power coefficients by calculating the component of relative velocity along free stream velocity, V_w for different rotor angles, α at different tip speed ratios, λ of a four Bladed Savonius rotor.

4.3.1 Prediction of Power Coefficient

The quasi-steady approach applied to the analysis of Darricus rotor has been considered for the prediction of performance of four bladed Savonius rotor. The static drag coefficient obtained experimentally at blade angle α, has been used in conjunction with the relative velocity V_r corresponding to a particular tip speed ratio, λ to evaluate the force acting on the blade. The power coefficient has been estimated by averaging the work done over a cycle.

4.3.1.a Velocity Triangles

Six sets of velocity triangles are drawn for six different tip speed ratios of 0.5, 0.8, 0.9, 1.1, 1.2 and 1.5. In each set, nine velocity triangle diagrams have been drawn for angle of rotation (α) ranging from 0^0 to 80^0. Typical diagrams are shown in figures 4.2(a) to 4.2(f).

Velocity triangle diagrams are drawn on the basis of the following calculations:

Blade diameter,

$d = 125mm = 0.125m$

i.e., $r = 0.0625m$

Overlap distance,

$a = 25mm = 0.025m$

Overlap ratio,

$S = a/d = 0.2$

Diameter of the rotor, $\qquad D = 2d - a = 0.225m$

$R = 0.1125m$

$U_0 = 13m/s$

At Tip speed ratio, $\lambda = 0.5$

$\lambda = 0.5 = R\omega / U_0$

$\therefore \omega = 57.78$ rad / s

$r \omega = 0.0625 \times 57.78 = 3.6$ m/s

Similarly,

At, $\lambda = 0.8$, $r \omega = 5.8$ m/s

$\lambda = 0.9$, $r \omega = 6.5$ m/s

$\lambda = 1.1$, $r \omega = 8$ m/s

$\lambda = 1.2$, $r \omega = 8.6$ m/s

$\lambda = 1.5$, $r \omega = 10.8$ m/s

i. At $\alpha = 0^0$

ii. At $\alpha = 10^0$

Figure 4.1 (a)   Velocity triangles combining the effect of free stream velocity and blade rotation at $\lambda = 0.5$.

i. At $\alpha = 0^0$
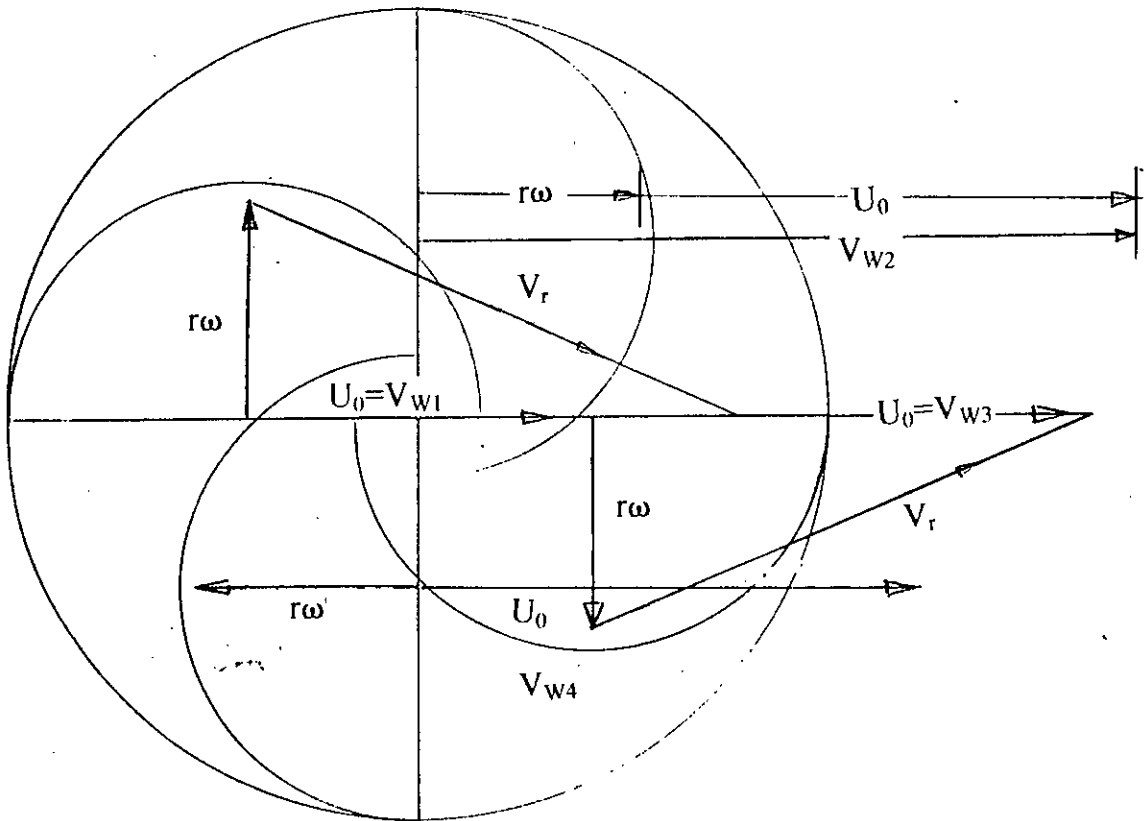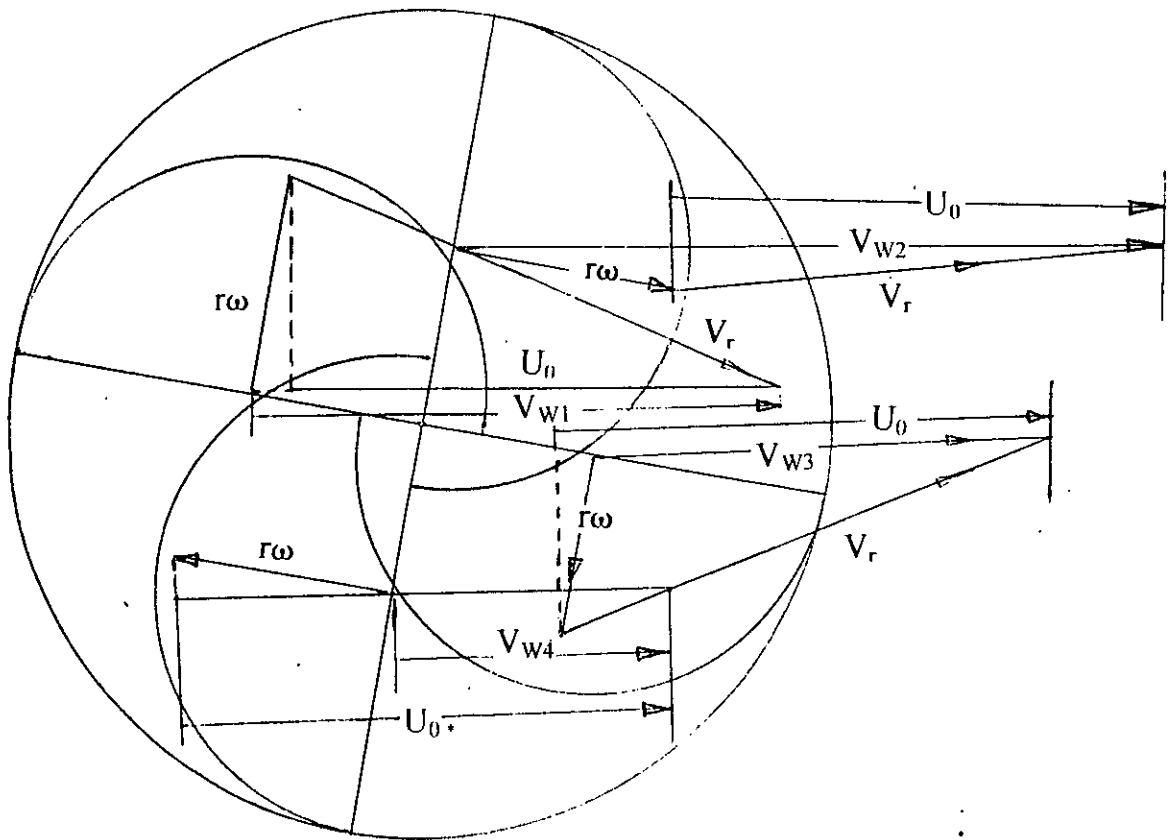
ii. At $\alpha = 10^0$

Figure 4.1(b)   Velocity triangles combining the effect of free stream velocity and blade rotation at $\lambda = 0.8$.

i.   At $\alpha = 0^0$
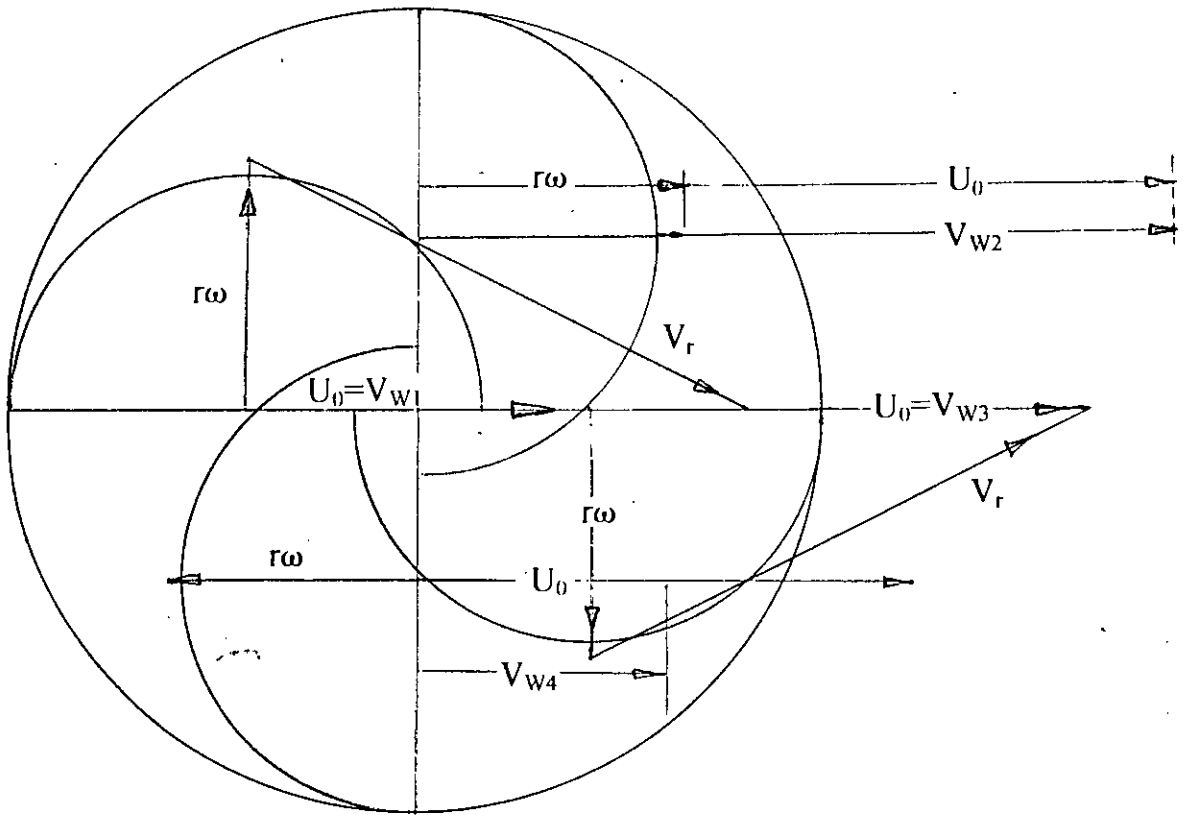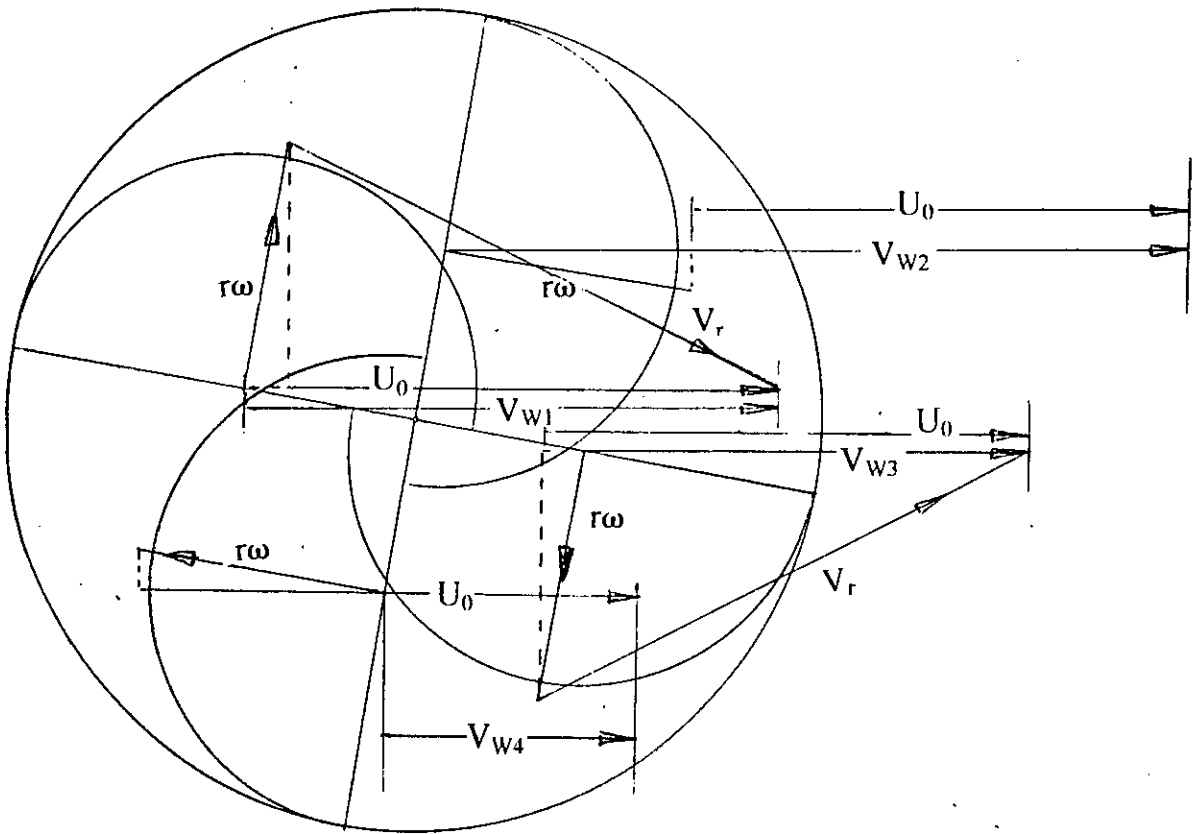
ii.   At $\alpha = 10^0$

Figure 4.1 (c)   Velocity triangles combining the effect of free stream velocity and blade rotation at $\lambda = 0.9$.

i.   At $\alpha = 0^0$
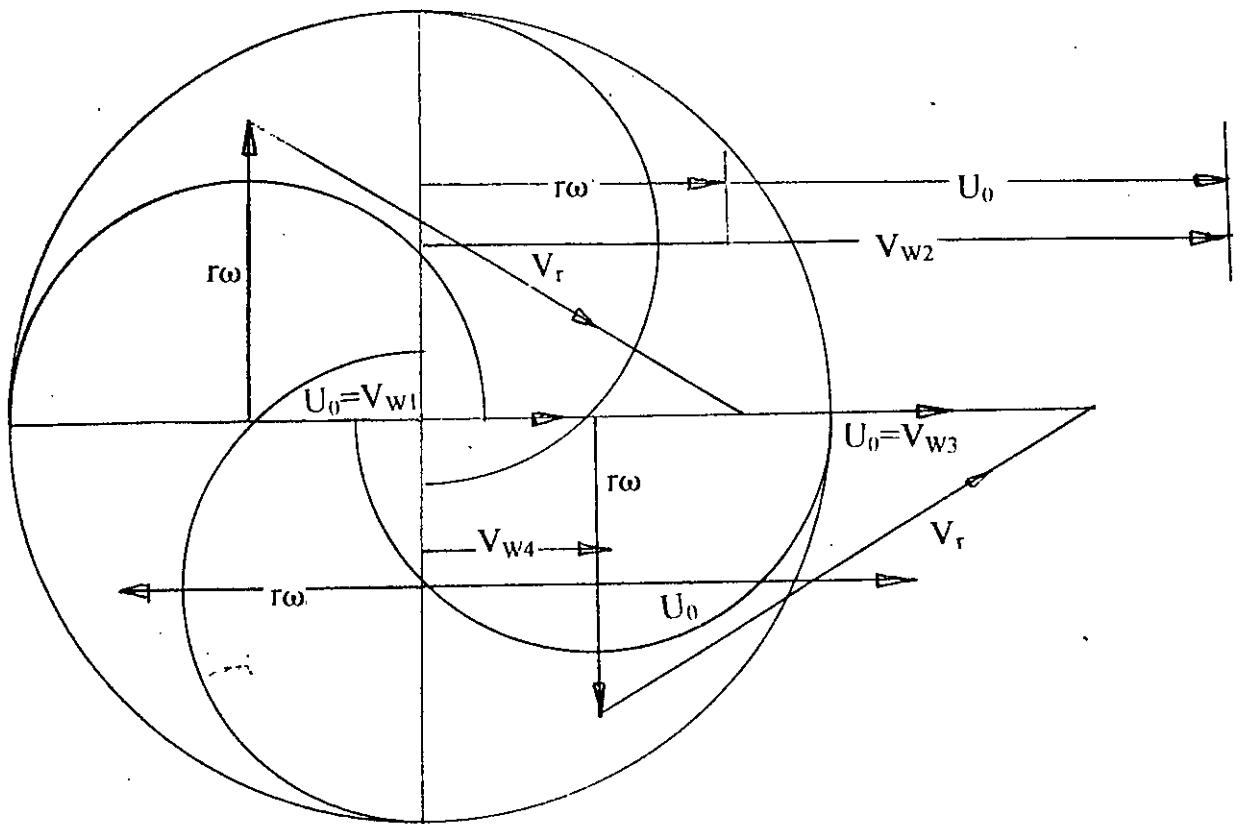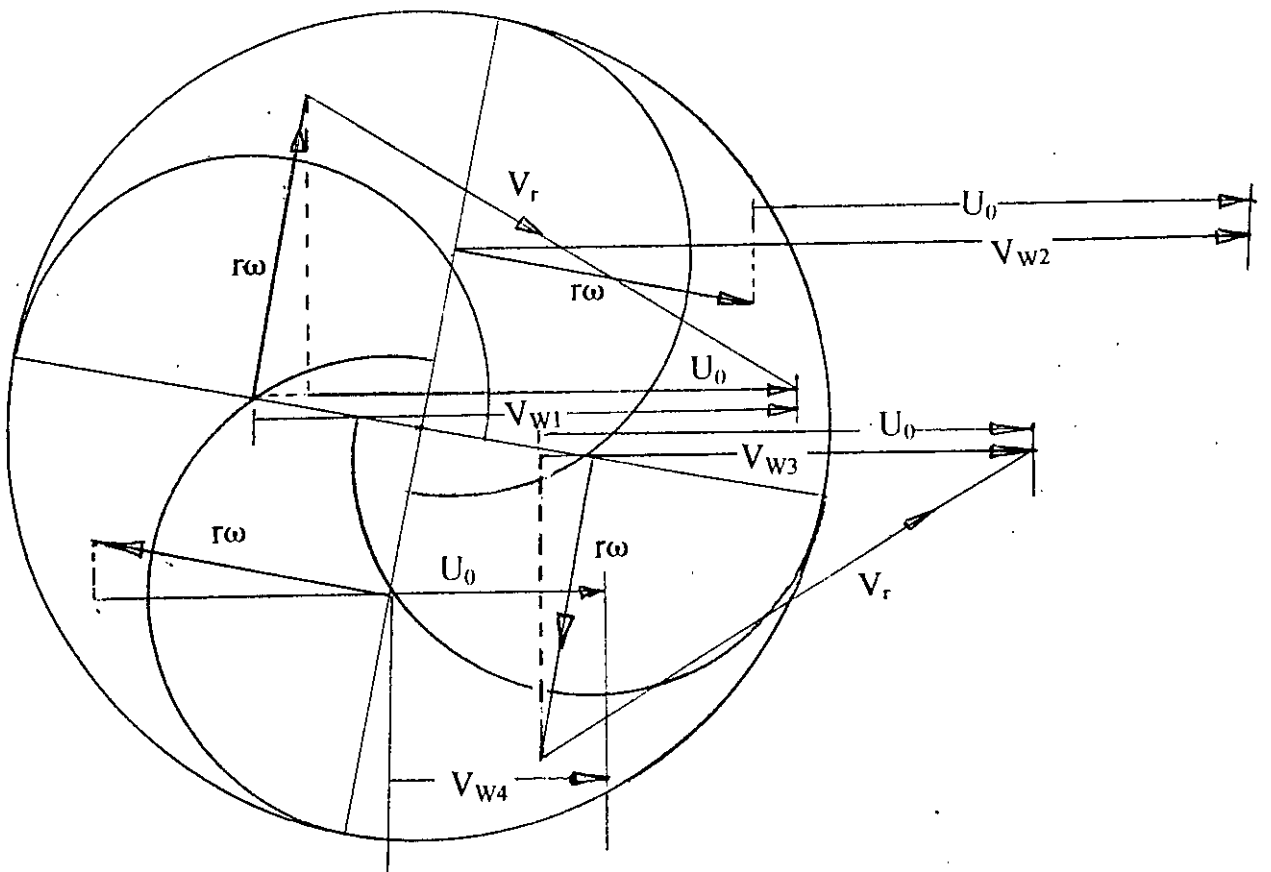
ii.   At $\alpha = 10^0$

Figure 4. 1 (d)   Velocity triangles combining the effect of free stream velocity and blade rotation at $\lambda = 1.1$.

i. At $\alpha = 0^0$
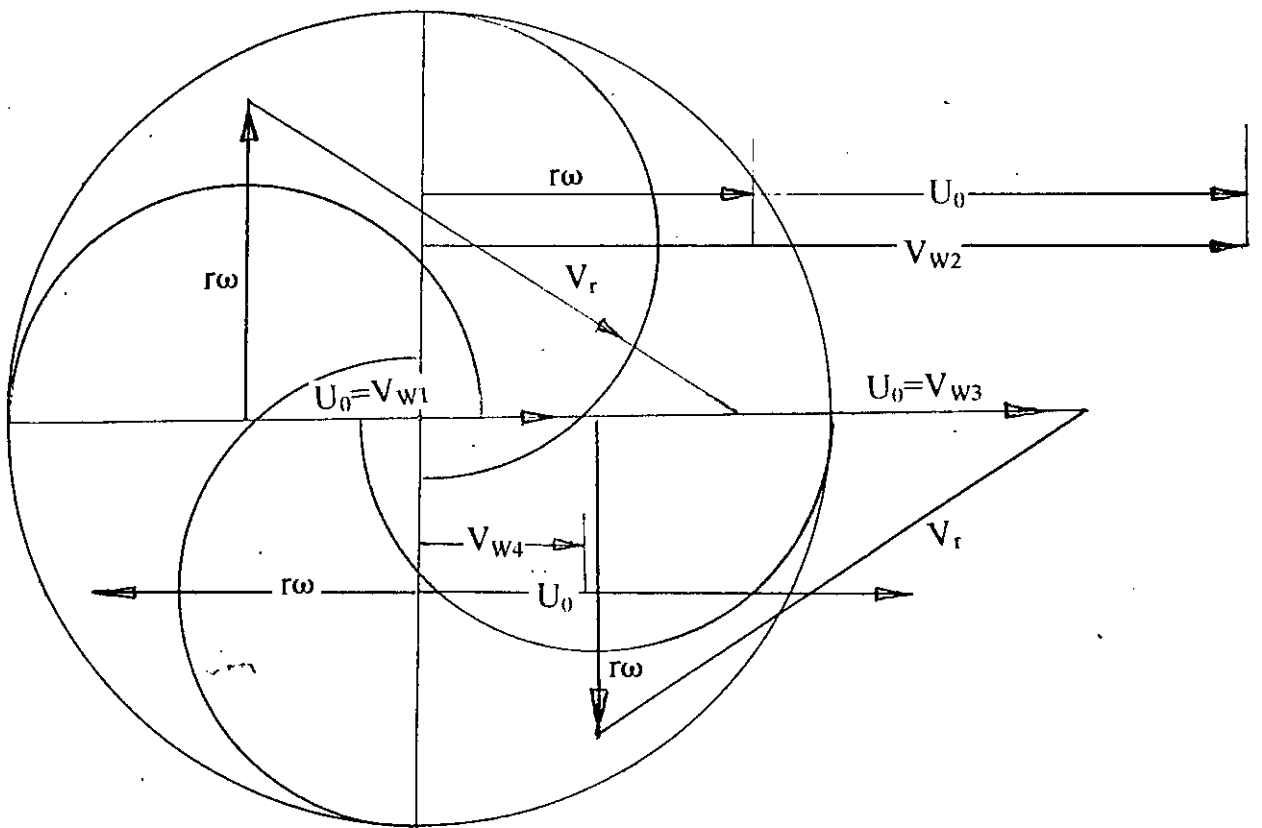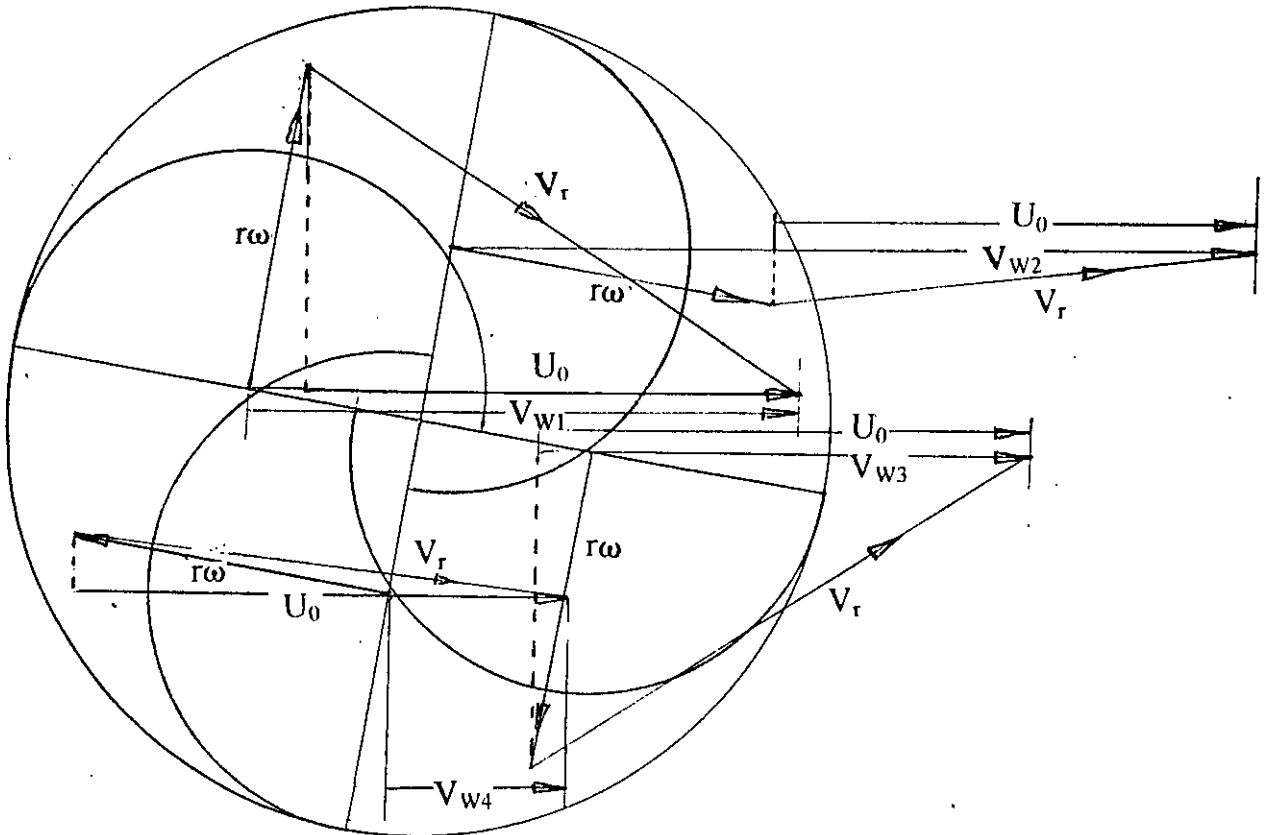
ii. At $\alpha = 10^0$

Figure 4.1 (e)   Velocity triangles combining the effect of free stream velocity and blade rotation at $\lambda = 1.2$.

i. At $\alpha = 0^0$
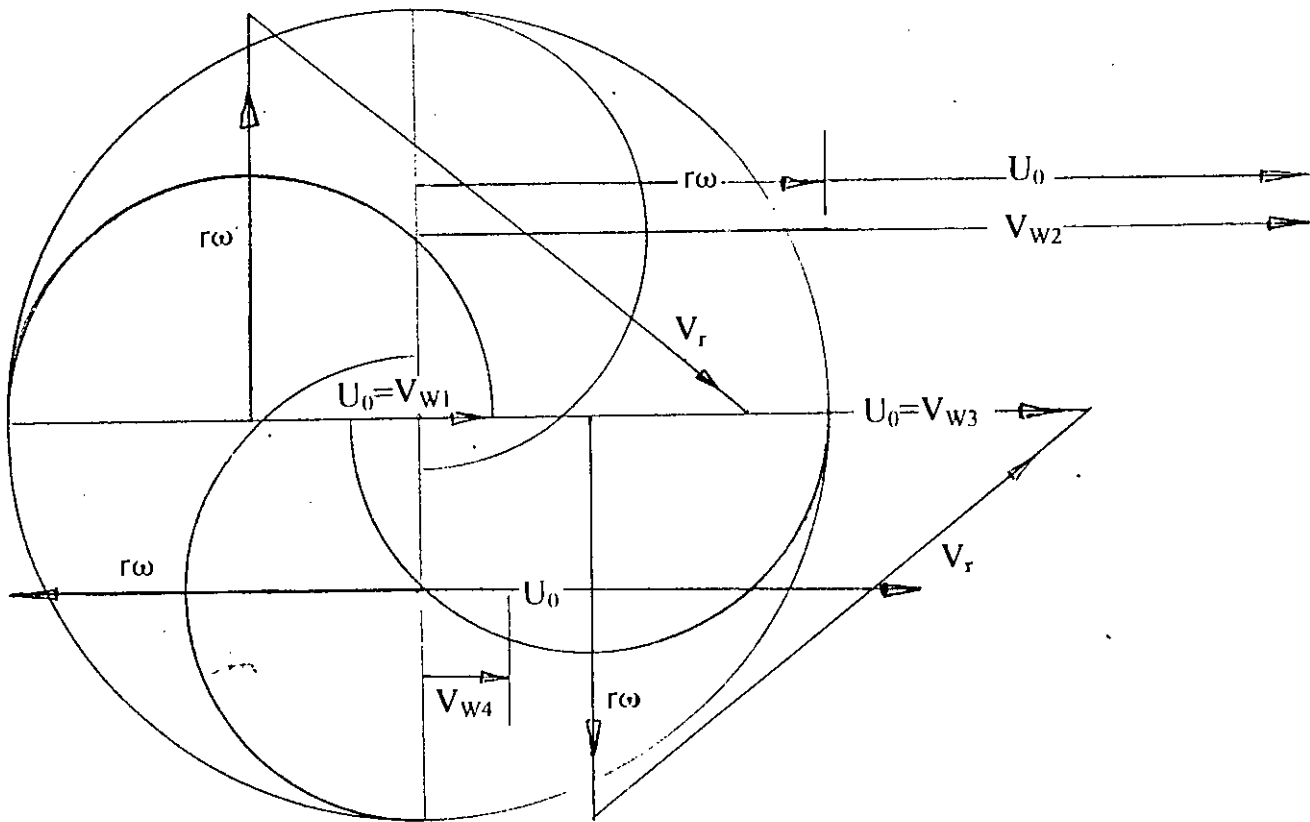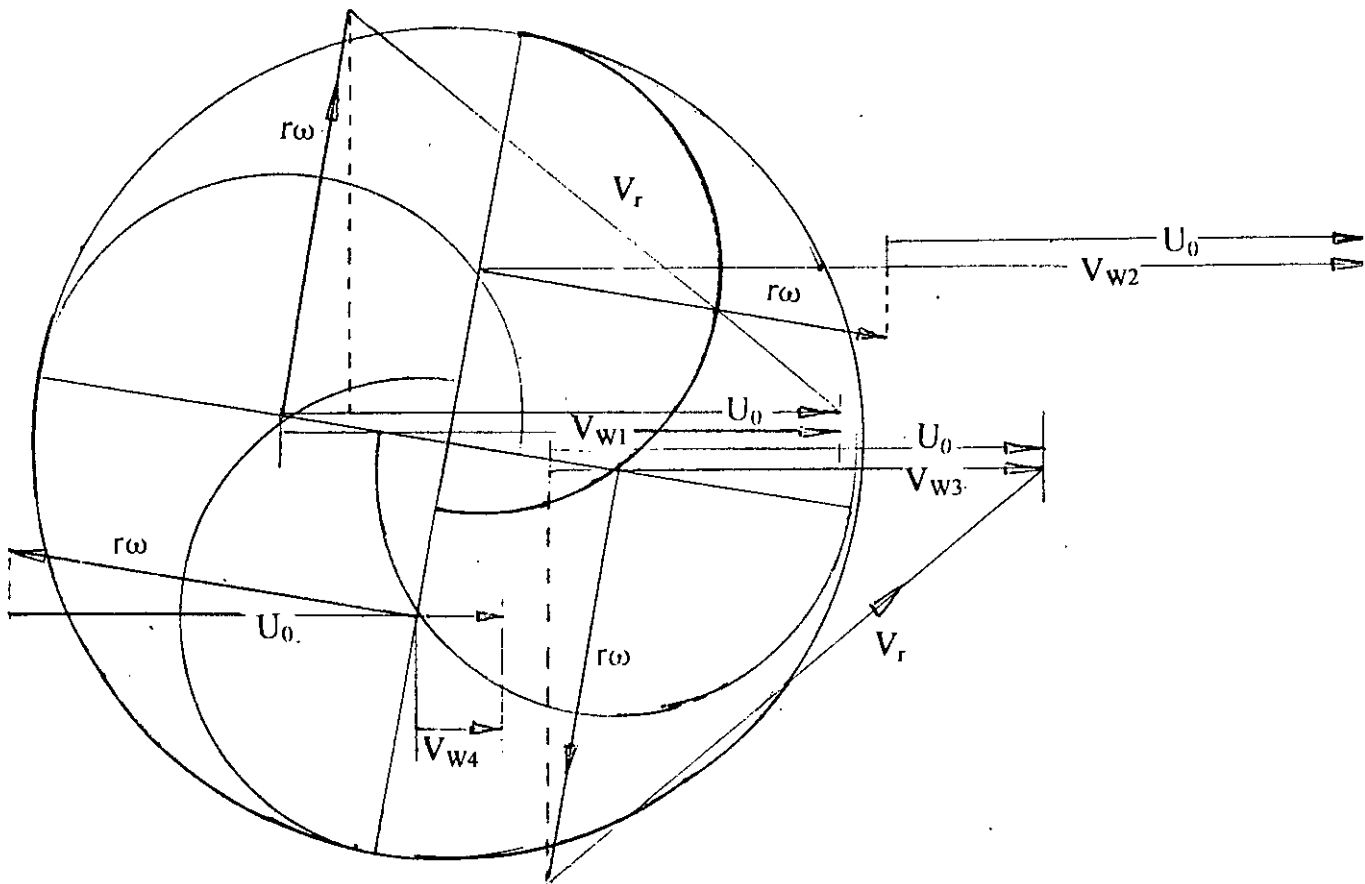
ii. At $\alpha = 10^0$

Figure 4.1 (f)   Velocity triangles combining the effect of free stream velocity and
blade rotation at $\lambda = 1.5$.

4.3.1.b Power Co-efficient

The following equations have been used to estimate the power coefficient at a blade angle α.

$$C_n{}'(\alpha) = C_n(\alpha) \times (V_{w1}/U_o)^2 \qquad (4.7)$$

$$C_n{}'(90^0+\alpha) = C_n(90^0+\alpha) \times (V_{w2}/U_o)^2 \qquad (4.8)$$

$$C_n{}'(180^0+\alpha) = C_n(180^0+\alpha) \times (V_{w3}/U_o)^2 \qquad (4.9)$$

$$C_n{}'(270^0+\alpha) = C_n(270^0+\alpha) \times (V_{w4}/U_o)^2 \qquad (4.10)$$

Torque coefficient at α,

$$C_Q{}'(\alpha) = [C_n{}'(\alpha) + C_n{}'(90^0+\alpha) + C_n{}'(180^0+\alpha) + C_n{}'(270^0+\alpha)] \times \frac{(1-s)}{(2-s)^2} \qquad (4.11)$$

Power coefficient at α,

$$C_P(\alpha) = C_Q{}'(\alpha).\lambda \qquad (4.12)$$

4.3.2 Numerical Prediction

A computer programme was developed to calculate the power coefficient (C_p) using the value of the component of relative velocity V_w along U_o and static normal drag coefficient $C_n(\alpha)$ for three different tip speed ratios with the help of equations (4.7) to (4.12). The programme output gave four sets of dynamic torque coefficients and power coefficient and finally four average values of power coefficient $C_{Pave.}$

Power coefficient vs. tip speed ratio of the present prediction and previous researchers' prediction were plotted on the same graph for analysis. Finally, comparisons were made of power coefficient vs tip speed ratio for different Reynolds number.

CHAPTER 5
RESULTS AND DISCUSSIONS

Chapter-5

RESULTS AND DISCUSSIONS

5.1   Introduction

In this chapter, the results of the pressure distribution over the convex and concave surfaces of each blade at different angle of rotation are analyzed first. The nature of the drag and static torque characteristics are also analyzed. In addition comparative study of the existing research works and the present investigation on the prediction of dynamic characteristics are also presented in this chapter.

5.2   Static Aerodynamic Characteristics

This topic includes the analysis of pressure distribution, drag coefficients, C_n and C_t, torque coefficient, C_q and total static torque coefficient, C_Q.

5.2.1   Pressure Distribution

The pressure distribution over the surfaces of the blades were measured at every 10^0 interval of rotor angle between $0^0 \leq \alpha \leq 80^0$. The results are presented in figure 5.1(a) to 5.1(i).

At $\alpha=0^0$ (Figure 5.1(a)) on the concave surface the pressure remains almost constant on the first, second and fourth blade. The pressure coefficient, C_{pc} is positive on the first blade and very near to atmospheric pressure on the second blade. On the third and fourth blades the pressure coefficient is negative. On the third blade the pressure fluctuates.
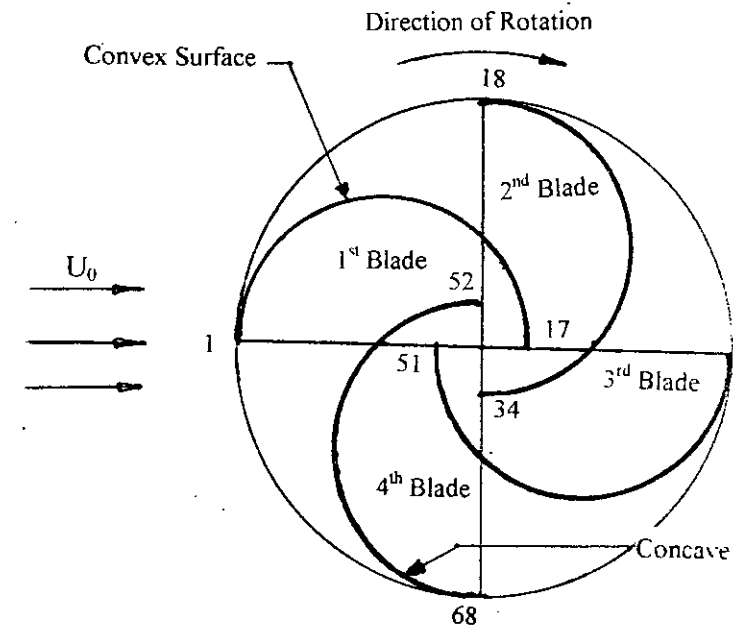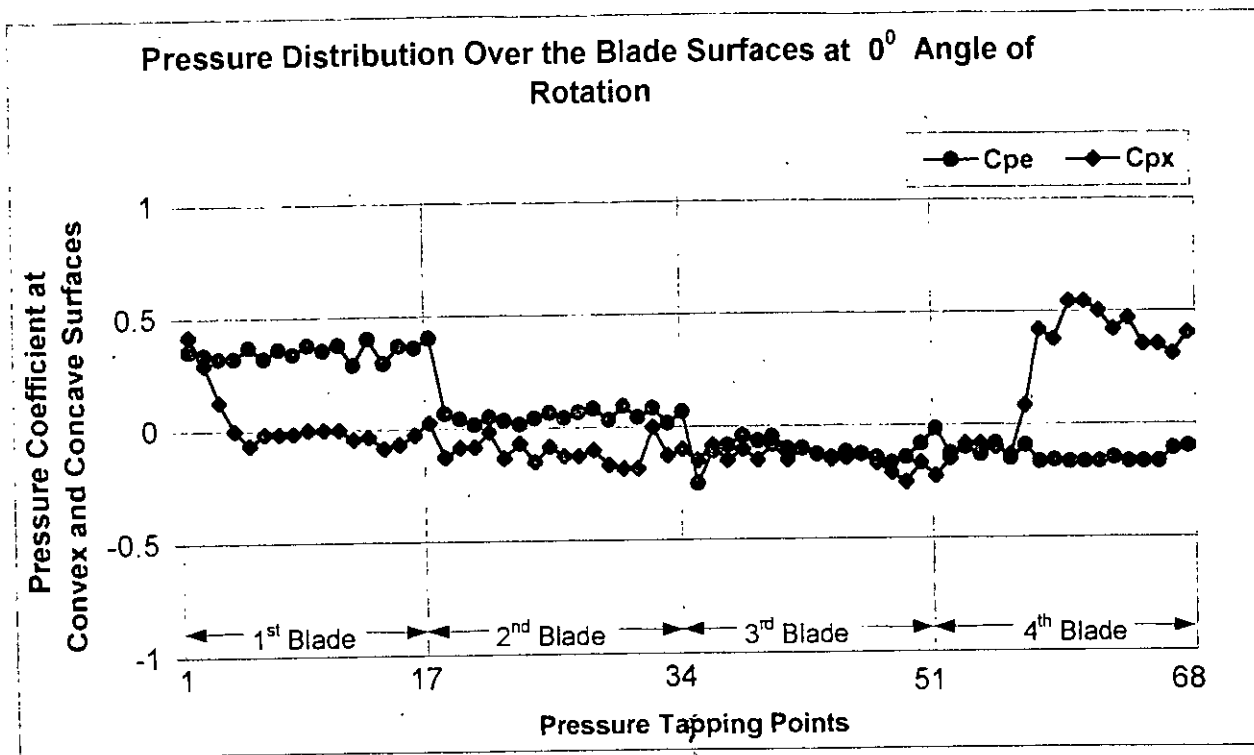
Figure 5.1(a) : Pressure Distribution over the Blade Surfaces at 0^0 Angle of Rotation
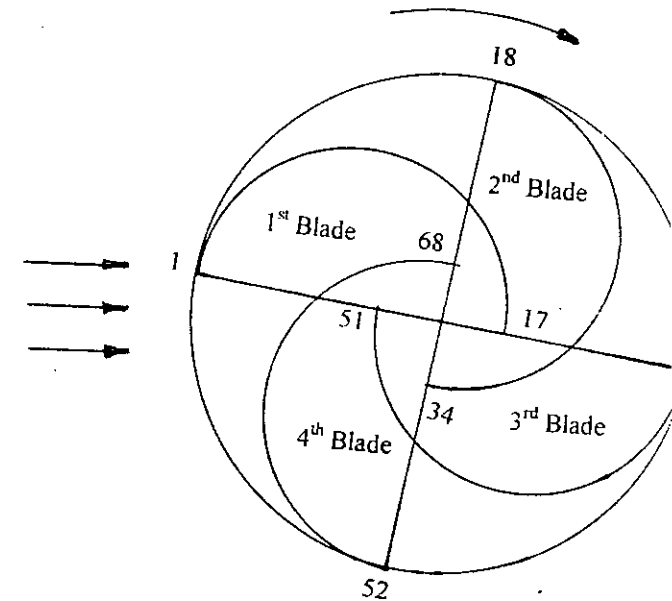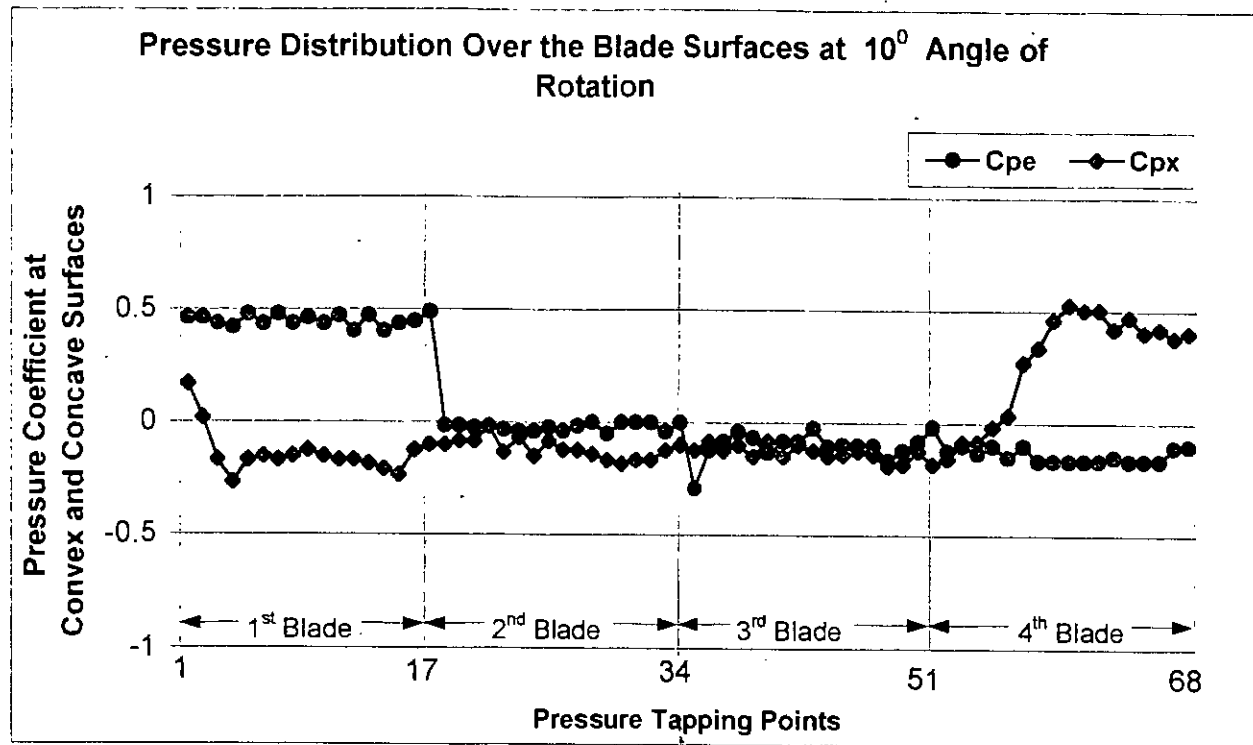
Figure 5.1(b) : Pressure Distribution over the Blade Surfaces at 10^0 Angle of Rotation
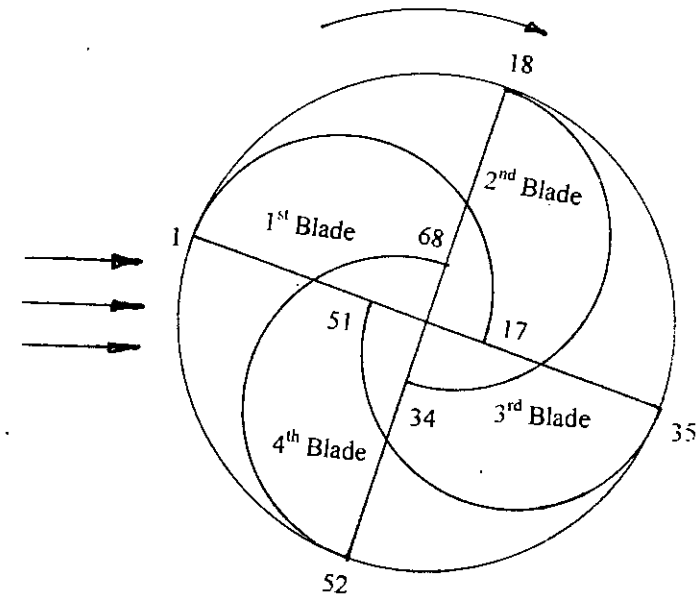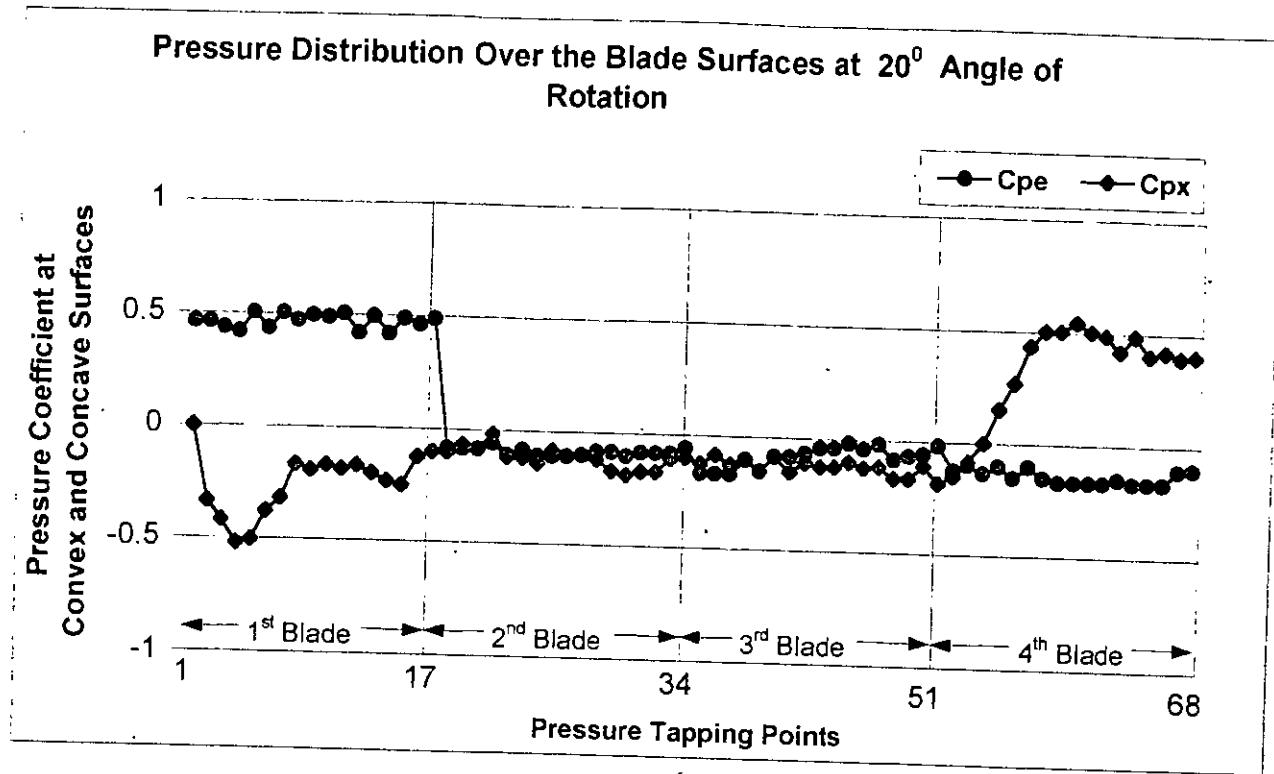
Figure 5.1(c) : Pressure Distribution over the Blade Surfaces at 20^0 Angle of Rotation
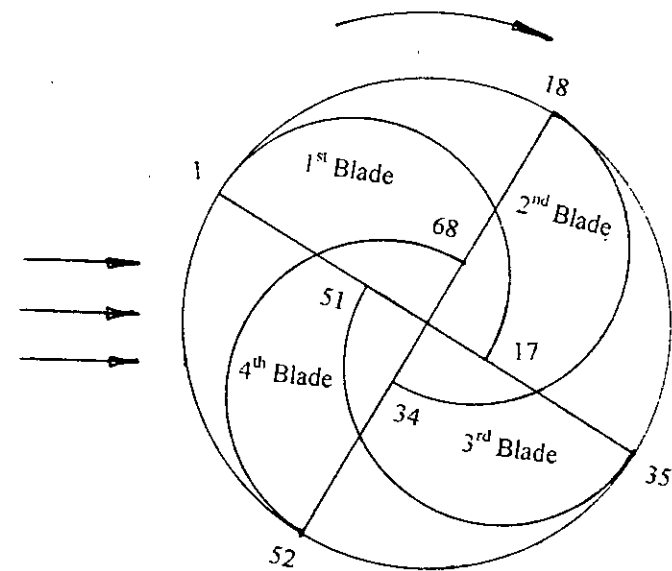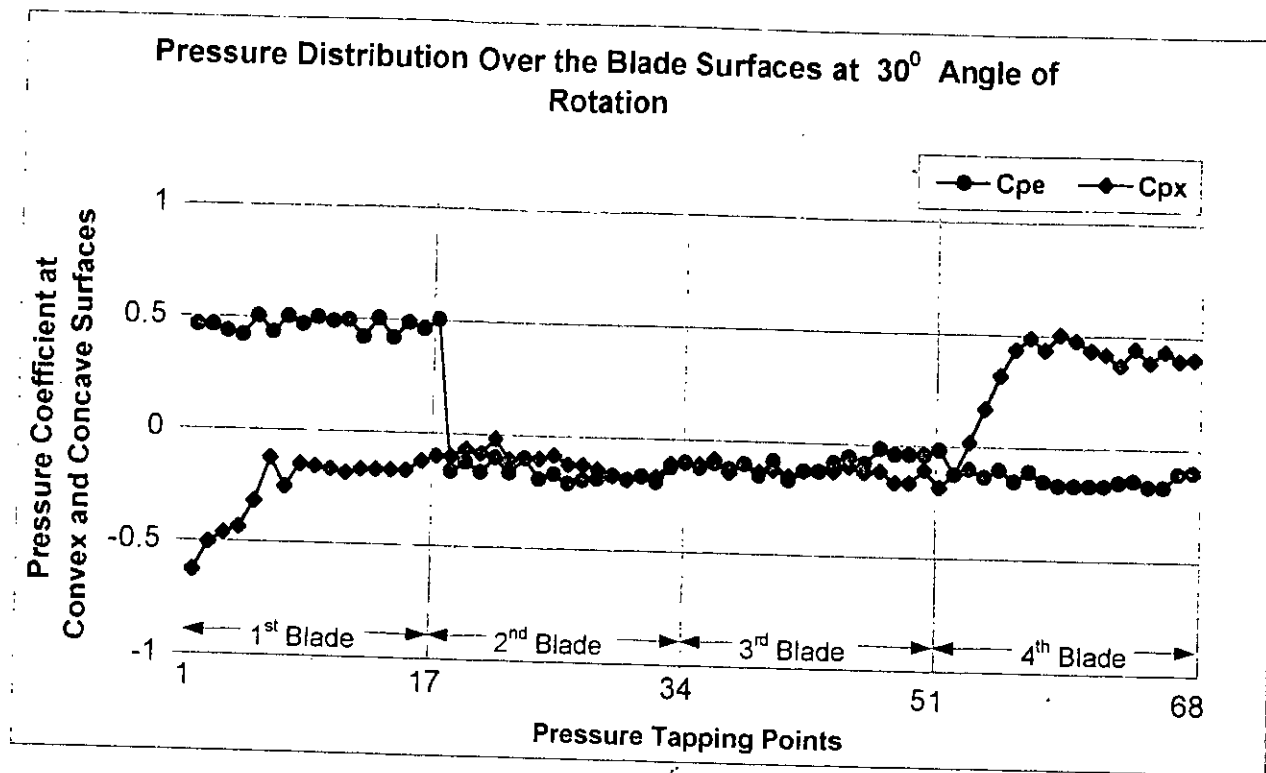
Figure 5.1(d) : Pressure Distribution over the Blade Surfaces at 30^0 Angle of Rotation
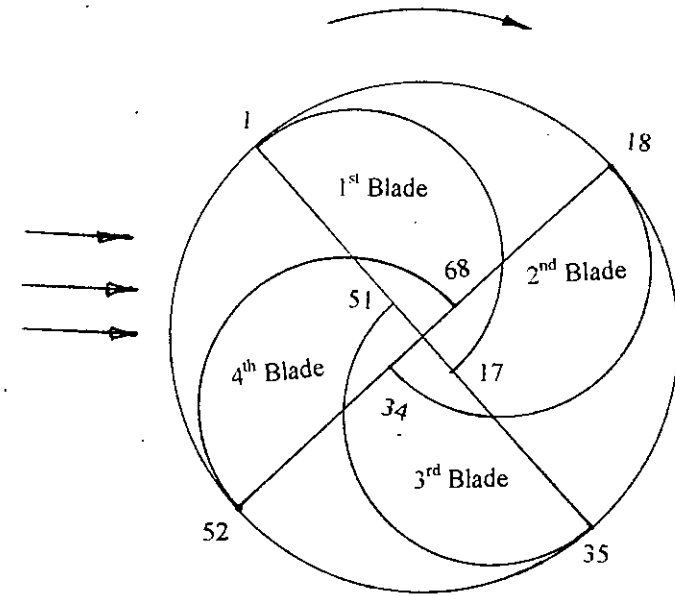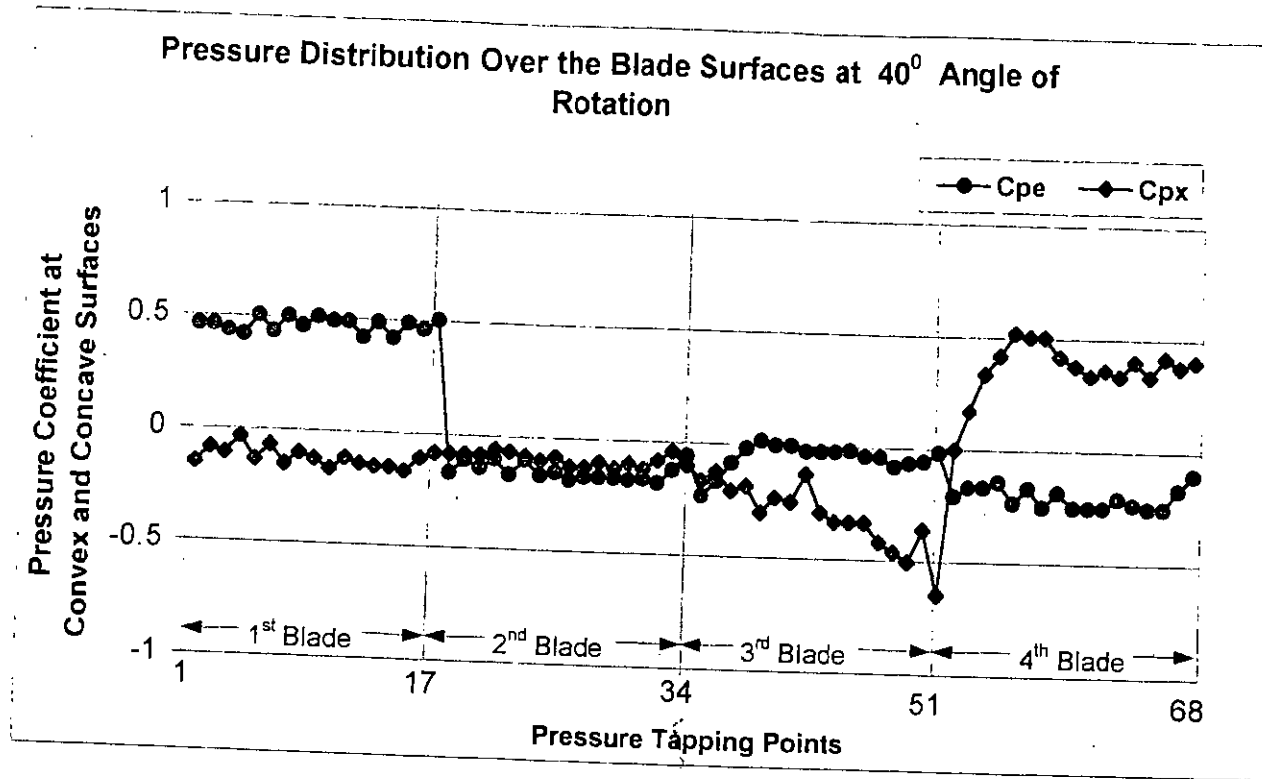
Figure 5.1(e) : Pressure Distribution over the Blade Surfaces at 40^0 Angle of Rotation
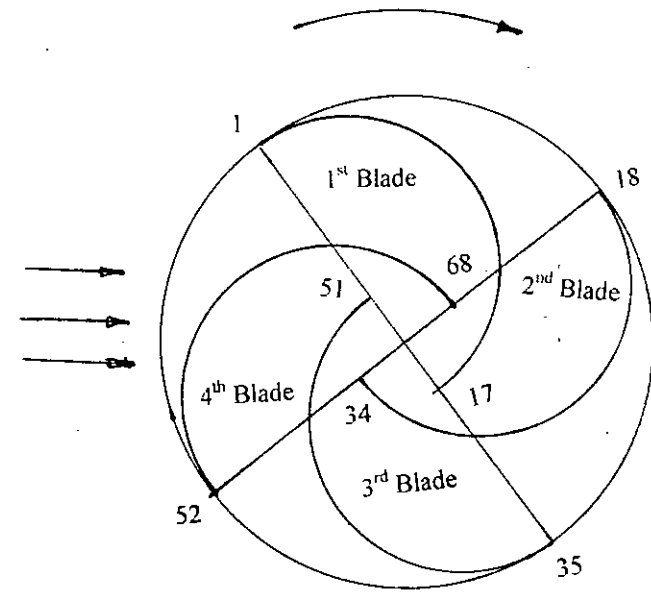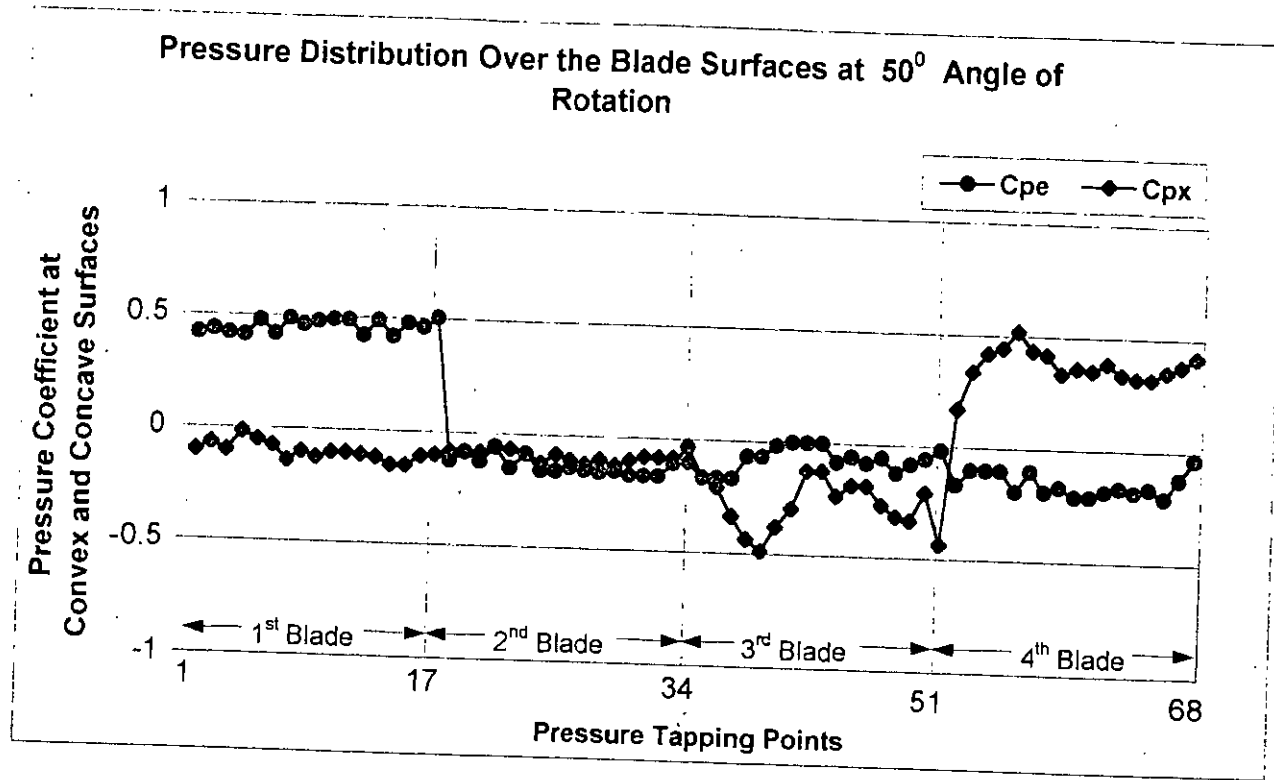
Figure 5.1(f) : Pressure Distribution over the Blade Surfaces at 50^0 Angle of Rotation
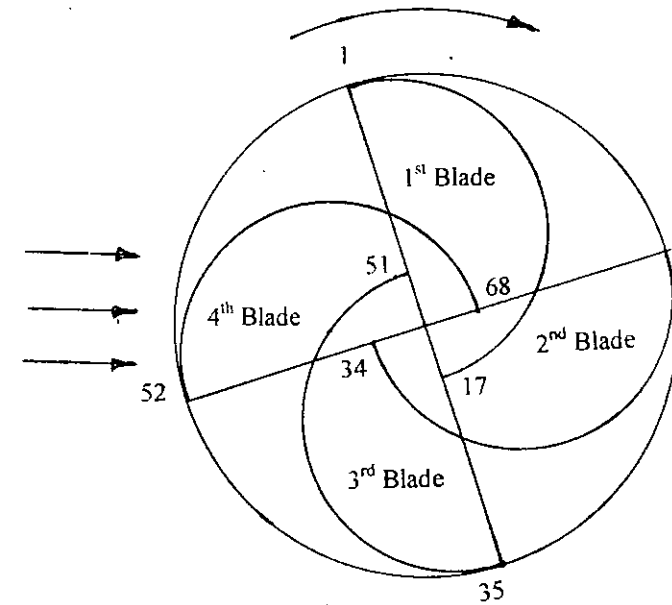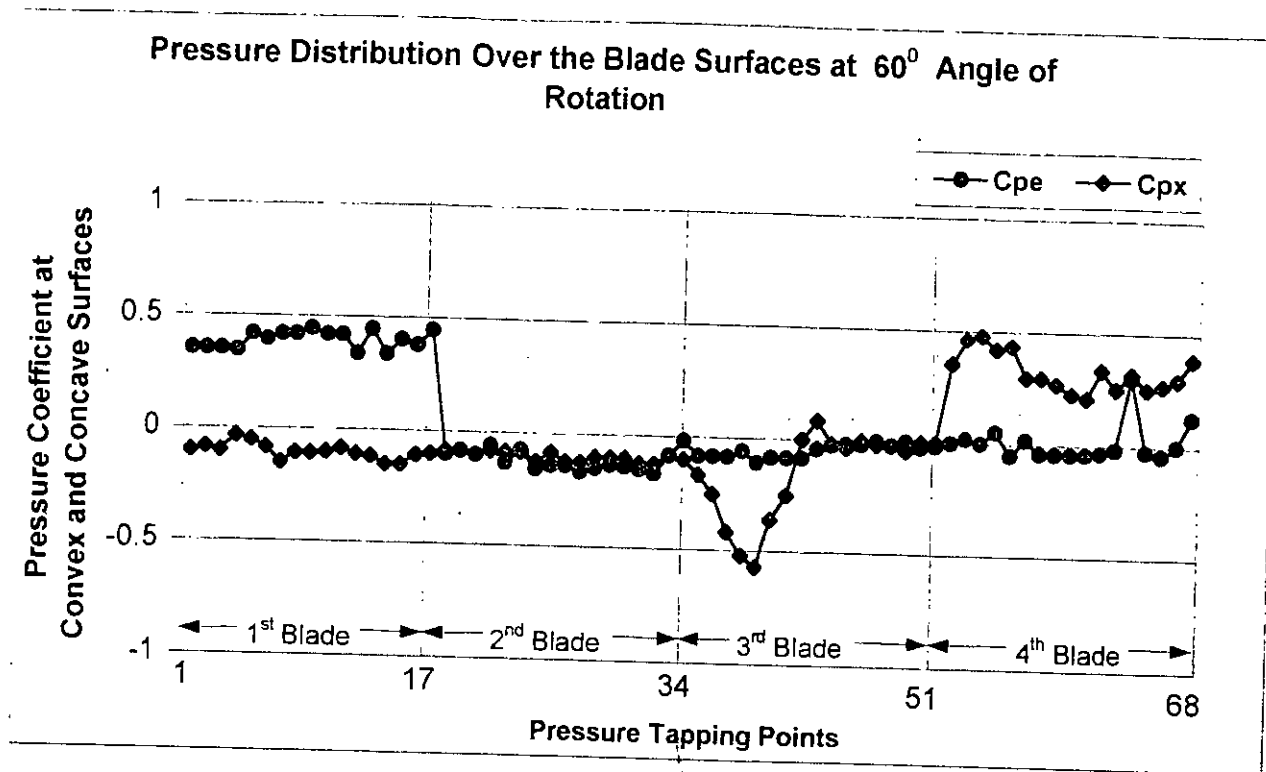
Figure 5.1(g) : Pressure Distribution over the Blade Surfaces at 60^0 Angle of Rotation
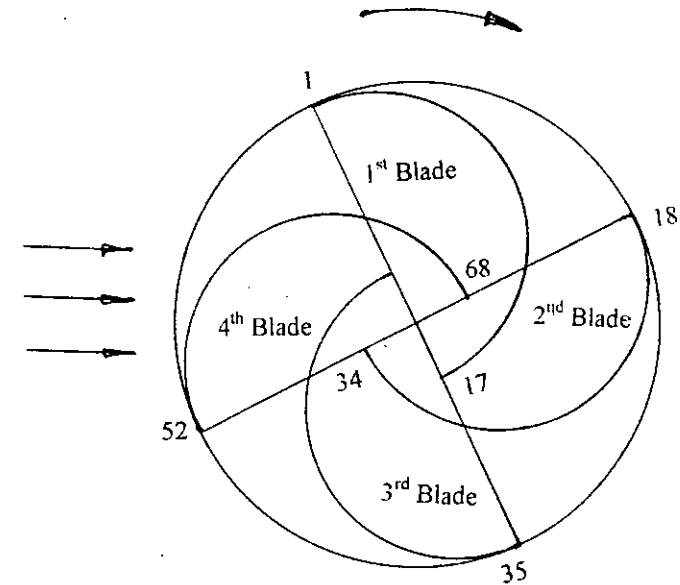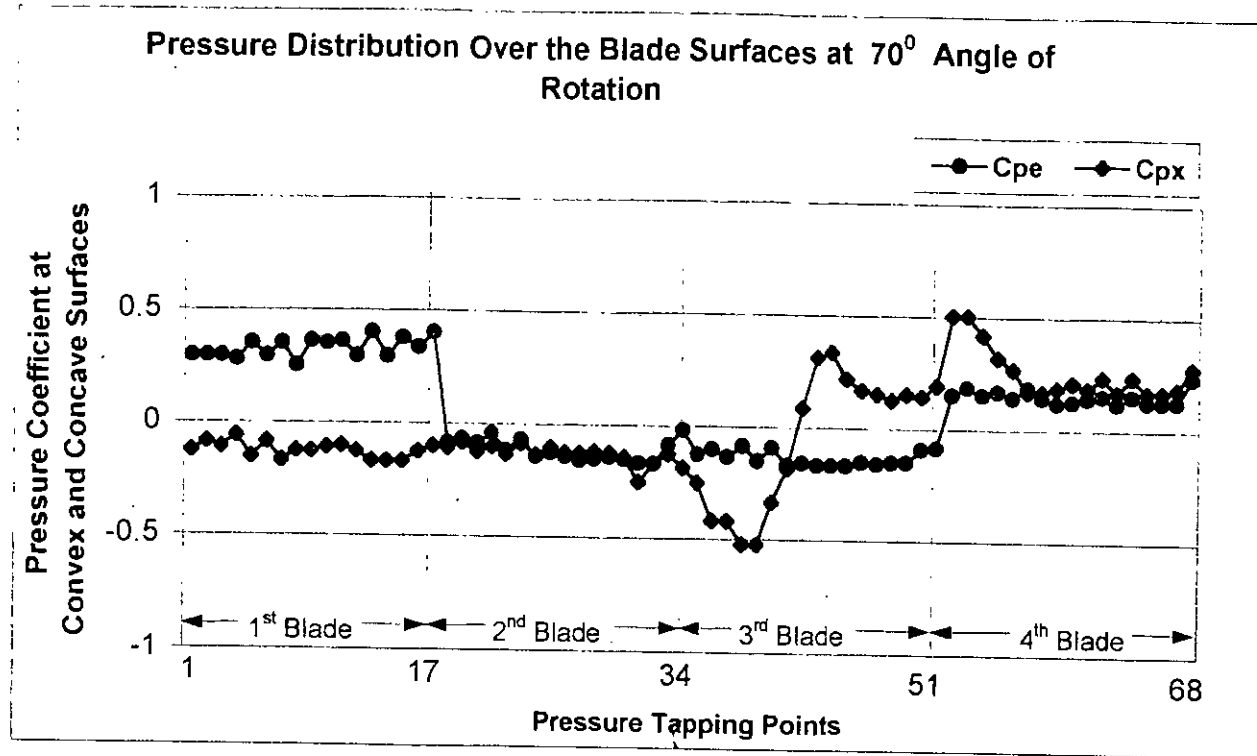
Figure 5.1(h) : Pressure Distribution over the Blade Surfaces at 70^0 Angle of Rotation
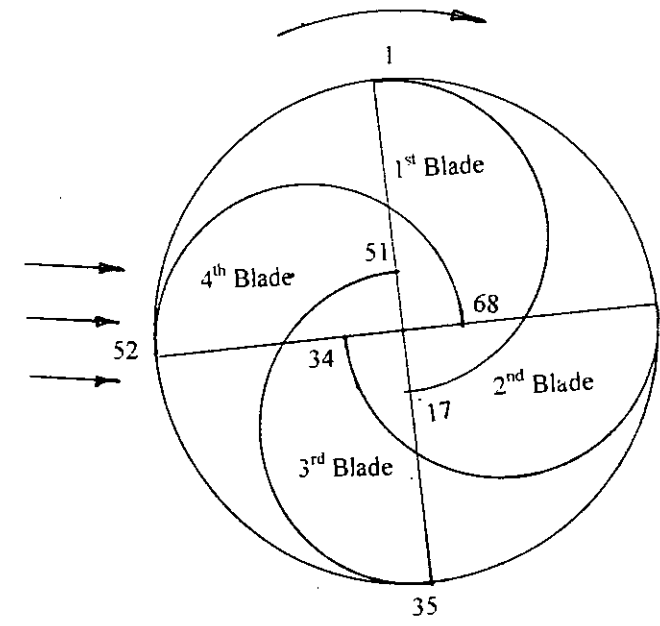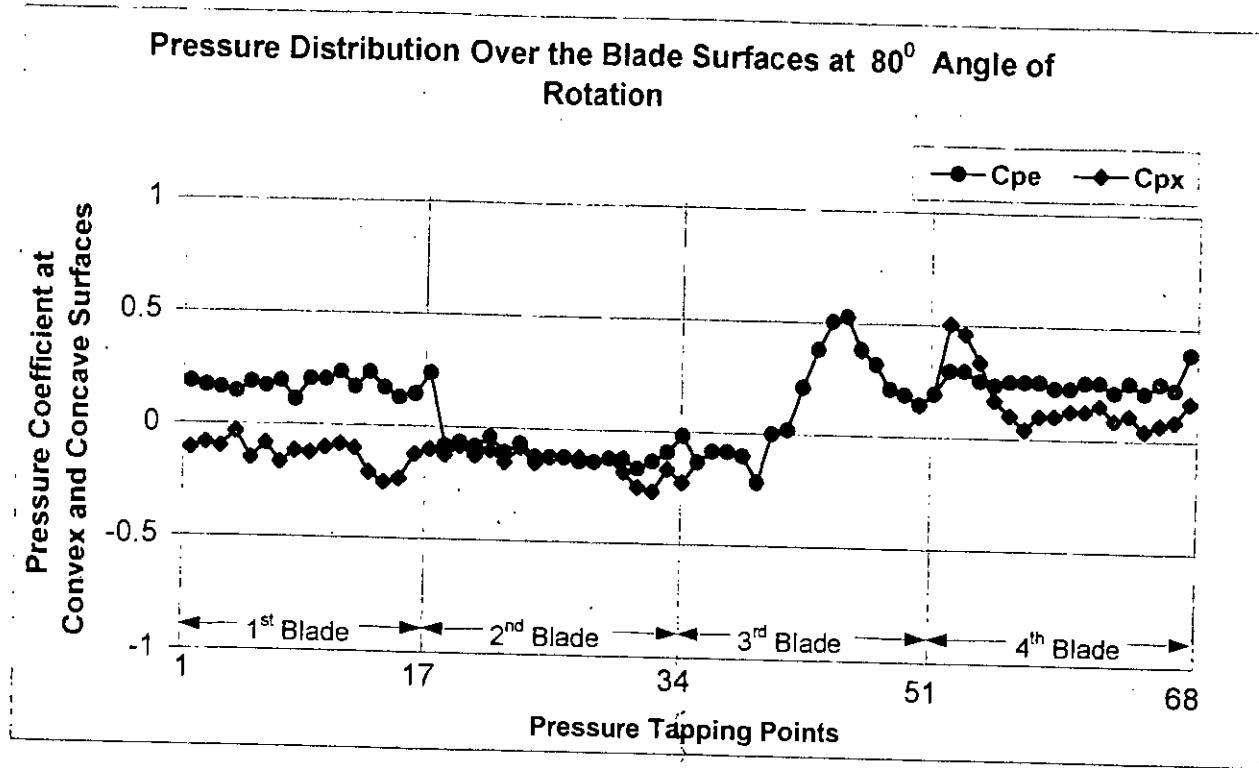
Figure 5.1(i) : Pressure Distribution over the Blade Surfaces at 80^0 Angle of Rotation

On the convex surface for the first blade the pressure drastically reduces from $\phi = 0^0$ to 40^0 and then it almost remains near to atmospheric pressure. On the second and third blade the pressure fluctuates with negative pressure coefficient, C_{px}. On the fourth blade again the pressure rapidly increases.

At $\alpha=10^0$ (Figure 5.1(b)) on the concave surface the pressure remains constant on the first and second blade. On the third and fourth blade the pressure coefficient fluctuates. On the first blade C_{pc} is positive and on the second blade the pressure remains at atmospheric level. On the third and fourth blades the C_{pc} is negative. On convex surface the C_{px} fluctuates for all the blades. It remains at negative value on the first, second and third blade. On the fourth blade the C_{px} is positive.

At $\alpha=20^0$ (Figure 5.1(c)) on the concave surface the pressure remains positive and the C_{pe} value remains at atmospheric level for all other blades. On the convex surface in the first blade the pressure coefficient is negative and in the fourth blade the C_{px} increases and remains with maximum value. For all other blades C_{pc} almost overlaps with the C_{px}. On the fourth blade the C_{px} is positive.

At $\alpha=30^0$ (Figure 5.1(d)) on the concave surface the pressure remains positive on first blade and the C_{pe} value remains at atmospheric level for all other blades. On the convex surface of the first blade the pressure coefficient is extremely negative for $\phi = 0^0$ and then gradually increases. At $\phi = 50^0$, the C_{px} increases and remains at atmospheric level. For all other blades C_{pc} overlaps the C_{px} except on the fourth blade. On the fourth blade C_{px} is positive.

At $\alpha=40^0$ (Figure 5.1(e)) on the concave surface the C_{pc} remains positive on the first blade and for all other blades C_{pe} is almost at atmospheric level. On the convex surface the pressure coefficient is nearly at atmospheric level on the first

and second blades. The C_{px} is negative on the third blade. On the fourth blade C_{px} increases and remains at maximum value.

At $\alpha= 50^0$ (Figure 5.1(f)) C_{pc} is positive on the first blade and for all other blades the C_{pc} remains nearer to atmospheric value. On the convex surface for the first and second blades, the C_{px} is nearer to atmospheric level. On the third blade C_{px} is negative and it fluctuates. On the fourth blade the C_{px} is maximum with positive values.

At $\alpha= 60^0$ (Figure 5.1(g)) C_{pc} is positive only on the first blade and for all other blades the C_{pc} remains nearer to atmospheric value. On the convex surface for the first and second blades, the C_{px} is nearer to atmospheric value but it is negative in the third blade. On the fourth blade the C_{px} is positive.

At $\alpha= 70^0$ (Figure 5.1(h)) C_{pc} is as it was at $\alpha= 60^0$ for the first, second and third blades and in the fourth blade C_{pc} is positive. On the convex surface C_{px} variates on the third and fourth blades. The peak positive value of C_{px} is obtained on the fourth blade.

At $\alpha= 80^0$ (Figure 5.1(i)) C_{pc} is positive in the first, third and fourth blade. But on the second blades C_{pc} is positive. In the convex surface, C_{px} is negative in the first and second blades. In the third blade C_{px} is maximum and in the fourth blade C_{px} is negative.

5.2.2 Normal Drag Coefficient

Normal drag coefficient, C_n of an individual blade effect of four-bladed Savonius rotor and three-bladed Savonius rotor [1] are shown in figure 5.2(a) for different rotor angles.

For the flow over the four-bladed system, considering the first blade the normal drag coefficient $C_n(\alpha)$ increases with the increase of the rotor angle from $\alpha=0^0$ to 20^0. From this point the drag coefficient C_n decreases with the increase of rotor angle α, up to 90^0. Between $\alpha=0^0$ to $\alpha=90^0$, drag coefficient $C_n(\alpha)$, is positive for a rotor angle of 0^0 to 60^0 and reaches its maximum value at $\alpha=20^0$. At $\alpha=100^0$, the value of C_n increases, after which it remains constant till $\alpha=150^0$. Between $\alpha=150^0$ to $\alpha=160^0$, the value of C_n drops slightly and then remains constant till $\alpha=180^0$. The C_n decreases between $\alpha=180^0$ to $\alpha=210^0$. From $\alpha=210^0$, C_n increases sharply till $\alpha=250^0$. From $\alpha=260^0$ to $\alpha=320^0$, C_n falls sharply and becomes negative. From then onwards, the value of C_n increases till $\alpha=340^0$. At $\alpha=350^0$, C_n falls slightly again it rises at 360^0. Between $\alpha=220^0$ and $\alpha=300^0$, C_n is responsible for maximum torque production. Negative C_n is available between $\alpha=60^0$ to 90^0, $\alpha=160^0$ to 210^0 and $\alpha=310^0$ to 350^0.

For the flow over the three-bladed Savonius Rotor [1], for the first blades, normal drag coefficient $C_n(\alpha)$ increases with the increase of rotor angle from $\alpha=0^0$ to 60^0 and then decreases with the increase of the rotor angle α, up to 120^0. It remains constant from $\alpha=120^0$ to 220^0. From $\alpha=230^0$, drag coefficient increases till $\alpha=260^0$. C_n decreases from $\alpha=270^0$ to 340^0. At $\alpha=340^0$, C_n increases and becomes zero at $\alpha=350^0$.

Normal drag coefficient, C_n with four blades' combined effect and three blades' combined effect [1] are shown in the figure 5.2(b).

For four-bladed system C_n increases steadily from $\alpha=0^0$ to 20^0. It decreases drastically at $\alpha=30^0$. It then increases at $\alpha=40^0$, again it falls at $\alpha=50^0$. It then remains constant, rising once at $\alpha=70^0$. The maximum value is obtained at 20^0 angle of rotation. The system repeats from $\alpha=90^0$ to $\alpha=170^0$, $\alpha=180^0$ to $\alpha=260^0$ and $\alpha=260^0$ to $\alpha=350^0$.

In consideration to the combined effect of the three blades of a three-bladed Savonius rotor [1], normal drag coefficient C_n increases with increase of the rotor angle ranging from $\alpha=0^0$ to 60^0 and after that it decreases with the increase of the rotor angle up to $\alpha=90^0$. From $\alpha=90^0$ C_n increases till 110^0. The system repeats from $\alpha=120^0$ to $\alpha=230^0$ and from $\alpha=240^0$ to $\alpha=350^0$.

Comparing the combined effect of four-bladed system with that of the three-bladed system, one finds that in the three-bladed system the normal drag coefficient rises and falls smoothly. On the other hand, in the four-bladed system the C_n rises and falls sharply. But the four-bladed system produces more normal drag coefficient compared to that of a three-bladed system.
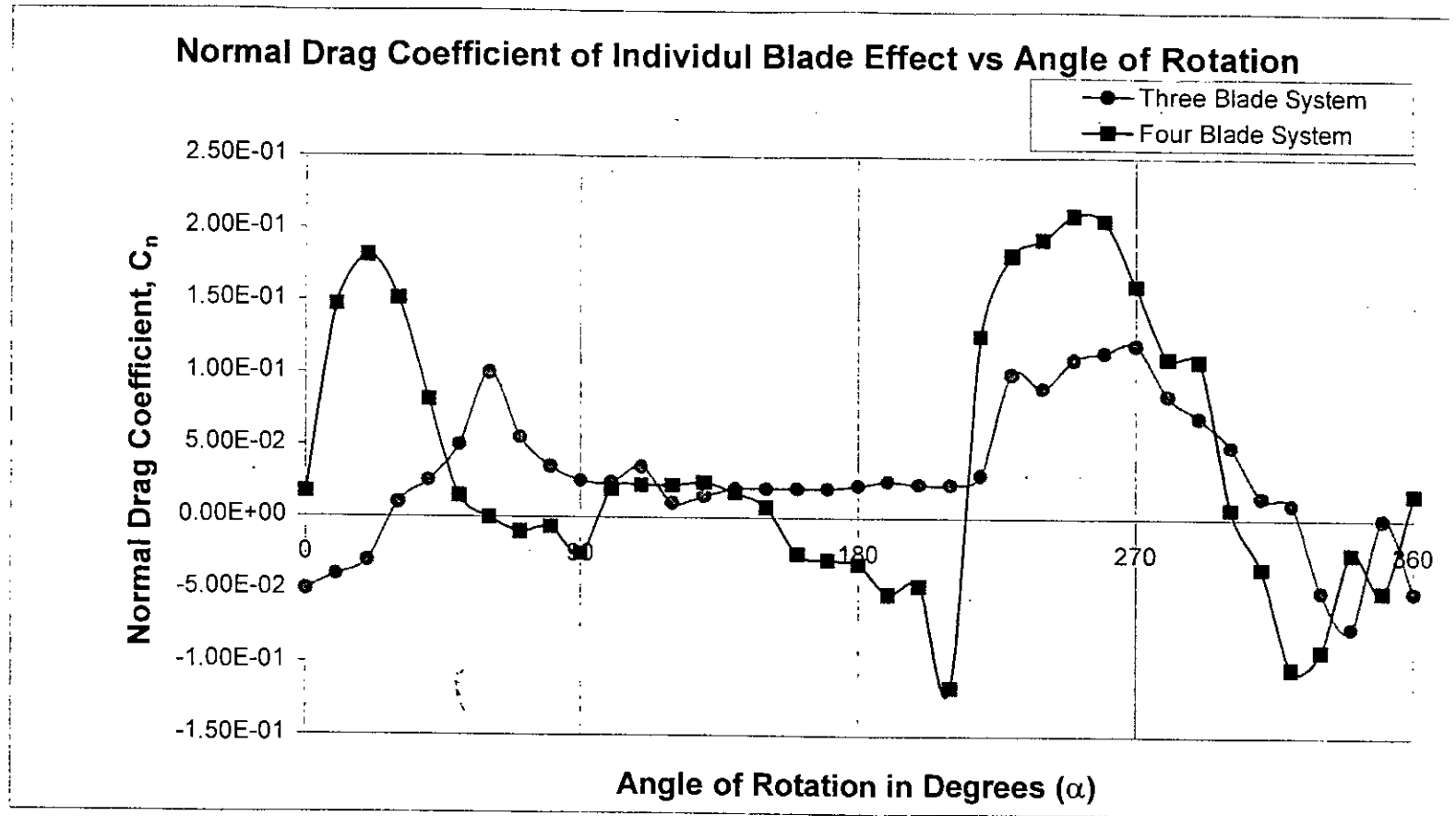
Figure 5.2(a) : Normal Drag Coefficient of Individual Blade Effect
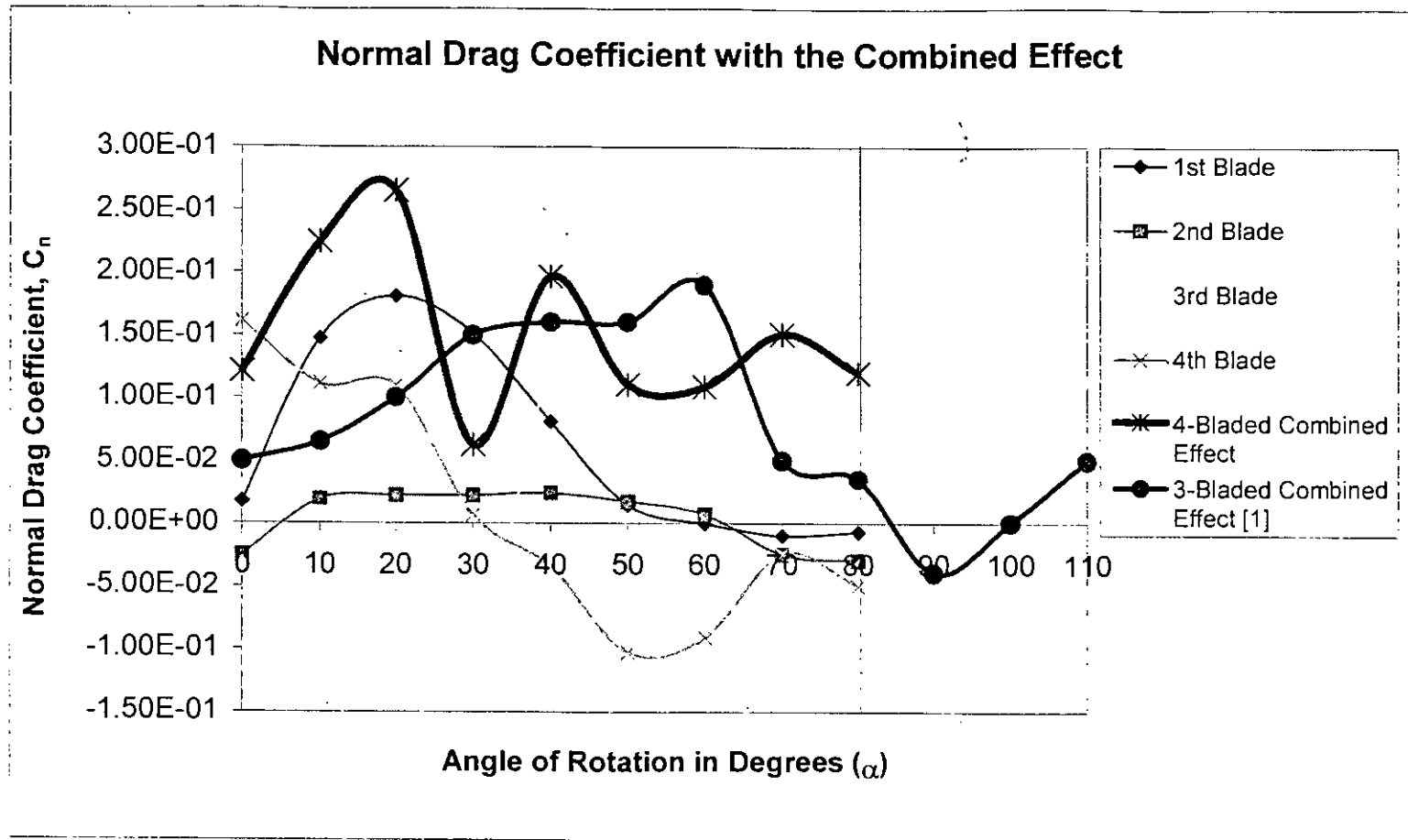
Figure 5.2(b)   :Normal Drag Coefficient with Combined Blade Effect

5.2.3 Tangential Drag Coefficient

Tangential drag coefficient, C_t with individual blade effect for both three-bladed [1] and four-bladed Savonius rotor are shown in figure 5.3(a) for different rotor angles.

For the four-bladed system, on the first blade, the tangential drag coefficient, C_t increases with the increase of rotor angle from $\alpha=0^0$ to $\alpha=20^0$. From this point the C_t decreases up to $\alpha=130^0$. From $\alpha=130^0$ to $\alpha=200^0$, the value is constant and nearly zero. From $\alpha=210^0$, the tangential drag increases till $\alpha=220^0$. The drag coefficient then decreases from $\alpha=220^0$ to $\alpha=310^0$. It increases from 320^0 to 360^0. The negative thrust is produced from $\alpha=270^0$ to $\alpha=340^0$. Finally, it produces positive thrust at $\alpha=350^0$. Maximum positive thrust is available between 0^0 to 110^0 angle of rotation and maximum negative thrust is available from 270^0 to 340^0 angle of rotation.

For three-bladed system [1] tangential drag coefficient, C_t increases with the increase of rotor angle from $\alpha=10^0$ to 60^0. It remains constant from 60^0 to 110^0. At 120^0, C_t decreases. It remains positive from 130^0 to 230^0. It decreases from 240^0 to 340^0 and then increases up to $\alpha=360^0$.

By comparing C_t of three-bladed system [1] with C_t of four bladed system, one can observe that the value of C_t for four-bladed system is greater. For three- bladed system positive thrust is obtained from 20^0 to 240^0. Negative thrust is obtained from 240^0 to 360^0. For four-bladed system positive thrust is obtained from 0^0 to 110^0 and from 190^0 to 260^0. Negative thrust is obtained from 270^0 to 360^0.
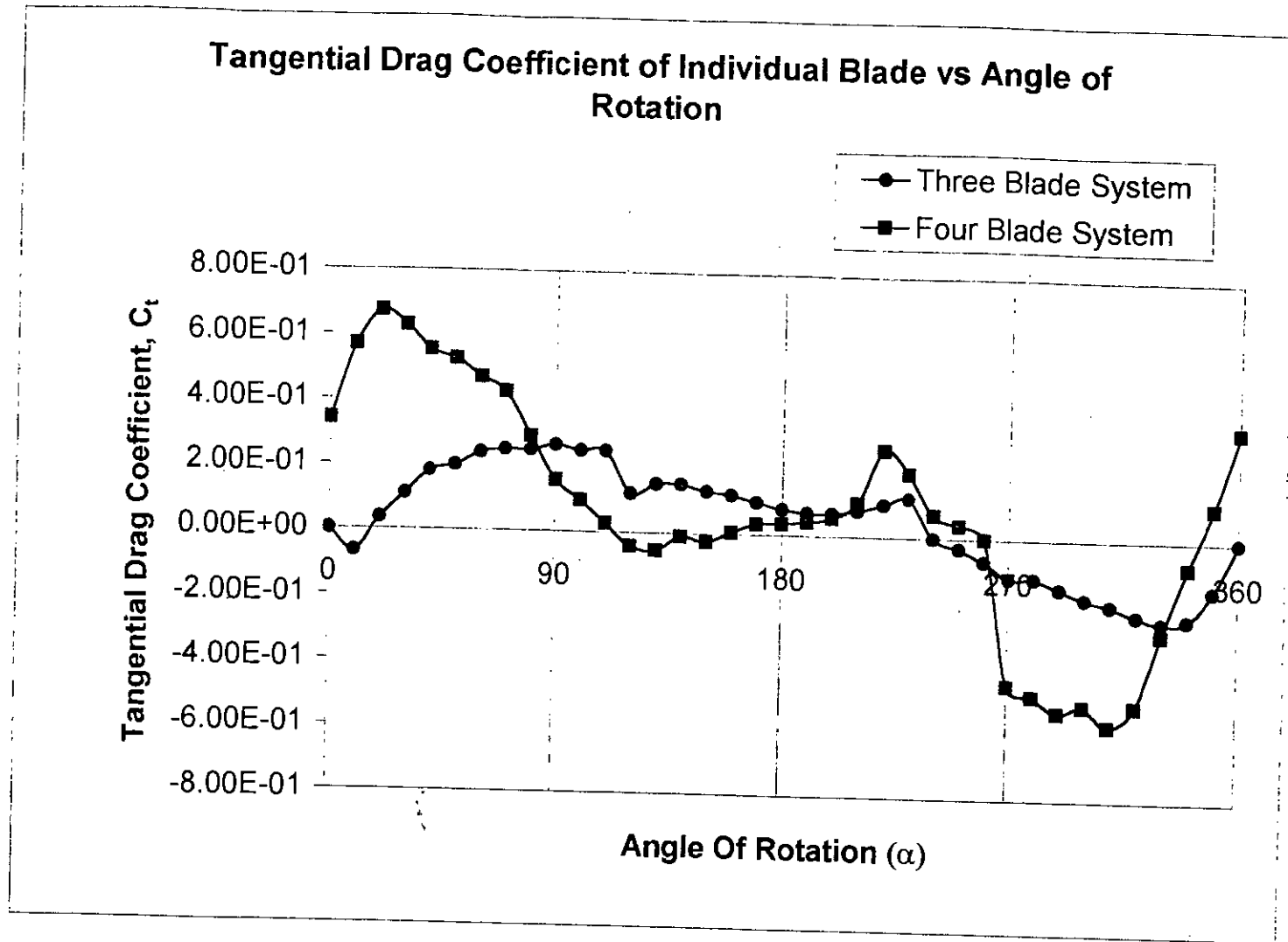
Figure 5.3(a) :Tangential Drag Coefficient of Individual Blade Effect
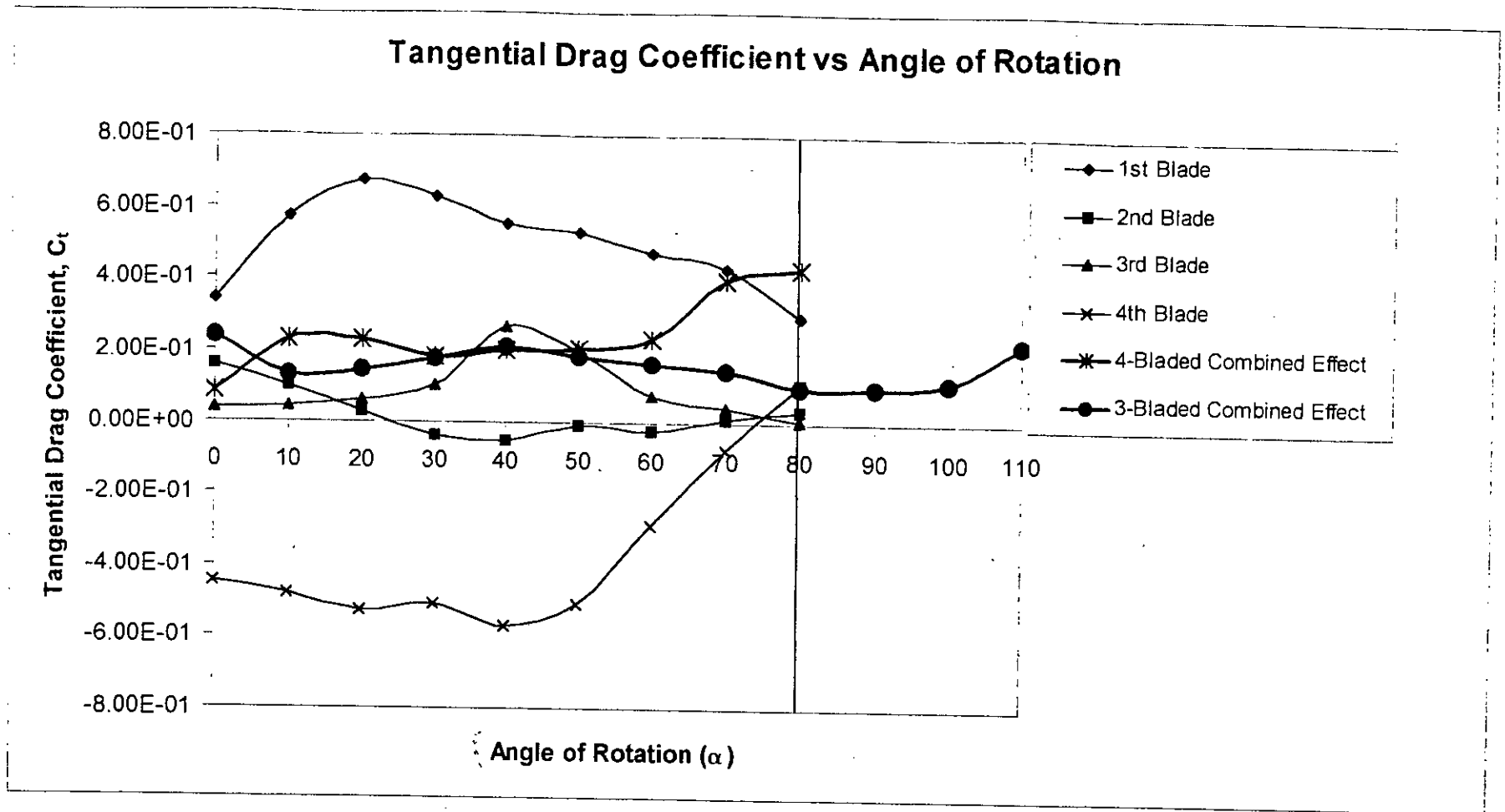
Figure 5.3(b) : Tangential Drag Coefficient of Individual Blade Effect

Tangential drag coefficient, C_t with three [1] and four blades, the combined effect is shown in figure 5.3(b) for different rotor angles.

The drag coefficient increases for $\alpha=0^0$ to 10^0 and remains constant till $\alpha=20^0$ and decreases at $\alpha=30^0$. From $\alpha=40^0$ to 60^0 the value remains constant. The tangential drag coefficient rapidly increases from $\alpha=60^0$ to $\alpha=80^0$. For rotor angle, $\alpha=90^0$ to $\alpha=170^0$, $\alpha=180^0$ to $\alpha=260^0$ and $\alpha=270^0$ to $\alpha=350^0$ the values repeat in the same pattern.

For the three-bladed system with three blades combined effect [1], one can observe that little decrease and increase occur in the tangential drag coefficient, C_t with respect to the increase of rotor angle. C_t decreases from $\alpha=0^0$ to $\alpha=10^0$ and increases from 10^0 to 40^0. C_t again decreases from $\alpha=40^0$ to $\alpha=80^0$ and remains constant from 80^0 to 100^0. It increases from $\alpha=100^0$ to $\alpha=110^0$. The system repeats from $\alpha=120^0$ to 230^0 and from $\alpha=240^0$ to 350^0.

By comparing four blades combined effect with three blades combined effect one can observe that four-bladed rotor shows better thrust effect than that of three-bladed rotor. However, the thrust pattern is not as smooth in case of four-bladed rotor than that in three-bladed rotor.

5.2.4 Torque Coefficient

Torque coefficient, C_q with individual blade effect is shown for both three-bladed [1] and four- bladed rotors in figure 5.4(a) for different rotor angles. The nature of torque coefficient, C_q is exactly similar to that of the normal drag coefficient, C_n with individual blade effect as shown in figure 5.2(a), which is responsible for producing torque. The only difference between the two graphs is that the value of torque coefficient is smaller than normal drag coefficient.

For the flow over the four-bladed system, on the first blade the torque coefficient C_q increases with the increase of the rotor angle from $\alpha=0^0$ to 20^0. From this point the torque coefficient C_q decreases with the increase of rotor angle, up to 90^0. Between $\alpha=90^0$ to 100^0, C_q increases, after which it remains constant till $\alpha=150^0$. Between $\alpha=150^0$ to 160^0, the C_q drops slightly and then again remains constant till $\alpha=180^0$. The C_q decreases between $\alpha=180^0$ to 210^0. From $\alpha=210^0$, C_q increases sharply till $\alpha=250^0$. At $\alpha=250^0$, C_q is maximum. Between $\alpha=260^0$ to 320^0, the C_t falls sharply and becomes negative. From then onwards, the C_q increases till $\alpha=340^0$.

For the flow over the three-bladed Savonius Rotor [1], for the first blade, torque coefficient C_q increase with the increase of rotor angle from $\alpha =0^0$ to 60^0 and then decreases with the increase of the rotor angle α, up to 90^0. It remains constant from $\alpha =90^0$ to 210^0. C_q increases from 220^0 to 270^0, again it falls from 270^0 to 340^0. At 340^0, C_q increases till $\alpha = 350^0$.

Torque coefficient, C_q with four blades combined effect and three blades combined effect [1] are shown in the figure 5.4(b). This figure is also similar to figure 5.2(b).

Torque Coefficient for Individual Blade with Different Rotor Angle
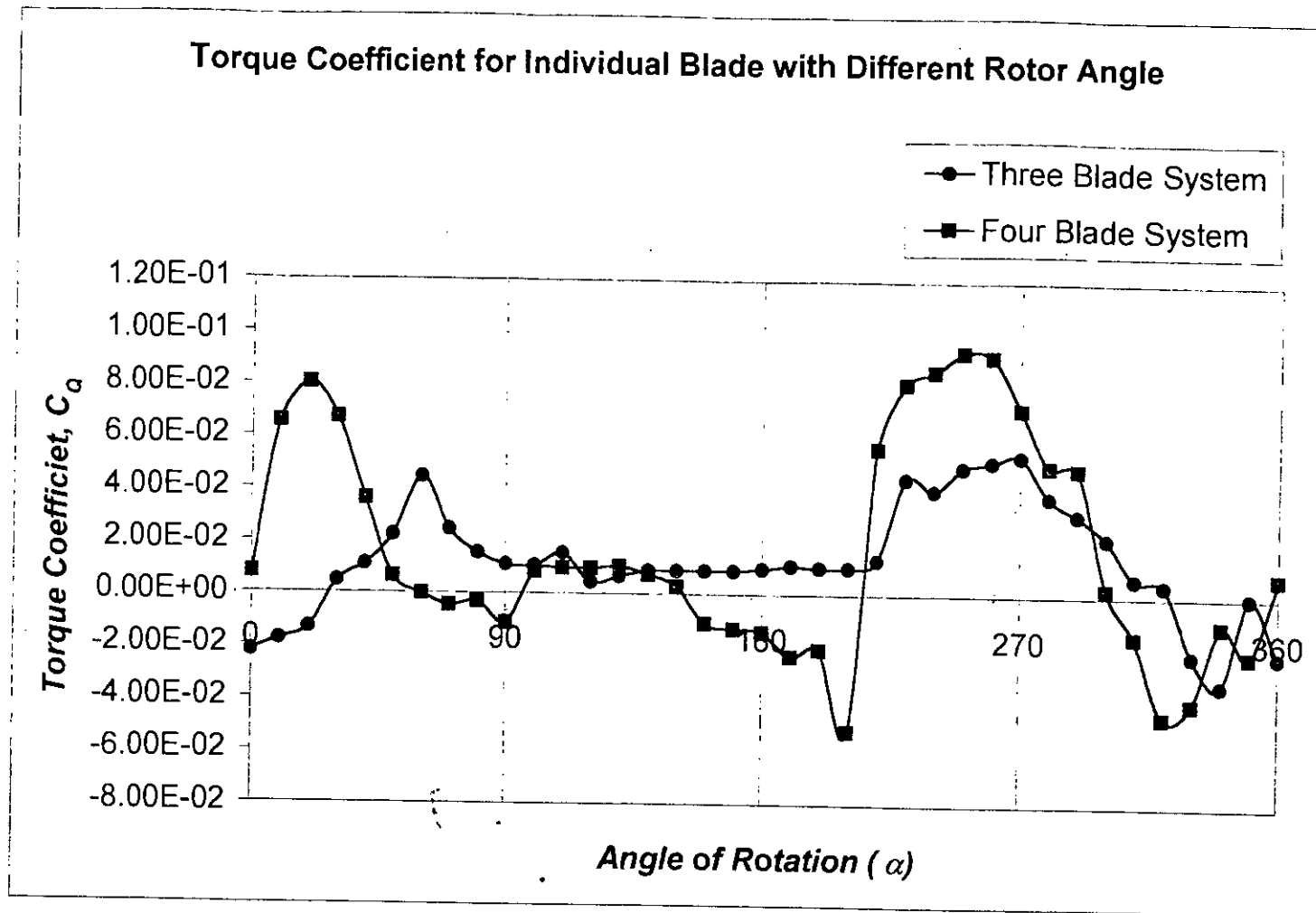
Figure 5.4(a)   :Torque Coefficient with Individual Blade Effect
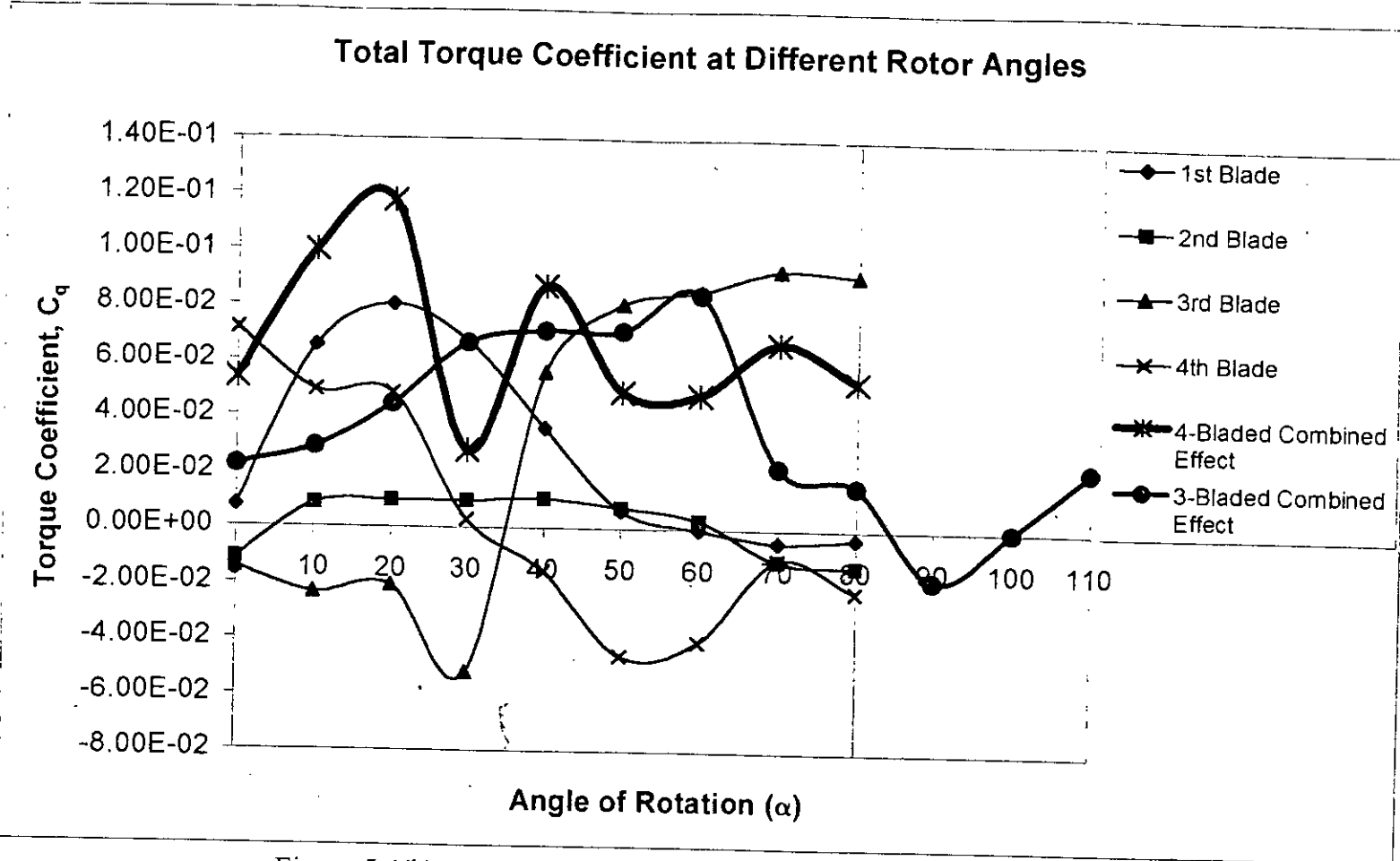
Figure 5.4(b) :Total Static Torque Coefficient at Different Rotor Angles

For four bladed system C_q increases steadily from $\alpha = 0^0$ to 20^0. After $\alpha = 20^0$, it decreases drastically till $\alpha = 30^0$. It then increases again till $\alpha = 40^0$, again it falls at $\alpha = 50^0$. It then remains constant, rising once at $\alpha = 70^0$. The maximum value is obtained at 30^0 angle of rotation. The system repeats from $\alpha = 90^0$ to 170^0, $\alpha = 180^0$ to 260^0 and $\alpha = 260^0$ to 350^0.

In consideration to the combined effect of the three blades of a three bladed Savonius rotor [1], torque coefficient C_q increases with increase of the rotor angle ranging from $\alpha = 0^0$ to 60^0 and after that it decreases with the increase of the rotor angle up to $\alpha = 90^0$. From $\alpha = 90^0$ to 110^0, C_q increases. The System repeats from $\alpha = 120^0$ to 230^0 and from $\alpha = 240^0$ to 350^0.

Comparing the combined effect four bladed system with that of the three bladed system, one finds that in the three bladed system the production of torque coefficient rises and falls smoothly. On the other hand, the C_q rises and falls drastically in the four bladed system. But the four bladed system produces more torque coefficient compared to that of a three bladed system.

5.3 Dynamic Aerodynamic Characteristics

5.3.1 Prediction of Power Coefficient

The predicted power coefficients, C_P for different tip speed ratios, λ are shown in figure 5.5 along with the measured data of Rahman [1], Ogawa and Yoshida [8] and Islam et al [12]. The overlap ratio considered in this study is same as the rotor of Rahman, Ogawa and Yoshida, Islam et al. The predicted power coefficient matches with the result of Rahman [1] but it deviates with the result of polynomial prediction by Islam at el [12] and Ogawa and Yoshida [8] only in magnitude. The natures of curve for all the cases are similar.

Comparison of power coefficients for different tip speed ratios for different Reynolds number are shown in figure 5.6. It is observed that the power coefficient increases with the increase of Reynolds number.
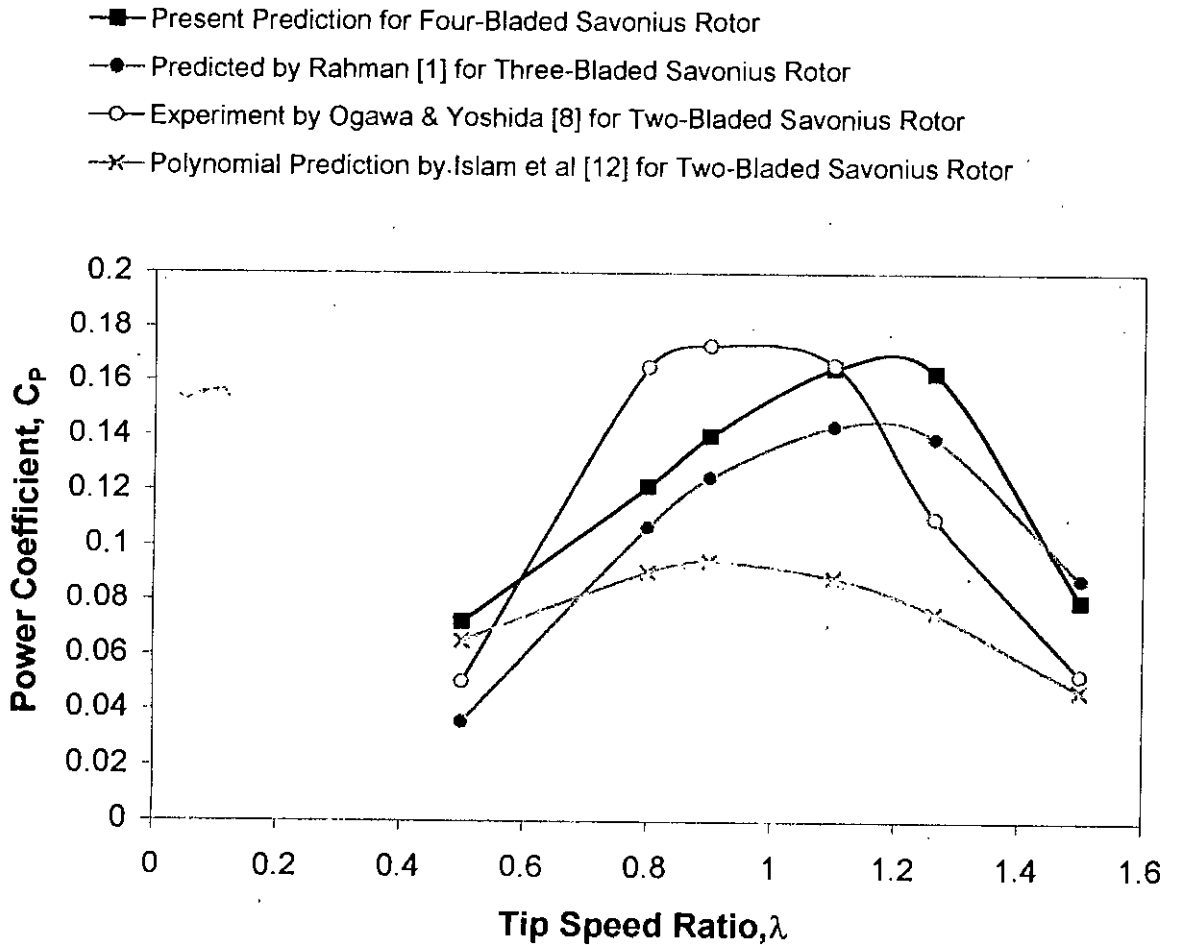
Figure 5.5 : Power Coefficient for Different Tip Speed Ratio
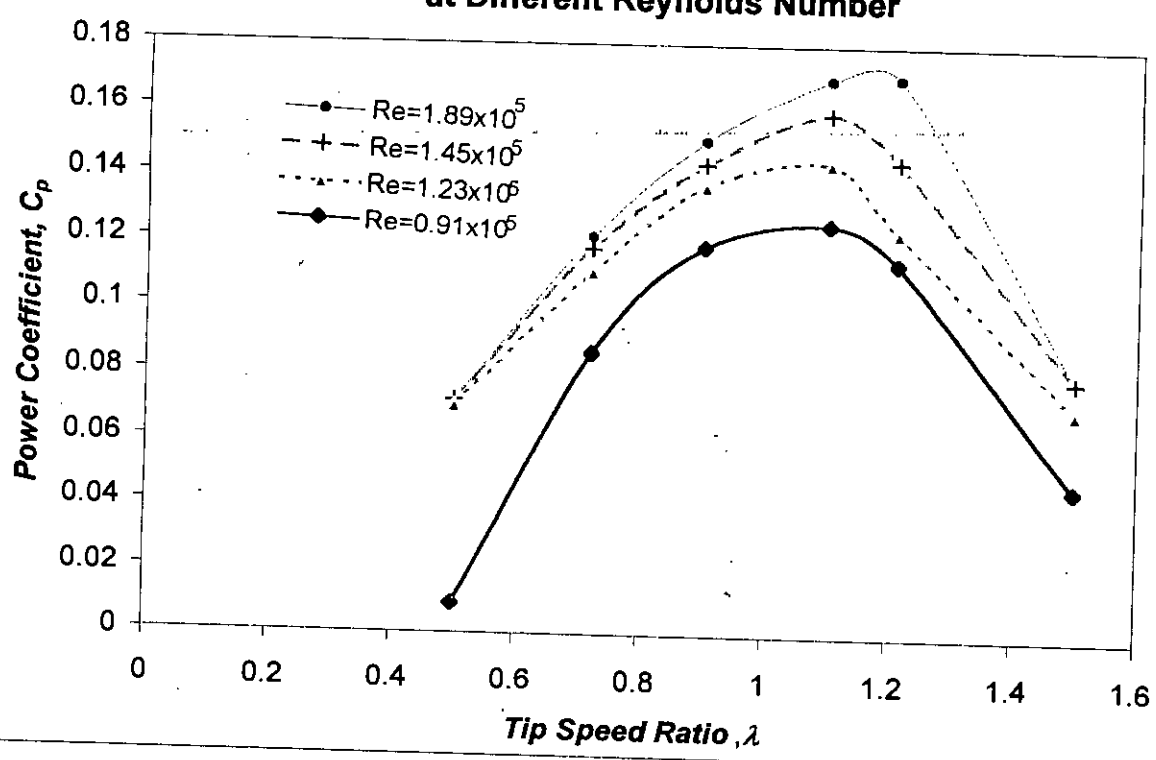
Figure 5.6 :Comparisons of C_P vs λ for different Reynolds number

CHAPTER 6
CONCLUSIONS AND RECOMMENDATIONS

Chapter-6

CONCLUSIONS AND RECOMMENDATIONS

6.1 Introduction

This chapter presents the conclusions drawn from the experimental investigation of flow over the four-bladed Savonius rotor. The scope of extension and development of the present study are also included in this chapter.

6.2 Conclusions

The present study concerns the pressure distribution over the four blades of the four-bladed Savonius rotor on both the convex and the concave surfaces at different angles of rotation. Three computer programming were performed using Microsoft Fortran to calculate forces experienced by the rotor blades, drag coefficients and torque coefficients by using raw data of pressure from the experiment. In the dynamic prediction part of this research work, the power coefficient (C_P) was calculated using the value of the component of relative velocity V_w, along the free stream velocity U_0 and the static normal drag coefficient C_n for different tip speed ratio, λ. From the study, analysis and results of this research work, the following conclusions can be made:

1.   From the pressure distribution on both the concave and convex surfaces of the four blades at different angle of rotation, it is found that the variation of pressure in the concave surfaces is almost constant for different angle of rotation. However for a particular angle of rotation, the pressure coefficient in the concave surfaces varies for different blades. For any given angle of rotation for a particular

blade the pressure coefficient in the concave surface is almost constant. For the first blade C_{pc} is positive and for all other cases C_{pc} is nearly zero or having little negative values.

The pressure coefficient varies significantly in the convex surfaces. For the first blade from 0^0 to 20^0 angle of rotation the pressure coefficient in the convex surfaces C_{px} decreases. So the pressure difference in the convex and concave surfaces increases. From 40^0 to 70^0 angle of rotation the pressure coefficient in the convex surfaces C_{px} is constant, so the pressure difference in the convex and concave surfaces remains constant. There is no pressure variation between convex and concave surfaces for the second blade at any angle of rotation between $0^0 \leq \alpha \leq 80^0$. On the third blade, there is no pressure variation between $0^0 \leq \alpha \leq 30^0$ angle of rotation, however between $40^0 \leq \alpha \leq 80^0$ the pressure coefficient in the convex surfaces varies sinosidially. On the fourth blade, the pressure difference between the convex and concave surfaces increases between $0^0 \leq \alpha \leq 50^0$, but it decreases between $60^0 \leq \alpha \leq 80^0$. The pattern of the pressure coefficient in the convex surface is also sinosidial.

2. For the flow over the four bladed Savonius rotor, normal drag coefficient C_n increases with the increase of rotor angle from $\alpha = 0^0$ to 30^0 and then it decreases with the increase of the rotor angle α, up to 80^0. The drag coefficient C_n remains almost positive value from 100^0 to 150^0. It remains at negative value up to 210^0, then it rapidly increases to the highest positive value till 300^0. From 300^0, the value reduces to lowest negative value at 320^0, then again it increases.

3. In consideration to the combined effect of the four blades of a four bladed Savonius rotor, normal drag coefficient, C_n increases with the increase of rotor

angle from $\alpha=0^0$ to 20^0, then decreases its value at 30^0 again increases at 40^0. The value of C_n decreases at 50^0 and remains constant from 50^0 to 80^0. The maximum value is obtained at 20^0 angle of rotation. This favors the torque production for all angle of rotation. The system repeats from $\alpha=90^0$ to $\alpha=170^0$, $\alpha=180^0$ to $\alpha=260^0$ and $\alpha=260^0$ to $\alpha=350^0$. So, first and third blades are responsible for the production of maximum positive torque, which is very much necessary for the application of a vertical axis wind turbine.

4.   In consideration of the tangential drag coefficient, C_t with individual blade effect for different rotor angles, for the first blade, the tangential drag coefficient, $C_t(\alpha)$ increases with the increase of rotor angle from $\alpha=0^0$ to $\alpha=20^0$ and decreases its value up to $\alpha=120^0$. From $\alpha=130^0$ to $\alpha=200^0$ the value is constant and near to zero. From $\alpha=200^0$ to $\alpha=220^0$ the tangential drag coefficient increases. It then again decreases from $\alpha=220^0$ to 310^0. From 310^0 C_t increases till 360^0. Maximum positive thrust is available from $\alpha=0^0$ to 110^0 and maximum negative thrust is available from $\alpha=260^0$ to 340^0.

5.   For the tangential drag coefficient, C_t with four blades combined effect for different rotor angles, the drag coefficient increases for $\alpha=0^0$ to $\alpha=10^0$ and remain constant from $\alpha=10^0$ to $\alpha=20^0$. The value decreases at $\alpha=30^0$. For $\alpha=30^0$ to $\alpha=60^0$ the value remains constant. The tangential drag coefficient rapidly increases from $\alpha=60^0$ to $\alpha=80^0$. For rotor angle $\alpha=90^0$ to $\alpha=170^0$, $\alpha=180^0$ to $\alpha=260^0$ and $\alpha=270^0$ to $\alpha=350^0$ the values repeat in the same pattern.

6.   For the case torque coefficient, C_q with individual blade effect for different rotor angles, the nature of drag is exactly similar to that of the normal drag coefficient C_n with individual blade effect, which is responsible for producing

torque. The only difference between the two graphs is that the value of torque coefficient is smaller than normal drag coefficient, because the torque coefficient is calculated by multiplying some factor with normal drag coefficient. The maximum positive torque coefficient is available from $\alpha=0^0$ to 60^0 and from $\alpha=220^0$ to 300^0. C_q is negative for $\alpha=160^0$ to 210^0 and from $\alpha=300^0$ to 350^0

7. Considering the total static torque Coefficient, C_Q at different rotor angles, the nature of the curve is exactly similar to the normal drag coefficient, C_n with four blades combined effect. Only difference is that the value of torque coefficient is greater than normal drag coefficient with combined blade effect. Here the total static torque coefficient increases rapidly at angle from $\alpha=0^0$ to $\alpha=20^0$. The torque coefficient sharply falls at $\alpha=30^0$, again increases at $\alpha=40^0$. However, the value remain constant for $\alpha=50^0$ to $\alpha=80^0$. The curve repeats its nature from $\alpha=90^0$ to $\alpha=170^0$, $\alpha=180^0$ to $\alpha=260^0$ and $\alpha=270^0$ to $\alpha=350^0$.

8. For the prediction of dynamic characteristic, the measured power coefficient C_P vs. tip speed ratio λ of the present work matches with the nature C_P vs λ curve of other researchers. The present predicted curve is steeper than the predicted curves of the other researchers (figure 5.5). So, it can be concluded that the increases in the number of blades make the nature of the C_P vs λ curve steeper that provides more power.

9. The power coefficient C_P increases with the increase of Reynolds number for the four bladed Savonius rotor (figure 5.6). The variation of Reynolds number were made by varying the velocity of wind.

10. The four bladed Savonius rotor provides more power coefficient than that of the two and three bladed Savonius rotor. The C_n, C_t and C_q curves against the

angle of rotation of three bladed Savonius rotor predicted by Rahman [3] gives smoother curves than the present prediction.

6.3 Recommendations

1. The same experiment can be done with different shapes of the blades in the Savonius rotor.

2. The effect of Reynolds number on the flow over four bladed Savonius rotor with varying overlap ratios may be investigated.

3. The same experiment can be done with flow visualization technique to get a better understanding about the pressure distribution, drag coefficient and torque coefficient.

4. Ogawa and Yashida [8] and Islam et al [12] predicted Savonius rotor dynamically for two bladed Savonius rotor, Rahman [1] predicted Savonius rotor dynamically for three bladed Savonius rotor but until now only a few researches worked for the prediction of a four bladed Savonius rotor dynamically. So, further research could be conducted in this field.

REFERENCES

References :

1. Rahman, M., "Aerodynamic Characteristics of a Three Bladed Savonius Rotor." M.Sc. Engg. Thesis (2000), Dept of Mech. Engg., BUET.

2. Lysen, E.H., Bos, H.G. and Cordes, E.H. (1978), "Savonius Rotors for Water Pumping", SWD publication, Amersfoort, The Netherlands.

3. Park, J, (1975), " Simplified Wind Power System for Experimentry", Helion Inc., California, USA.

4. Sivasegaram, S. (1977), "Design Parameters Affecting the Performance of Resistance Type Rotors", Wind Engineering, vol. 1, pp. 207-217.

5. Newman, B.G. (1974), "Measurements on a Savonius Rotor with a Variable Gap", Proc, Symposium on Wind Energy: Achievements and Potential, Sherbrooke, Canada.

6. Lysen, E.H. (1983), " Introduction to Wind Energy," Steering Committee of Wind Energy for Developing Countries, P.O. Box 85, Amersfoort, the Netherlands.

7. Wilson, R.E. and S.N. Walker (1981), "Performance Analysis Program for Propeller Type Wind Turbines", Oregon State University, March, USA.

8. Ogawa, T. and H. Yoshida (1986), " The Effects of a Deflecting Plate and Rotor and Plates", Bull. JSME, vol. 29, pp. 2115-2121.

9.   Islam, A.K.M.S., Islam, M.Q., Razzaque, M.M. and Ahsraf, R. (1995), "Static Torque and Drag Characteristics of an S-shaped Savonius Rotor and Prediction of Dynamic Characteristics," Wind Engineering, vol. 19, no.6.

10.   Huda, M.D., Selim, M.A., Islam, A.K.M.S. and Islam, M.Q. (1992), "The Performance of an S-shaped Savonius Rotor with a Deflecting Plate", RERIC Int. Energy Journal, vol.14 no. 1, pp. 25-32.

11.   Gavalda, J., Massons, J. and Diaz, F. (1991), "Drag and Lift Coefficients of the Savonius Wind Machine", Wind Engineering, vol. 15, pp. 240-246.

12.   Islam, A.K.M.S., Islam, M.Q., Mandal, A.C. and Razzaque, M.M. (1993) " Aerodynamic Characteristics of a Stationary Savonius Rotor", RERIC Int. Energy Journal, vol. 15 no.2,pp.125-135.

13.   Bowden, G.J and MeAleese, S.A. (1984), "The Properties of Isolated and Coupled Savonius Rotors", Wind Engineering, vol. 8, no. 4, pp.271-288.

14.   Templin, R.J. (1974), "Aerodynamic Performance Theory for the NRC Vertical-Axis Wind Turbine", National Research Council of Canada, Report LTR-LA-160.

15.   Noll, R.B. and Ham, N.D. (1980), "Analytical Evaluation of the Aerodynamic Performance of a Hi-Reliability Vertical-Axis Wind Turbine", Proceeding of AWEA National Conference.

16.   Wilson, R.E. and Lissaman, P.B.S. (1974), "Applied Aerodynamics of Wind Power Machines", Oregon State University.

17.   Strickland, J.H. (1975), "The Darrieus Turbine: A Performance Prediction Model Using Multiple Streamtubes, Sandia Laboratories Report", SAND75-0431.

18.   Currie, I. G. (1974), "Fundamental Mechanics of Fluids", McGraw Hill.

19.   Paraschivoiu, I. And Delclaux, F. (1983), "Double Multiple Stream Tube Model with Recent Improvements", Journal of Energy, vol. 7, no. 3, pp. 250-255.

20.   Paraschiviu, I., Fraunic, P. and Beguier, C. (1985), "Stream Tube Expansion Effects on the Darricus Wind Turbine", Journal of Propulsion, vol. I, no. 2, pp. 150-155.

21.   Fanucci, J.B. and Watters, R.E. (1976), "Innovative Wind Machines: The Theoretical Performance of a Vertical-Axis Wind Turbine", Proceedings of the Vertical-Axis Wind Turbine Technology Workshop, Sandia Laboratories, SAND 76-5586, pp. III-61-95.

22.   Holme, O. (1976), " A Contribution to the Aerodynamic Theory of the Vertical Axis Wind Turbine", proceedings of the International Symposium on Wind Energy Systems, Cambridge, pp. C4-55-72.

23.   Wilson, R.E. (1978), " Vortex Sheet Analysis of the Giromill", ASME Journal of Fluids Engineering, vol. 100, no. 3, pp. 340-342.

24.   Sawada, T., Nakamura, M. and Kamada, S.(1986), "Blade Force Measurement and Flow Visualization of Savonius Rotors", Bull. JSME, vol. 29, pp. 2095-2100.

25. Aldoss, T.K. and Obeidat, K.M. (1987), "Performance Analysis of Two Savonius Rotors Running Side by Side Using the Discrete Vortex Method", Wind Engineering, vol. 11,no.5.

26. Jones, C.N., Littler, R.D. and Manser, B.L. (1979), "The Savonius Rotor Performance and Flow", 1st BWEA Workshop.

27. Sivasegaram, S. and Sivapalan, S. (1983), "Augmentation of power in Slow Running Vertical-Axis Wind Rotors Using Multiple Vanes", Wind Engineering, vol. 7, no.1.

27. Mahfuz, M. U. (2001), "Wind Energy Status in Bangladesh.", Wind Engineering, vol 25, no. 3.

28. Jagadeesh, A. (1999) " Wind Energy Development in Tamil Nadu and Andra Pradesh: Institutional Dynamics and Barrier. A Case Study. ", ISREPA-99.

29. Mandal, A.C., Islam, M. Q. (2001), "Aerodynamics and Design of Wind Turbines.", BUET.

APPENDIX- A
FORTRAN PROGRAMMING WITH OUTPUTS

```
C   PROGRAM FOR CALCULATION OF NORMAL AND TANGENTIAL FORCE
C   AND TORQUE USING RAW DATA OF PRESSURE FROM EXPERIMENT
*************************************************************
C                VARIABLE IDENTIFICATION
*************************************************************

     REAL FN(100), FT(100), TQ(100), RAWDP(100, 100),
    +DP(100,100), DELL
*************************************************************
C              OPENING OF INPUT AND OUTPUT FILES
*************************************************************

     OPEN (7,  FILE= 'winds9.for',STATUS= 'unknown' )
     OPEN (4,  FILE= 'OUT.for' , STATUS= 'unknown' )
     OPEN (11, FILE= 'FN.for' , STATUS= 'unknown')
     OPEN (12, FILE= 'FT.for' , STATUS= 'unknown' )
     OPEN (13, FILE= 'TQ.for' , STATUS= 'unknown')
     OPEN (14, FILE='RAW.for', STATUS='unknown')


*************************************************************
C   INITIALIZATION
*************************************************************
     RO=1.2
     U=13
     GAMA=9.81
     PIE=22./7.
     d=0.125
     a=0.025
     DELL=(d*10*PIE) / (2.*180.)
     S=a/d


*************************************************************
     MN=17
     MM=36
*************************************************************
C             MAIN PROGRAM
*************************************************************
     DO I=1,36
       DO J=1,17
         READ ( 7,* ) RAWDP ( I, J )
         DP ( I, J ) = 25.4 * RAWDP ( I, J )
       ENDDO
     ENDDO

     DO I=1,36
       DO J=1,17
```

```
            WRITE ( 14, * ) DP ( I, J )
        ENDDO
      ENDDO

      DO I=1,36
        DO J=1,17

            ANG=J*(180./17.)-(180./17.)
            FN(I)=GAMA*DELL*0.342*DP(I,J)*COS(ANG*PIE/180.)
            FT(I)=GAMA*DELL*0.342*DP(I,J)*SIN(ANG*PIE/180.)
            TQ(I)=FN(I)*(d/2)*(1-S)

*************************************************************
C              WRITING STATEMENT
*************************************************************

            WRITE(4, *) FN (I), FT(I), TQ(I)
            WRITE(11, *) FN(I)
            WRITE(12, *) FT (I)
            WRITE(13, *) TQ (I)
        ENDDO

      WRITE(4, *) 'CALCULATION FOR' ,I, 'th SET IS COMPLETE'

      ENDDO
*************************************************************
      STOP
      END
```

```
************************************************************
C              PROGRAM FOR INTEGRATION
************************************************************
C              VARIABLE IDENTIFICATION
*
************************************************************
      REAL FN(100,100), FT(100,100), TQ(100,100), FNF, FTF,
     1 TQF,CN,CT,CQ

************************************************************
C              OPENING OF INPUT AND OUTPUT FILES

************************************************************
      OPEN (11, FILE= 'FN.for' , STATUS= 'UNKNOWN' )
      OPEN (12, FILE= 'FT.for' , STATUS= 'UNKNOWN' )
      OPEN (13, FILE= 'TQ.for' , STATUS= 'UNKNOWN' )
      OPEN (20, FILE= 'R.for' , STATUS= 'UNKNOWN' )
      OPEN (21, FILE= 'FNF.for' , STATUS= 'UNKNOWN' )
      OPEN (22, FILE= 'FTF.for' , STATUS= 'UNKNOWN' )
      OPEN (23, FILE= 'TQF.for' , STATUS= 'UNKNOWN' )
      OPEN (24, FILE= 'CN.for' , STATUS= 'UNKNOWN' )
      OPEN (25, FILE= 'CT.for' , STATUS= 'UNKNOWN' )
      OPEN (26, FILE= 'CQ.for' , STATUS= 'UNKNOWN' )


************************************************************
C              INITIALIZATION
C
C
************************************************************
      d=0.125
      a=0.025
      S=a/d
      RO=1.2
      U=13.
      PIE=22./7.
      DELL=(d*10.*PIE) / (2.*180.)


************************************************************
C        READING THE DATA FROM FILES
************************************************************
      DO I=1, 36
        DO J=1,17
          READ ( 11,* ) FN ( I, J )
          READ ( 12,* ) FT ( I, J )
          READ ( 13,* ) TQ ( I, J )
```

```
      ENDDO
      ENDDO
************************************************************
      WRITE(20,*) '*********** FNF********** FTF ******************
     1 TQF **********CN**********CT**********CQ'
************************************************************

C   INTEGRATING NORMAL, TANGENTIAL FORCE COMPONENT AND
C   TORQUE AND USING THESE RESULTANT FORCE COMPONENTS
C   DRAG COEFFICIENT IN THE NORMAL DIRECTION CN, DRAG
C   COEFFICIENT IN THE TRANSVERSE DIRECTION, CT OF THE
C   CHORD, STATIC TORQUE COEFFICIENT CQ FOR INDIVIDUAL
C   BLADE HAVE BEEN CALCULATED .

************************************************************
      DO I=1,36
         DO J=1,17
            FNF = FNF + FN( 1, J )
            FTF = FTF + FT( I, J )
            TQF = FQF + TQ( I, J )
         ENDDO

         WRITE (21,*) FNF
         WRITE (22,*) FTF
         WRITE (23,*) TQF
         CN=FNF/((1/2.0)*RO*(U**2.0)*d)
         CT=FTF/((1/2.0)*RO*(U**2.0)*d)
         CQ=CN* ((1-S) / (2-S))


************************************************************
C                 WRITING STATEMENT
************************************************************
         WRITE (24,*) CN
         WRITE (25,*) CT
         WRITE (26,*) CQ
         WRITE (20,909) FNF, FTF,TQF, CN, CT, CQ

909   FORMAT (4X, 6(F16.4))
************************************************************
         FNF=0.0
         FTF=0.0
         TQF=0.0
      ENDDO
      STOP
      END
```

```
****************************************************************
C   PROGRAM FOR COMBINING THE EFFECT OF THREE BLADES IN THE
C   AERODYNAMIC CHARACTERISTICS OF A THREE BLADED SAVONIUS
C   ROTOR
****************************************************************
C                 VARIABLE IDENTIFICATION
****************************************************************

      REAL FNF(37), FTF(37), TQF(37), CN(37), CT(37), CQ(36),
     1CFNF,CFTF, CTQF,CCN,CCT,CCQ


****************************************************************
C           OPENING OF INPUT AND OUTPUT FILES
****************************************************************

      OPEN (21, FILE= 'FNF.FOR' , STATUS= 'UNKNOWN' )
      OPEN (22, FILE= 'FTF.FOR' , STATUS= 'UNKNOWN' )
      OPEN (23, FILE= 'TQF.FOR' , STATUS= 'UNKNOWN' )
      OPEN (24, FILE= 'CN.FOR' , STATUS= 'UNKNOWN' )
      OPEN (25, FILE= 'CT.FOR' , STATUS= 'UNKNOWN' )
      OPEN (26, FILE= 'CQ.FOR' , STATUS= 'UNKNOWN' )
      OPEN (41, FILE= 'CFNF.FOR' , STATUS= 'UNKNOWN' )
      OPEN (42, FILE= 'CFTF.FOR' , STATUS= 'UNKNOWN' )
      OPEN (43, FILE= 'CTQF.FOR' , STATUS= 'UNKNOWN' )
      OPEN (44, FILE= 'CCN.FOR' , STATUS= 'UNKNOWN' )
      OPEN (45, FILE= 'CCT.FOR' , STATUS= 'UNKNOWN' )
      OPEN (46, FILE= 'CCQ.FOR' , STATUS= 'UNKNOWN' )
      OPEN (30, FILE= 'CR.FOR' , STATUS= 'UNKNOWN' )



****************************************************************
C                    INITIALIZATION
****************************************************************

      d=0.125
      a=0.025
      S=a/d

      MM=36
      WRITE (30, 90)
90    FORMAT(6X,'CFNF',6X,'CFTF',6X,'CTQF',6X,'CCN',6X,'CCT',
     1 6X,'CCQ')

****************************************************************
C               READING THE DATA FROM FILES
```

```
***********************************************************
      DO I=1, MM

          READ ( 21,* ) FNF ( I )
          READ ( 22,* ) FTF ( I )
          READ ( 23,* ) TQF ( I )
          READ ( 24,* ) CN(I)
          READ ( 25,* ) CT(I)
          READ ( 26,* ) CQ(I)

      ENDDO


***********************************************************
C       COMBINING EFFECT OF AERODYNAMIC CHARACTERISTICS
***********************************************************
      DO J=1,4
      DO I=1,9

      CFNF = FNF(I) + FNF( I+9 ) +FNF( I+18 ) +FNF( I+27 )
      CFTF = FTF(I) + FTF( I+9 ) +FTF( I+18 ) +FTF( I+27 )
      CTQF = TQF (I)+ TQF( I+9 ) +TQF( I+18 ) +TQF( I+27 )
      CCN =  CN(I)  + CN ( I+9 ) +CN ( I+18 ) +CN ( I+27 )
      CCT =  CT(I)  + CT ( I+9 ) +CT ( I+18 ) +CT ( I+27)
      CCQ = (CN (I)+ CN( I+9 ) +CN( I+18 )+CN(I+27))*
     1  ((1-S)/((2-S)**2))


***********************************************************
C                 WRITING STATEMENT
***********************************************************

      WRITE (30,900) CFNF,CFTF,CTQF,CCN,CCT,CCQ
      WRITE (41,*) CFNF
      WRITE (42,*) CFTF
      WRITE (43,*) CTQF
      WRITE (44,*) CCN
      WRITE (45,*) CCT
      WRITE (46,*) CCQ

      ENDDO
      ENDDO

900  FORMAT (4X, 6(F16.4))
***********************************************************
      STOP
      END
```

```
************************************************************
C    PROGRAM FOR CALCULATING THE DYNAMIC TORQUE COEFFICIENT
C    CQ, POWER COEFFICIENT CP AND AVERAGE POWER COEFFICIENT
C    OF A THREE BLADED SAVONIUS ROTOR FOR THE TIP SPEED
C    RATIO LAMDA=0.5
************************************************************
C              VARIABLE IDENTIFICATION

************************************************************
     REAL CN(36),VW5(36),CND(36), CQ(9), CP(9), CPAV
     REAL LAMDA
************************************************************
C           OPENING OF INPUT AND OUTPUT FILES

************************************************************


     OPEN (44, FILE= 'CCN.for' , STATUS= 'UNKNOWN' )
     OPEN (10, FILE= 'VW5.for' , STATUS= 'UNKNOWN' )
     OPEN (11, FILE= 'POWER.for' , STATUS= 'UNKNOWN' )


************************************************************
C              INITIALIZATION
************************************************************

     U=13.
     LAMDA=.50
     S=.2


************************************************************
C       READING THE DATA FROM FILES
************************************************************
     DO I=1, 36
     READ (44,* ) CN(I)
     READ (10,* ) VW5(I)
     ENDDO


************************************************************
C    MAIN PROGRAMME
************************************************************
     DO I=1, 36
     CND(I) =CN(I)*((VW5(I)/U)**2.0)
     END DO
     ADD=0.0
     DO I=1,9
     J=9+I
```

```
      K=18+I
      L=27+I
      CQ(I)=( CND(I)+ CND(J)+ CND(K)+CND(L))*((1-S)/(2-S)**2.0)
      CP(I)=CQ(I)*LAMDA

C*********************************************************
C     WRITING OUTPUT FILES
C*********************************************************

      WRITE (11,*) CQ(I), CP(I)
      ADD=ADD+CP(I)
      ENDDO
      CPAV=ADD/9.0
      WRITE(11,*) 'AVERAGE VALUE OF Cp=', CPAV
      STOP
      END
```

The FORTRAN gives the following Total Static Torque Coefficient, C_T and Power Coefficient C_p output for different value of λ and corresponding V_w

```
1.484272E-01   7.421359E-02
1.238090E-01   6.190450E-02
1.840210E-01   9.201049E-02
2.194096E-01   1.097048E-01
-3.256782E-02  -1.628391E-02
-1.718145E-02  -8.590723E-03
4.078414E-02   2.039207E-02
1.506869E-01   7.534347E-02
1.362207E-01   6.811033E-02
```
AVERAGE VALUE OF Cp= 5.297829E-02   for λ=0.5


```
1.571373E-01   1.257098E-01
1.310744E-01   1.048595E-01
1.948198E-01   1.558559E-01
2.322852E-01   1.858281E-01
-3.447898E-02  -2.758319E-02
-1.818970E-02  -1.455176E-02
4.317747E-02   3.454198E-02
1.595296E-01   1.276237E-01
1.442145E-01   1.153716E-01
```
AVERAGE VALUE OF Cp= 8.973953E-02   for λ=0.8


```
1.607778E-01   1.447000E-01
1.341111E-01   1.207000E-01
1.993333E-01   1.794000E-01
2.376667E-01   2.139000E-01
-3.527778E-02  -3.175000E-02
-1.861111E-02  -1.675000E-02
4.417778E-02   3.976000E-02
1.632255E-01   1.469030E-01
1.475556E-01   1.328000E-01
```
AVERAGE VALUE OF Cp= 1.032959E-01   for λ=0.9


```
1.699741E-01   1.869716E-01
1.417821E-01   1.559604E-01
2.107350E-01   2.318085E-01
2.512610E-01   2.763871E-01
-3.729564E-02  -4.102521E-02
```

-1.967565E-02 -2.164322E-02
 4.670471E-02   5.137518E-02
 1.725619E-01   1.898181E-01
 1.559956E-01   1.715952E-01
AVERAGE VALUE OF Cp= 1.334720E-01   for λ=1.1

 1.885242E-01   2.262291E-01
 1.584584E-01   1.901501E-01
 2.159562E-01   2.591475E-01
 2.574863E-01   3.089836E-01
-3.821968E-02 -4.586362E-02
-2.016314E-02 -2.419577E-02
 4.786188E-02   5.743426E-02
 1.768373E-01   2.122048E-01
 1.598606E-01   1.918327E-01
AVERAGE VALUE OF Cp= 1.528803E-01   for λ=1.2

 1.922314E-01   2.883472E-01
 1.603479E-01   2.405218E-01
 2.383298E-01   3.574947E-01
 2.841625E-01   4.262437E-01
-4.217933E-02 -6.326899E-02
-2.225208E-02 -3.337813E-02
 5.282047E-02   7.923071E-02
 1.951581E-01   2.927372E-01
 1.764225E-01   2.646338E-01
AVERAGE VALUE OF Cp= 2.058402E-01   for λ=1.5

 2.310776E-01   4.621552E-01
 1.927509E-01   3.855019E-01
 2.864915E-01   5.729829E-01
 3.415860E-01   6.831719E-01
-5.070292E-02 -1.014058E-01
-2.674879E-02 -5.349757E-02
 6.349443E-02   1.269889E-01
 2.345956E-01   4.691912E-01
 2.120740E-01   4.241479E-01
AVERAGE VALUE OF Cp= 3.299152E-01 for λ==2

However only the realistic values for Power Coefficient, C_p has been considered for the prediction. The filtering was done within the range of $0<C_p<0.22$.

λ	Modified $C_{p\,average}$
0.5	0.0716
0.8	0.1213
0.9	0.1397
1.1	0.1646
1.2	0.1629
1.5	0.0792

For $\lambda>1.5$ there is hardly any realistic value so they were not considered.

APPENDIX- B
EXPERIMENTAL DATA

Data for 0⁰ Angle of Rotation

Tapping Points	Initial Reading (in of H_2O)	$\alpha= 0^0$ (in of H_2O) (Convex surface)		Initial Reading (in of H_2O)	$\alpha= 0^0$ (in of H_2O) (Concave surface)		Pressure Diff. DP (in of H_2O)
1	1.7	1.2	0.5	1.7	1.28	0.42	-0.08
2	1.7	1.35	0.35	1.7	1.3	0.4	0.05
3	1.7	1.55	0.15	1.7	1.32	0.38	0.23
4	1.68	1.68	0	1.68	1.3	0.38	0.38
5	1.72	1.8	-0.08	1.72	1.28	0.44	0.52
6	1.7	1.72	-0.02	1.7	1.32	0.38	0.4
7	1.8	1.82	-0.02	1.8	1.37	0.43	0.45
8	1.7	1.72	-0.02	1.7	1.3	0.4	0.42
9	1.75	1.75	0.00	1.75	1.3	0.45	0.45
10	1.7	1.7	0.00	1.7	1.28	0.42	0.42
11	1.68	1.68	0.00	1.68	1.23	0.45	0.45
12	1.6	1.65	-0.05	1.6	1.26	0.34	0.39
13	1.78	1.82	-0.04	1.78	1.3	0.48	0.52
14	1.5	1.6	-0.10	1.5	1.15	0.35	0.45
15	1.6	1.68	-0.08	1.6	1.16	0.44	0.52
16	1.65	1.68	-0.03	1.65	1.22	0.43	0.46
17	1.68	1.65	0.03	1.68	1.2	0.48	0.45

Data for 10⁰ Angle of Rotation

Tapping Points	Initial Reading (in of H_2O)	$\alpha= 10^0$ (in of H_2O) (Convex surface)		Initial Reading (in of H_2O)	$\alpha= 10^0$ (in of H_2O) (Concave surface)		Pressure Diff. DP (in of H_2O)
1	1.7	1.5	0.2	1.7	1.15	0.55	0.35
2	1.7	1.68	0.02	1.7	1.15	0.55	0.53
3	1.7	1.9	-0.2	1.7	1.18	0.52	0.72
4	1.68	2	-0.32	1.68	1.18	0.5	0.82
5	1.72	1.92	-0.2	1.72	1.15	0.57	0.77
6	1.7	1.88	-0.18	1.7	1.18	0.52	0.7
7	1.8	2	-0.2	1.8	1.23	0.57	0.77
8	1.7	1.88	-0.18	1.7	1.18	0.52	0.7
9	1.75	1.9	-0.15	1.75	1.2	0.55	0.7
10	1.7	1.88	-0.18	1.7	1.18	0.52	0.7
11	1.68	1.88	-0.2	1.68	1.12	0.56	0.76
12	1.6	1.8	-0.2	1.6	1.12	0.48	0.68
13	1.78	2	-0.22	1.78	1.22	0.56	0.78
14	1.5	1.75	-0.25	1.5	1.02	0.48	0.73
15	1.6	1.88	-0.28	1.6	1.08	0.52	0.8
16	1.65	1.8	-0.15	1.65	1.12	0.53	0.68
17	1.68	1.8	-0.12	1.68	1.1	0.58	0.7

Data for 20⁰ Angle of Rotation

Tapping Points	Initial Reading (in of H_2O)	α= 20⁰ (in of H_2O) (Convex surface)		Initial Reading (in of H_2O)	α= 20⁰ (in of H_2O) (Concave surface)		Pressure Diff. DP (in of H_2O)
1	1.7	1.9	-0.2	1.7	1.15	0.55	0.75
2	1.7	2.1	-0.4	1.7	1.15	0.55	0.95
3	1.7	2.2	-0.5	1.7	1.18	0.52	1.02
4	1.68	2.3	-0.62	1.68	1.18	0.5	1.12
5	1.72	2.32	-0.6	1.72	1.12	0.6	1.2
6	1.7	2.15	-0.45	1.7	1.18	0.52	0.97
7	1.8	2.18	-0.38	1.8	1.2	0.6	0.98
8	1.7	1.9	-0.2	1.7	1.14	0.56	0.76
9	1.75	1.98	-0.23	1.75	1.16	0.59	0.82
10	1.7	1.9	-0.2	1.7	1.12	0.58	0.78
11	1.68	1.9	-0.22	1.68	1.08	0.6	0.82
12	1.6	1.8	-0.2	1.6	1.1	0.5	0.7
13	1.78	2.02	-0.24	1.78	1.19	0.59	0.83
14	1.5	1.78	-0.28	1.5	1	0.5	0.78
15	1.6	1.9	-0.3	1.6	1.02	0.58	0.88
16	1.65	1.8	-0.15	1.65	1.1	0.55	0.7
17	1.68	1.8	-0.12	1.68	1.1	0.58	0.7

Data for 30⁰ Angle of Rotation

Tapping Points	Initial Reading (in of H_2O)	α=30⁰ (in of H_2O) (Convex surface)		Initial Reading (in of H_2O)	α= 30⁰ (in of H_2O) (Concave surface)		Pressure Diff. DP (in of H_2O)
1	1.7	2.45	-0.75	1.7	1.15	0.55	1.3
2	1.7	2.3	-0.6	1.7	1.15	0.55	1.15
3	1.7	2.25	-0.55	1.7	1.18	0.52	1.07
4	1.68	2.2	-0.52	1.68	1.18	0.5	1.02
5	1.72	2.1	-0.38	1.72	1.12	0.6	0.98
6	1.7	1.85	-0.15	1.7	1.18	0.52	0.67
7	1.8	2.1	-0.3	1.8	1.2	0.6	0.9
8	1.7	1.88	-0.18	1.7	1.14	0.56	0.74
9	1.75	1.94	-0.19	1.75	1.15	0.6	0.79
10	1.7	1.9	-0.2	1.7	1.12	0.58	0.78
11	1.68	1.9	-0.22	1.68	1.09	0.59	0.81
12	1.6	1.8	-0.2	1.6	1.1	0.5	0.7
13	1.78	1.98	-0.2	1.78	1.18	0.6	0.8
14	1.5	1.7	-0.2	1.5	1	0.5	0.7
15	1.6	1.8	-0.2	1.6	1.02	0.58	0.78
16	1.65	1.8	-0.15	1.65	1.1	0.55	0.7
17	1.68	1.8	-0.12	1.68	1.08	0.6	0.72

Data for 40⁰ Angle of Rotation

Tapping Points	Initial Reading (in of H_2O)	α=40⁰ (in of H_2O) (Convex surface)		Initial Reading (in of H_2O)	α= 40⁰ (in of H_2O) (Concave surface)		Pressure Diff. DP (in of H_2O)
1	1.7	1.88	-0.18	1.7	1.15	0.55	0.73
2	1.7	1.8	-0.1	1.7	1.15	0.55	0.65
3	1.7	1.83	-0.13	1.7	1.18	0.52	0.65
4	1.68	1.72	-0.04	1.68	1.18	0.5	0.54
5	1.72	1.88	-0.16	1.72	1.12	0.6	0.76
6	1.7	1.78	-0.08	1.7	1.18	0.52	0.6
7	1.8	1.98	-0.18	1.8	1.2	0.6	0.78
8	1.7	1.82	-0.12	1.7	1.15	0.55	0.67
9	1.75	1.9	-0.15	1.75	1.15	0.6	0.75
10	1.7	1.9	-0.2	1.7	1.12	0.58	0.78
11	1.68	1.82	-0.14	1.68	1.1	0.58	0.72
12	1.6	1.77	-0.17	1.6	1.1	0.5	0.67
13	1.78	1.96	-0.18	1.78	1.2	0.58	0.76
14	1.5	1.68	-0.18	1.5	1	0.5	0.68
15	1.6	1.8	-0.2	1.6	1.02	0.58	0.78
16	1.65	1.78	-0.13	1.65	1.1	0.55	0.68
17	1.68	1.8	-0.1	1.68	1.08	0.6	0.7

Data for 50⁰ Angle of Rotation

Tapping Points	Initial Reading (in of H_2O)	α = 50⁰ (in of H_2O) (Convex surface)		Initial Reading (in of H_2O)	α = 50⁰ (in of H_2O) (Concave surface)		Pressure Diff. DP (in of H_2O)
1	1.7	1.82	-0.12	1.7	1.2	0.5	0.62
2	1.7	1.78	-0.08	1.7	1.18	0.52	0.6
3	1.7	1.82	-0.12	1.7	1.2	0.5	0.62
4	1.68	1.7	-0.02	1.68	1.19	0.49	0.51
5	1.72	1.78	-0.06	1.72	1.15	0.57	0.63
6	1.7	1.79	-0.09	1.7	1.2	0.5	0.59
7	1.8	1.97	-0.17	1.8	1.22	0.58	0.75
8	1.7	1.82	-0.12	1.7	1.15	0.55	0.67
9	1.75	1.9	-0.15	1.75	1.18	0.57	0.72
10	1.7	1.82	-0.12	1.7	1.12	0.58	0.7
11	1.68	1.8	-0.12	1.68	1.1	0.58	0.7
12	1.6	1.73	-0.13	1.6	1.1	0.5	0.63
13	1.78	1.92	-0.14	1.78	1.2	0.58	0.72
14	1.5	1.68	-0.18	1.5	1	0.5	0.68
15	1.6	1.78	-0.18	1.6	1.03	0.57	0.75
16	1.65	1.78	-0.13	1.65	1.1	0.55	0.68
17	1.68	1.8	-0.12	1.68	1.08	0.6	0.72

Data for 60⁰ Angle of Rotation

Tapping Points	Initial Reading (in of H_2O)	$\alpha = 60^0$ (in of H_2O) (Convex surface)		Initial Reading (in of H_2O)	$\alpha = 60^0$ (in of H_2O) (Concave surface)		Pressure Diff. DP (in of H_2O)
1	1.7	1.82	-0.12	1.7	1.28	0.42	0.54
2	1.7	1.8	-0.1	1.7	1.28	0.42	0.52
3	1.7	1.82	-0.12	1.7	1.28	0.42	0.54
4	1.68	1.72	-0.04	1.68	1.27	0.41	0.45
5	1.72	1.78	-0.06	1.72	1.22	0.5	0.56
6	1.7	1.8	-0.1	1.7	1.23	0.47	0.57
7	1.8	1.98	-0.18	1.8	1.3	0.5	0.68
8	1.7	1.83	-0.13	1.7	1.2	0.5	0.63
9	1.75	1.88	-0.13	1.75	1.22	0.53	0.66
10	1.7	1.82	-0.12	1.7	1.2	0.5	0.62
11	1.68	1.78	-0.1	1.68	1.18	0.5	0.6
12	1.6	1.73	-0.13	1.6	1.2	0.4	0.53
13	1.78	1.92	-0.14	1.78	1.25	0.53	0.67
14	1.5	1.68	-0.18	1.5	1.1	0.4	0.58
15	1.6	1.78	-0.18	1.6	1.12	0.48	0.66
16	1.65	1.78	-0.13	1.65	1.2	0.45	0.58
17	1.68	1.8	-0.12	1.68	1.15	0.53	0.65

Data for 70⁰ Angle of Rotation

Tapping Points	Initial Reading (in of H_2O)	$\alpha = 70^0$ (in of H_2O) (Convex surface)		Initial Reading (in of H_2O)	$\alpha = 70^0$ (in of H_2O) (Concave surface)		Pressure Diff. DP (in of H_2O)
1	1.7	1.85	-0.15	1.7	1.35	0.35	0.5
2	1.7	1.8	-0.1	1.7	1.35	0.35	0.45
3	1.7	1.83	-0.13	1.7	1.35	0.35	0.48
4	1.68	1.75	-0.07	1.68	1.35	0.33	0.4
5	1.72	1.9	-0.18	1.72	1.3	0.42	0.6
6	1.7	1.8	-0.1	1.7	1.35	0.35	0.45
7	1.8	2	-0.2	1.8	1.38	0.42	0.62
8	1.7	1.85	-0.15	1.7	1.4	0.3	0.45
9	1.75	1.9	-0.15	1.75	1.32	0.43	0.58
10	1.7	1.83	-0.13	1.7	1.28	0.42	0.55
11	1.68	1.8	-0.12	1.68	1.25	0.43	0.55
12	1.6	1.75	-0.15	1.6	1.25	0.35	0.5
13	1.78	1.98	-0.2	1.78	1.3	0.48	0.68
14	1.5	1.7	-0.2	1.5	1.15	0.35	0.55
15	1.6	1.8	-0.2	1.6	1.15	0.45	0.65
16	1.65	1.8	-0.15	1.65	1.25	0.4	0.55
17	1.68	1.8	-0.12	1.68	1.2	0.48	0.6

Data for 80⁰ Angle of Rotation

Tapping Points	Initial Reading (in of H_2O)	$\alpha = 80^0$ (in of H_2O) (Convex surface)		Initial Reading (in of H_2O)	$\alpha = 80^0$ (in of H_2O) (Concave surface)		Pressure Diff. DP (in of H_2O)
1	1.7	1.83	-0.13	1.7	1.48	0.22	0.35
2	1.7	1.8	-0.1	1.7	1.5	0.2	0.3
3	1.7	1.82	-0.12	1.7	1.51	0.19	0.31
4	1.68	1.72	-0.04	1.68	1.51	0.17	0.21
5	1.72	1.9	-0.18	1.72	1.5	0.22	0.4
6	1.7	1.8	-0.1	1.7	1.5	0.2	0.3
7	1.8	2	-0.2	1.8	1.57	0.23	0.43
8	1.7	1.84	-0.14	1.7	1.57	0.13	0.27
9	1.75	1.9	-0.15	1.75	1.51	0.24	0.39
10	1.7	1.82	-0.12	1.7	1.46	0.24	0.36
11	1.68	1.78	-0.1	1.68	1.4	0.28	0.38
12	1.6	1.72	-0.12	1.6	1.4	0.2	0.32
13	1.78	2.03	-0.25	1.78	1.5	0.28	0.53
14	1.5	1.8	-0.3	1.5	1.3	0.2	0.5
15	1.6	1.88	-0.28	1.6	1.45	0.15	0.43
16	1.65	1.8	-0.15	1.65	1.48	0.17	0.32
17	1.68	1.8	-0.12	1.68	1.4	0.28	0.4

Data for 90⁰ Angle of Rotation

Tapping Points	Initial Reading (in of H_2O)	$\alpha = 90^0$ (in of H_2O) (Convex surface)		Initial Reading (in of H_2O)	$\alpha = 90^0$ (in of H_2O) (Concave surface)		Pressure Diff. DP (in of H_2O)
1	1.7	1.85	-0.15	1.7	1.62	0.08	0.23
2	1.7	1.8	-0.1	1.7	1.65	0.05	0.15
3	1.7	1.8	-0.1	1.7	1.68	0.02	0.12
4	1.68	1.7	-0.02	1.68	1.62	0.06	0.08
5	1.72	1.88	-0.16	1.72	1.68	0.04	0.2
6	1.7	1.78	-0.08	1.7	1.68	0.02	0.1
7	1.8	1.98	-0.18	1.8	1.75	0.05	0.23
8	1.7	1.8	-0.1	1.7	1.62	0.08	0.18
9	1.75	1.9	-0.15	1.75	1.7	0.05	0.2
10	1.7	1.85	-0.15	1.7	1.62	0.08	0.23
11	1.68	1.8	-0.12	1.68	1.58	0.1	0.22
12	1.6	1.8	-0.2	1.6	1.56	0.04	0.24
13	1.78	2	-0.22	1.78	1.67	0.11	0.33
14	1.5	1.72	-0.22	1.5	1.45	0.05	0.27
15	1.8	1.8	0	1.6	1.5	0.1	0.1
16	1.65	1.8	-0.15	1.65	1.63	0.02	0.17
17	1.68	1.8	-0.12	1.68	1.6	0.08	0.2

98

Data for 100^0 Angle of Rotation

Tapping Points	Initial Reading (in of H_2O)	$\alpha = 100^0$ (in of H_2O) (Convex surface)		Initial Reading (in of H_2O)	$\alpha = 100^0$ (in of H_2O) (Concave surface)		Pressure Diff. DP (in of H_2O)
1	1.7	1.82	-0.12	1.7	1.72	-0.02	0.1
2	1.7	1.8	-0.1	1.7	1.72	-0.02	0.08
3	1.7	1.8	-0.1	1.7	1.73	-0.03	0.07
4	1.68	1.7	-0.02	1.68	1.7	-0.02	0
5	1.72	1.88	-0.16	1.72	1.76	-0.04	0.12
6	1.7	1.78	-0.08	1.7	1.75	-0.05	0.03
7	1.8	1.98	-0.18	1.8	1.85	-0.05	0.13
8	1.7	1.8	-0.1	1.7	1.73	-0.03	0.07
9	1.75	1.9	-0.15	1.75	1.8	-0.05	0.1
10	1.7	1.85	-0.15	1.7	1.72	-0.02	0.13
11	1.68	1.85	-0.17	1.68	1.68	0	0.17
12	1.6	1.8	-0.2	1.6	1.66	-0.06	0.14
13	1.78	2	-0.22	1.78	1.78	0	0.22
14	1.5	1.7	-0.2	1.5	1.5	0	0.2
15	1.6	1.8	-0.2	1.6	1.6	0	0.2
16	1.65	1.8	-0.15	1.65	1.7	-0.05	0.1
17	1.68	1.8	-0.12	1.68	1.68	0	0.12

Data for 110^0 Angle of Rotation

Tapping Points	Initial Reading (in of H_2O)	$\alpha = 110^0$ (in of H_2O) (Convex surface)		Initial Reading (in of H_2O)	$\alpha = 110^0$ (in of H_2O) (Concave surface)		Pressure Diff. DP (in of H_2O)
1	1.7	1.82	-0.12	1.7	1.8	-0.1	0.02
2	1.7	1.78	-0.08	1.7	1.8	-0.1	-0.02
3	1.7	1.8	-0.1	1.7	1.8	-0.1	0
4	1.68	1.7	-0.02	1.68	1.75	-0.07	-0.05
5	1.72	1.86	-0.14	1.72	1.85	-0.13	0.01
6	1.7	1.84	-0.14	1.7	1.8	-0.1	0.04
7	1.8	1.97	-0.17	1.8	1.93	-0.13	0.04
8	1.7	1.8	-0.1	1.7	1.83	-0.13	-0.03
9	1.75	1.88	-0.13	1.75	1.88	-0.13	0
10	1.7	1.82	-0.12	1.7	1.82	-0.12	-1.1E-16
11	1.68	1.82	-0.14	1.68	1.78	-0.1	0.04
12	1.6	1.8	-0.2	1.6	1.7	-0.1	0.1
13	1.78	2	-0.22	1.78	1.9	-0.12	0.1
14	1.5	1.7	-0.2	1.5	1.6	-0.1	0.1
15	1.6	1.8	-0.2	1.6	1.7	-0.1	0.1
16	1.65	1.78	-0.13	1.65	1.75	-0.1	0.03
17	1.68	1.8	-0.12	1.68	1.75	-0.07	0.05

99

Data for 120⁰ Angle of Rotation

Tapping Points	Initial Reading (in of H_2O)	$\alpha = 120^0$ (in of H_2O) (Convex surface)		Initial Reading (in of H_2O)	$\alpha = 120^0$ (in of H_2O) (Concave surface)		Pressure Diff. DP (in of H_2O)
1	1.7	1.82	-0.12	1.7	1.9	-0.2	-0.08
2	1.7	1.78	-0.08	1.7	1.85	-0.15	-0.07
3	1.7	1.8	-0.1	1.7	1.9	-0.2	-0.1
4	1.68	1.7	-0.02	1.68	1.8	-0.12	-0.1
5	1.72	1.85	-0.13	1.72	1.92	-0.2	-0.07
6	1.7	1.82	-0.12	1.7	1.82	-0.12	-1.1E-16
7	1.8	1.92	-0.12	1.8	2.03	-0.23	-0.11
8	1.7	1.8	-0.1	1.7	1.9	-0.2	-0.1
9	1.75	1.9	-0.15	1.75	2	-0.25	-0.1
10	1.7	1.85	-0.15	1.7	1.93	-0.23	-0.08
11	1.68	1.85	-0.17	1.68	1.9	-0.22	-0.05
12	1.6	1.8	-0.2	1.6	1.8	-0.2	0
13	1.78	2	-0.22	1.78	2	-0.22	0
14	1.5	1.7	-0.2	1.5	1.7	-0.2	0
15	1.6	1.8	-0.2	1.6	1.83	-0.23	-0.03
16	1.65	1.78	-0.13	1.65	1.8	-0.15	-0.02
17	1.68	1.8	-0.12	1.68	1.8	-0.12	-1.1E-16

Data for 130⁰ Angle of Rotation

Tapping Points	Initial Reading (in of H_2O)	$\alpha = 130^0$ (in of H_2O) (Convex surface)		Initial Reading (in of H_2O)	$\alpha = 130^0$ (in of H_2O) (Concave surface)		Pressure Diff. DP (in of H_2O)
1	1.7	1.8	-0.1	1.7	1.9	-0.2	-0.1
2	1.7	1.8	-0.1	1.7	1.83	-0.13	-0.03
3	1.7	1.8	-0.1	1.7	1.87	-0.17	-0.07
4	1.68	1.75	-0.07	1.68	1.8	-0.12	-0.05
5	1.72	1.8	-0.08	1.72	1.92	-0.2	-0.12
6	1.7	1.8	-0.1	1.7	1.82	-0.12	-0.02
7	1.8	1.92	-0.12	1.8	2	-0.2	-0.08
8	1.7	1.8	-0.1	1.7	1.88	-0.18	-0.08
9	1.75	1.9	-0.15	1.75	1.97	-0.22	-0.07
10	1.7	1.85	-0.15	1.7	1.9	-0.2	-0.05
11	1.68	1.8	-0.12	1.68	1.88	-0.2	-0.08
12	1.6	1.75	-0.15	1.6	1.8	-0.2	-0.05
13	1.78	1.9	-0.12	1.78	1.99	-0.21	-0.09
14	1.5	1.65	-0.15	1.5	1.7	-0.2	-0.05
15	1.6	1.7	-0.1	1.6	1.82	-0.22	-0.12
16	1.65	1.7	-0.05	1.65	1.8	-0.15	-0.1
17	1.68	1.8	-0.12	1.68	1.75	-0.07	0.05

Data for 140⁰ Angle of Rotation

Tapping Points	Initial Reading (in of H_2O)	$\alpha = 140^0$ (in of H_2O) (Convex surface)		Initial Reading (in of H_2O)	$\alpha = 140^0$ (in of H_2O) (Concave surface)		Pressure Diff. DP (in of H_2O)
1	1.7	1.8	-0.1	1.7	1.85	-0.15	-0.05
2	1.7	1.8	-0.1	1.7	1.8	-0.1	0
3	1.7	1.8	-0.1	1.7	1.85	-0.15	-0.05
4	1.68	1.75	-0.07	1.68	1.75	-0.07	0
5	1.72	1.8	-0.08	1.72	1.9	-0.18	-0.1
6	1.7	1.8	-0.1	1.7	1.8	-0.1	0
7	1.8	1.95	-0.15	1.8	1.99	-0.19	-0.04
8	1.7	1.8	-0.1	1.7	1.86	-0.16	-0.06
9	1.75	1.88	-0.13	1.75	1.92	-0.17	-0.04
10	1.7	1.85	-0.15	1.7	1.88	-0.18	-0.03
11	1.68	1.8	-0.12	1.68	1.87	-0.19	-0.07
12	1.6	1.75	-0.15	1.6	1.78	-0.18	-0.03
13	1.78	1.9	-0.12	1.78	1.98	-0.2	-0.08
14	1.5	1.6	-0.1	1.5	1.7	-0.2	-0.1
15	1.6	1.7	-0.1	1.6	1.8	-0.2	-0.1
16	1.65	1.75	-0.1	1.65	1.78	-0.13	-0.03
17	1.68	1.8	-0.12	1.68	1.72	-0.04	0.08

Data for 150⁰ Angle of Rotation

Tapping Points	Initial Reading (in of H_2O)	$\alpha = 150^0$ (in of H_2O) (Convex surface)		Initial Reading (in of H_2O)	$\alpha = 150^0$ (in of H_2O) (Concave surface)		Pressure Diff. DP (in of H_2O)
1	1.7	1.8	-0.1	1.7	1.82	-0.12	-0.02
2	1.7	1.8	-0.1	1.7	1.8	-0.1	0
3	1.7	1.82	-0.12	1.7	1.82	-0.12	-1.1E-16
4	1.68	1.78	-0.1	1.68	1.75	-0.07	0.03
5	1.72	1.82	-0.1	1.72	1.88	-0.16	-0.06
6	1.7	1.8	-0.1	1.7	1.79	-0.09	0.01
7	1.8	1.95	-0.15	1.8	1.99	-0.19	-0.04
8	1.7	1.8	-0.1	1.7	1.87	-0.17	-0.07
9	1.75	1.9	-0.15	1.75	1.92	-0.17	-0.02
10	1.7	1.85	-0.15	1.7	1.9	-0.2	-0.05
11	1.68	1.8	-0.12	1.68	1.86	-0.18	-0.06
12	1.6	1.72	-0.12	1.6	1.76	-0.16	-0.04
13	1.78	1.9	-0.12	1.78	1.95	-0.17	-0.05
14	1.5	1.65	-0.15	1.5	1.68	-0.18	-0.03
15	1.6	1.75	-0.15	1.6	1.8	-0.2	-0.05
16	1.65	1.75	-0.1	1.65	1.75	-0.1	0

Data for 160⁰ Angle of Rotation

Data for 160^0 Angle of Rotation

Tapping Points	Initial Reading (in of H_2O)	$\alpha = 160^0$ (in of H_2O) (Convex surface)		Initial Reading (in of H_2O)	$\alpha = 160^0$ (in of H_2O) (Concave surface)		Pressure Diff. DP (in of H_2O)
1	1.7	1.83	-0.13	1.7	1.8	-0.1	0.03
2	1.7	1.8	-0.1	1.7	1.78	-0.08	0.02
3	1.7	1.85	-0.15	1.7	1.8	-0.1	0.05
4	1.68	1.8	-0.12	1.68	1.73	-0.05	0.07
5	1.72	1.88	-0.16	1.72	1.86	-0.14	0.02
6	1.7	1.8	-0.1	1.7	1.78	-0.08	0.02
7	1.8	1.96	-0.16	1.8	1.97	-0.17	-0.01
8	1.7	1.82	-0.12	1.7	1.85	-0.15	-0.03
9	1.75	1.9	-0.15	1.75	1.92	-0.17	-0.02
10	1.7	1.85	-0.15	1.7	1.89	-0.19	-0.04
11	1.68	1.82	-0.14	1.68	1.86	-0.18	-0.04
12	1.6	1.75	-0.15	1.6	1.77	-0.17	-0.02
13	1.78	1.95	-0.17	1.78	1.96	-0.18	-0.01
14	1.5	1.8	-0.3	1.5	1.7	-0.2	0.1
15	1.6	1.8	-0.2	1.6	1.8	-0.2	0
16	1.65	1.8	-0.15	1.65	1.75	-0.1	0.05
17	1.68	1.9	-0.22	1.68	1.7	-0.02	0.2

Data for 170^0 Angle of Rotation

Tapping Points	Initial Reading (in of H_2O)	$\alpha = 170^0$ (in of H_2O) (Convex surface)		Initial Reading (in of H_2O)	$\alpha = 170^0$ (in of H_2O) (Concave surface)		Pressure Diff. DP (in of H_2O)
1	1.7	1.85	-0.15	1.7	1.8	-0.1	0.05
2	1.7	1.8	-0.1	1.7	1.78	-0.08	0.02
3	1.7	1.85	-0.15	1.7	1.8	-0.1	0.05
4	1.68	1.8	-0.12	1.68	1.73	-0.05	0.07
5	1.72	1.9	-0.18	1.72	1.85	-0.13	0.05
6	1.7	1.8	-0.1	1.7	1.78	-0.08	0.02
7	1.8	1.98	-0.18	1.8	1.95	-0.15	0.03
8	1.7	1.85	-0.15	1.7	1.85	-0.15	0
9	1.75	1.9	-0.15	1.75	1.9	-0.15	0
10	1.7	1.85	-0.15	1.7	1.87	-0.17	-0.02
11	1.68	1.85	-0.17	1.68	1.85	-0.17	0
12	1.6	1.75	-0.15	1.6	1.75	-0.15	0
13	1.78	2	-0.22	1.78	1.93	-0.15	0.07
14	1.5	1.8	-0.3	1.5	1.7	-0.2	0.1
15	1.6	1.92	-0.32	1.6	1.76	-0.16	0.16
16	1.65	1.85	-0.2	1.65	1.76	-0.11	0.09
17	1.68	1.95	-0.27	1.68	1.7	-0.02	0.25

Data for 180^0 Angle of Rotation

Tapping Points	Initial Reading (in of H_2O)	$\alpha = 180^0$ (in of H_2O) (Convex surface)		Initial Reading (in of H_2O)	$\alpha = 180^0$ (in of H_2O) (Concave surface)		Pressure Diff. DP (in of H_2O)
1	1.7	1.88	-0.18	1.7	2	-0.3	-0.12
2	1.7	1.8	-0.1	1.7	1.83	-0.13	-0.03
3	1.7	1.88	-0.18	1.7	1.8	-0.1	0.08
4	1.68	1.8	-0.12	1.68	1.73	-0.05	0.07
5	1.72	1.9	-0.18	1.72	1.8	-0.08	0.1
6	1.7	1.8	-0.1	1.7	1.756	-0.056	0.044
7	1.8	1.98	-0.18	1.8	1.92	-0.12	0.06
8	1.7	1.82	-0.12	1.7	1.82	-0.12	-1.1E-16
9	1.75	1.9	-0.15	1.75	1.9	-0.15	0
10	1.7	1.88	-0.18	1.7	1.87	-0.17	0.01
11	1.68	1.85	-0.17	1.68	1.82	-0.14	0.03
12	1.6	1.75	-0.15	1.6	1.75	-0.15	0
13	1.78	1.98	-0.2	1.78	1.95	-0.17	0.03
14	1.5	1.75	-0.25	1.5	1.7	-0.2	0.05
15	1.6	1.9	-0.3	1.6	1.77	-0.17	0.13
16	1.65	1.85	-0.2	1.65	1.75	-0.1	0.1
17	1.68	1.95	-0.27	1.68	1.7	-0.02	0.25

Data for 190^0 Angle of Rotation

Tapping Points	Initial Reading (in of H_2O)	$\alpha = 190^0$ (in of H_2O) (Convex surface)		Initial Reading (in of H_2O)	$\alpha = 190^0$ (in of H_2O) (Concave surface)		Pressure Diff. DP (in of H_2O)
1	1.7	1.85	-0.15	1.7	2.05	-0.35	-0.2
2	1.7	1.8	-0.1	1.7	1.85	-0.15	-0.05
3	1.7	1.85	-0.15	1.7	1.8	-0.1	0.05
4	1.68	1.8	-0.12	1.68	1.73	-0.05	0.07
5	1.72	1.9	-0.18	1.72	1.8	-0.08	0.1
6	1.7	1.8	-0.1	1.7	1.86	-0.16	-0.06
7	1.8	1.98	-0.18	1.8	1.9	-0.1	0.08
8	1.7	1.82	-0.12	1.7	1.8	-0.1	0.02
9	1.75	1.9	-0.15	1.75	1.78	-0.03	0.12
10	1.7	1.88	-0.18	1.7	1.83	-0.13	0.05
11	1.68	1.85	-0.17	1.68	1.8	-0.12	0.05
12	1.6	1.75	-0.15	1.6	1.72	-0.12	0.03
13	1.78	1.95	-0.17	1.78	1.9	-0.12	0.05
14	1.5	1.73	-0.23	1.5	1.7	-0.2	0.03
15	1.6	1.82	-0.22	1.6	1.75	-0.15	0.07
16	1.65	1.8	-0.15	1.65	1.75	-0.1	0.05
17	1.68	1.9	-0.22	1.68	1.7	-0.02	0.2

Data for 200⁰ Angle of Rotation

Tapping Points	Initial Reading (in of H_2O)	$\alpha = 200^0$ (in of H_2O) (Convex surface)		Initial Reading (in of H_2O)	$\alpha = 200^0$ (in of H_2O) (Concave surface)		Pressure Diff. DP (in of H_2O)
1	1.7	1.85	-0.15	1.7	1.9	-0.2	-0.05
2	1.7	1.8	-0.1	1.7	1.9	-0.2	-0.1
3	1.7	1.85	-0.15	1.7	1.9	-0.2	-0.05
4	1.68	1.8	-0.12	1.68	1.8	-0.12	-1.1E-16
5	1.72	1.9	-0.18	1.72	1.9	-0.18	0
6	1.7	1.8	-0.1	1.7	1.8	-0.1	0
7	1.8	1.98	-0.18	1.8	1.9	-0.1	0.08
8	1.7	1.83	-0.13	1.7	1.78	-0.08	0.05
9	1.75	1.9	-0.15	1.75	1.8	-0.05	0.1
10	1.7	1.85	-0.15	1.7	1.75	-0.05	0.1
11	1.68	1.8	-0.12	1.68	1.7	-0.02	0.1
12	1.6	1.75	-0.15	1.6	1.65	-0.05	0.1
13	1.78	1.92	-0.14	1.78	1.8	-0.02	0.12
14	1.5	1.7	-0.2	1.5	1.6	-0.1	0.1
15	1.6	1.8	-0.2	1.6	1.68	-0.08	0.12
16	1.65	1.78	-0.13	1.65	1.72	-0.07	0.06
17	1.68	1.9	-0.22	1.68	1.7	-0.02	0.2

Data for 210⁰ Angle of Rotation

Tapping Points	Initial Reading (in of H_2O)	$\alpha = 210^0$ (in of H_2O) (Convex surface)		Initial Reading (in of H_2O)	$\alpha = 210^0$ (in of H_2O) (Concave surface)		Pressure Diff. DP (in of H_2O)
1	1.7	1.83	-0.13	1.7	1.85	-0.15	-0.02
2	1.7	1.8	-0.1	1.7	1.82	-0.12	-0.02
3	1.7	1.87	-0.17	1.7	1.85	-0.15	0.02
4	1.68	1.8	-0.12	1.68	1.8	-0.12	-1.1E-16
5	1.72	1.88	-0.16	1.72	1.9	-0.18	-0.02
6	1.7	1.85	-0.15	1.7	1.8	-0.1	0.05
7	1.8	1.98	-0.18	1.8	2	-0.2	-0.02
8	1.7	1.85	-0.15	1.7	1.85	-0.15	0
9	1.75	1.9	-0.15	1.75	1.9	-0.15	0
10	1.7	1.85	-0.15	1.7	1.8	-0.1	0.05
11	1.68	1.8	-0.12	1.68	1.75	-0.07	0.05
12	1.6	1.75	-0.15	1.6	1.7	-0.1	0.05
13	1.78	1.92	-0.14	1.78	1.8	-0.02	0.12
14	1.5	1.7	-0.2	1.5	1.55	-0.05	0.15
15	1.6	1.8	-0.2	1.6	1.65	-0.05	0.15
16	1.65	1.78	-0.13	1.65	1.7	-0.05	0.08
17	1.68	1.9	-0.22	1.68	1.7	-0.02	0.2

Data for 220⁰ Angle of Rotation

Tapping Points	Initial Reading (in of H_2O)	α = 220⁰ (in of H_2O) (Convex surface)		Initial Reading (in of H_2O)	α = 220⁰ (in of H_2O) (Concave surface)		Pressure Diff. DP (in of H_2O)
1	1.7	1.9	-0.2	1.7	1.98	-0.28	-0.08
2	1.7	1.85	-0.15	1.7	1.9	-0.2	-0.05
3	1.7	1.95	-0.25	1.7	1.8	-0.1	0.15
4	1.68	1.9	-0.22	1.68	1.7	-0.02	0.2
5	1.72	2.08	-0.36	1.72	1.7	0.02	0.38
6	1.7	1.98	-0.28	1.7	1.7	0	0.28
7	1.8	2.1	-0.3	1.8	1.8	0	0.3
8	1.7	1.85	-0.15	1.7	1.73	-0.03	0.12
9	1.75	2.1	-0.35	1.75	1.78	-0.03	0.32
10	1.7	2.1	-0.4	1.7	1.73	-0.03	0.37
11	1.68	2.08	-0.4	1.68	1.7	-0.02	0.38
12	1.6	2	-0.4	1.6	1.65	-0.05	0.35
13	1.78	2.28	-0.5	1.78	1.83	-0.05	0.45
14	1.5	2.05	-0.55	1.5	1.6	-0.1	0.45
15	1.6	2.2	-0.6	1.6	1.68	-0.08	0.52
16	1.65	2.08	-0.43	1.65	1.72	-0.07	0.36
17	1.68	2.45	-0.77	1.68	1.7	-0.02	0.75

Data for 230⁰ Angle of Rotation

Tapping Points	Initial Reading (in of H_2O)	α = 230⁰ (in of H_2O) (Convex surface)		Initial Reading (in of H_2O)	α = 230⁰ (in of H_2O) (Concave surface)		Pressure Diff. DP (in of H_2O)
1	1.7	1.9	-0.2	1.7	1.9	-0.2	0
2	1.7	1.95	-0.25	1.7	1.9	-0.2	0.05
3	1.7	2.1	-0.4	1.7	1.9	-0.2	0.2
4	1.68	2.2	-0.52	1.68	1.76	-0.08	0.44
5	1.72	2.3	-0.58	1.72	1.8	-0.08	0.5
6	1.7	2.15	-0.45	1.7	1.72	-0.02	0.43
7	1.8	2.15	-0.35	1.8	1.8	0	0.35
8	1.7	1.85	-0.15	1.7	1.7	0	0.15
9	1.75	1.9	-0.15	1.75	1.75	0	0.15
10	1.7	1.98	-0.28	1.7	1.8	-0.1	0.18
11	1.68	1.9	-0.22	1.68	1.75	-0.07	0.15
12	1.6	1.82	-0.22	1.6	1.7	-0.1	0.12
13	1.78	2.1	-0.32	1.78	1.85	-0.07	0.25
14	1.5	1.88	-0.38	1.5	1.65	-0.15	0.23
15	1.6	2	-0.4	1.6	1.7	-0.1	0.3
16	1.65	1.9	-0.25	1.65	1.72	-0.07	0.18
17	1.68	2.2	-0.52	1.68	1.7	-0.02	0.5

Data for 240^0 Angle of Rotation

Tapping Points	Initial Reading (in of H_2O)	$\alpha = 240^0$ (in of H_2O) (Convex surface)		Initial Reading (in of H_2O)	$\alpha = 240^0$ (in of H_2O) (Concave surface)		Pressure Diff. DP (in of H_2O)
1	1.7	1.9	-0.2	1.7	1.8	-0.1	0.1
2	1.7	2	-0.3	1.7	1.8	-0.1	0.2
3	1.7	2.2	-0.5	1.7	1.8	-0.1	0.4
4	1.68	2.3	-0.62	1.68	1.75	-0.07	0.55
5	1.72	2.4	-0.68	1.72	1.85	-0.13	0.55
6	1.7	2.13	-0.43	1.7	1.8	-0.1	0.33
7	1.8	2.1	-0.3	1.8	1.9	-0.1	0.2
8	1.7	1.7	0	1.7	1.8	-0.1	-0.1
9	1.75	1.65	0.1	1.75	1.8	-0.05	-0.15
10	1.7	1.72	-0.02	1.7	1.73	-0.03	-0.01
11	1.68	1.72	-0.04	1.68	1.7	-0.02	0.02
12	1.6	1.6	0	1.6	1.62	-0.02	-0.02
13	1.78	1.8	-0.02	1.78	1.78	0	0.02
14	1.5	1.52	-0.02	1.5	1.52	-0.02	0
15	1.6	1.65	-0.05	1.6	1.6	0	0.05
16	1.65	1.65	0	1.65	1.68	-0.03	-0.03
17	1.68	1.68	0	1.68	1.7	-0.02	-0.02

Data for 250^0 Angle of Rotation

Tapping Points	Initial Reading (in of H_2O)	$\alpha = 250^0$ (in of H_2O) (Convex surface)		Initial Reading (in of H_2O)	$\alpha = 250^0$ (in of H_2O) (Concave surface)		Pressure Diff. DP (in of H_2O)
1	1.7	2	-0.3	1.7	1.85	-0.15	0.15
2	1.7	2.2	-0.5	1.7	1.82	-0.12	0.38
3	1.7	2.2	-0.5	1.7	1.86	-0.16	0.34
4	1.68	2.3	-0.62	1.68	1.78	-0.1	0.52
5	1.72	2.34	-0.62	1.72	1.9	-0.18	0.44
6	1.7	2.1	-0.4	1.7	1.81	-0.11	0.29
7	1.8	2.02	-0.22	1.8	2	-0.2	0.02
8	1.7	1.6	0.1	1.7	1.89	-0.19	-0.29
9	1.75	1.38	0.37	1.75	1.95	-0.2	-0.57
10	1.7	1.3	0.4	1.7	1.9	-0.2	-0.6
11	1.68	1.42	0.26	1.68	1.88	-0.2	-0.46
12	1.6	1.4	0.2	1.6	1.78	-0.18	-0.38
13	1.78	1.6	0.18	1.78	1.97	-0.19	-0.37
14	1.5	1.35	0.15	1.5	1.68	-0.18	-0.33
15	1.6	1.42	0.18	1.6	1.78	-0.18	-0.36
16	1.65	1.48	0.17	1.65	1.76	-0.11	-0.28
17	1.68	1.45	0.23	1.68	1.78	-0.1	-0.33

Data for 260^0 Angle of Rotation

Tapping Points	Initial Reading (in of H_2O)	$\alpha = 260^0$ (in of H_2O) (Convex surface)		Initial Reading (in of H_2O)	$\alpha = 260^0$ (in of H_2O) (Concave surface)		Pressure Diff. DP (in of H_2O)
1	1.7	1.86	-0.16	1.7	1.86	-0.16	0
2	1.7	1.8	-0.1	1.7	1.8	-0.1	0
3	1.7	1.8	-0.1	1.7	1.8	-0.1	0
4	1.68	1.8	-0.12	1.68	1.8	-0.12	-1.1E-16
5	1.72	1.98	-0.26	1.72	1.98	-0.26	0
6	1.7	1.7	0	1.7	1.7	0	0
7	1.8	1.78	0.02	1.8	1.78	0.02	0
8	1.7	1.45	0.25	1.7	1.45	0.25	0
9	1.75	1.3	0.45	1.75	1.3	0.45	0
10	1.7	1.1	0.6	1.7	1.1	0.6	0
11	1.68	1.05	0.63	1.68	1.05	0.63	0
12	1.6	1.15	0.45	1.6	1.145	0.455	0.005
13	1.78	1.4	0.38	1.78	1.4	0.38	0
14	1.5	1.25	0.25	1.5	1.25	0.25	0
15	1.6	1.38	0.22	1.6	1.38	0.22	0
16	1.65	1.48	0.17	1.65	1.48	0.17	0
17	1.68	1.45	0.23	1.68	1.45	0.23	0

Data for 270^0 Angle of Rotation

Tapping Points	Initial Reading (in of H_2O)	$\alpha = 270^0$ (in of H_2O) (Convex surface)		Initial Reading (in of H_2O)	$\alpha = 270^0$ (in of H_2O) (Concave surface)		Pressure Diff. DP (in of H_2O)
1	1.7	1.88	-0.18	1.7	1.85	-0.15	0.03
2	1.7	1.8	-0.1	1.7	1.82	-0.12	-0.02
3	1.7	1.8	-0.1	1.7	1.86	-0.16	-0.06
4	1.68	1.8	-0.12	1.68	1.78	-0.1	0.02
5	1.72	1.88	-0.16	1.72	1.9	-0.18	-0.02
6	1.7	1.6	0.1	1.7	1.81	-0.11	-0.21
7	1.8	1.3	0.5	1.8	2	-0.2	-0.7
8	1.7	1.25	0.45	1.7	1.89	-0.19	-0.64
9	1.75	1.1	0.65	1.75	1.95	-0.2	-0.85
10	1.7	1.05	0.65	1.7	1.9	-0.2	-0.85
11	1.68	1.08	0.6	1.68	1.88	-0.2	-0.8
12	1.6	1.1	0.5	1.6	1.78	-0.18	-0.68
13	1.78	1.22	0.56	1.78	1.98	-0.2	-0.76
14	1.5	1.08	0.42	1.5	1.7	-0.2	-0.62
15	1.6	1.18	0.42	1.6	1.8	-0.2	-0.62
16	1.65	1.28	0.37	1.65	1.78	-0.13	-0.5
17	1.68	1.2	0.48	1.68	1.8	-0.12	-0.6

107

Data for 280⁰ Angle of Rotation

Tapping Points	Initial Reading (in of H_2O)	$\alpha = 280^0$ (in of H_2O) (Convex surface)		Initial Reading (in of H_2O)	$\alpha = 280^0$ (in of H_2O) (Concave surface)		Pressure Diff. DP (in of H_2O)
1	1.7	1.89	-0.19	1.7	1.85	-0.15	0.04
2	1.7	1.8	-0.1	1.7	1.82	-0.12	-0.02
3	1.7	1.8	-0.1	1.7	1.86	-0.16	-0.06
4	1.68	1.7	-0.02	1.68	1.8	-0.12	-0.1
5	1.72	1.68	0.04	1.72	1.9	-0.18	-0.22
6	1.7	1.38	0.32	1.7	1.82	-0.12	-0.44
7	1.8	1.4	0.4	1.8	2	-0.2	-0.6
8	1.7	1.15	0.55	1.7	1.9	-0.2	-0.75
9	1.75	1.12	0.63	1.75	1.95	-0.2	-0.83
10	1.7	1.1	0.6	1.7	1.9	-0.2	-0.8
11	1.68	1.08	0.6	1.68	1.88	-0.2	-0.8
12	1.6	1.1	0.5	1.6	1.78	-0.18	-0.68
13	1.78	1.22	0.56	1.78	1.98	-0.2	-0.76
14	1.5	1.02	0.48	1.5	1.7	-0.2	-0.68
15	1.6	1.1	0.5	1.6	1.8	-0.2	-0.7
16	1.65	1.2	0.45	1.65	1.78	-0.13	-0.58
17	1.68	1.2	0.48	1.68	1.8	-0.12	-0.6

Data for 290⁰ Angle of Rotation

Tapping Points	Initial Reading (in of H_2O)	$\alpha = 290^0$ (in of H_2O) (Convex surface)		Initial Reading (in of H_2O)	$\alpha = 290^0$ (in of H_2O) (Concave surface)		Pressure Diff. DP (in of H_2O)
1	1.7	1.88	-0.18	1.7	1.85	-0.15	0.03
2	1.7	1.8	-0.1	1.7	1.82	-0.12	-0.02
3	1.7	1.7	0	1.7	1.86	-0.16	-0.16
4	1.68	1.5	0.18	1.68	1.8	-0.12	-0.3
5	1.72	1.4	0.32	1.72	1.9	-0.18	-0.5
6	1.7	1.18	0.52	1.7	1.82	-0.12	-0.64
7	1.8	1.2	0.6	1.8	1.98	-0.18	-0.78
8	1.7	1.1	0.6	1.7	1.9	-0.2	-0.8
9	1.75	1.1	0.65	1.75	1.95	-0.2	-0.85
10	1.7	1.1	0.6	1.7	1.9	-0.2	-0.8
11	1.68	1.1	0.58	1.68	1.88	-0.2	-0.78
12	1.6	1.1	0.5	1.6	1.78	-0.18	-0.68
13	1.78	1.2	0.58	1.78	1.98	-0.2	-0.78
14	1.5	1.02	0.48	1.5	1.7	-0.2	-0.68
15	1.6	1.1	0.5	1.6	1.8	-0.2	-0.7
16	1.65	1.18	0.47	1.65	1.78	-0.13	-0.6
17	1.68	1.2	0.48	1.68	1.8	-0.12	-0.6

Data for 300⁰ Angle of Rotation

Data for 300^0 Angle of Rotation

Tapping Points	Initial Reading (in of H_2O)	$\alpha = 300^0$ (in of H_2O) (Convex surface)		Initial Reading (in of H_2O)	$\alpha = 300^0$ (in of H_2O) (Concave surface)		Pressure Diff. DP (in of H_2O)
1	1.7	1.85	-0.15	1.7	1.85	-0.15	0
2	1.7	1.68	0.02	1.7	1.82	-0.12	-0.14
3	1.7	1.5	0.2	1.7	1.86	-0.16	-0.36
4	1.68	1.3	0.38	1.68	1.8	-0.12	-0.5
5	1.72	1.2	0.52	1.72	1.9	-0.18	-0.7
6	1.7	1.12	0.58	1.7	1.83	-0.13	-0.71
7	1.8	1.28	0.52	1.8	1.98	-0.18	-0.7
8	1.7	1.1	0.6	1.7	1.9	-0.2	-0.8
9	1.75	1.18	0.57	1.75	1.95	-0.2	-0.77
10	1.7	1.18	0.52	1.7	1.9	-0.2	-0.72
11	1.68	1.18	0.5	1.68	1.88	-0.2	-0.7
12	1.6	1.16	0.44	1.6	1.78	-0.18	-0.62
13	1.78	1.25	0.53	1.78	1.95	-0.17	-0.7
14	1.5	1.04	0.46	1.5	1.7	-0.2	-0.66
15	1.6	1.08	0.52	1.6	1.8	-0.2	-0.72
16	1.65	1.18	0.47	1.65	1.78	-0.13	-0.6
17	1.68	1.2	0.48	1.68	1.8	-0.12	-0.6

Data for 310^0 Angle of Rotation

Tapping Points	Initial Reading (in of H_2O)	$\alpha = 310^0$ (in of H_2O) (Convex surface)		Initial Reading (in of H_2O)	$\alpha = 320^0$ (in of H_2O) (Concave surface)		Pressure Diff. DP (in of H_2O)
1	1.7	1.7	0	1.7	1.95	-0.25	-0.25
2	1.7	1.5	0.2	1.7	1.9	-0.2	-0.4
3	1.7	1.3	0.4	1.7	1.9	-0.2	-0.6
4	1.68	1.18	0.5	1.68	1.85	-0.17	-0.67
5	1.72	1.1	0.62	1.72	2	-0.28	-0.9
6	1.7	1.1	0.6	1.7	1.9	-0.2	-0.8
7	1.8	1.2	0.6	1.8	2.1	-0.3	-0.9
8	1.7	1.2	0.5	1.7	1.92	-0.22	-0.72
9	1.75	1.3	0.45	1.75	2.05	-0.3	-0.75
10	1.7	1.3	0.4	1.7	2	-0.3	-0.7
11	1.68	1.25	0.43	1.68	1.98	-0.3	-0.73
12	1.6	1.2	0.4	1.6	1.85	-0.25	-0.65
13	1.78	1.3	0.48	1.78	2.06	-0.28	-0.76
14	1.5	1.1	0.4	1.5	1.8	-0.3	-0.7
15	1.6	1.1	0.5	1.6	1.9	-0.3	-0.8
16	1.65	1.2	0.45	1.65	1.85	-0.2	-0.65
17	1.68	1.2	0.48	1.68	1.8	-0.12	-0.6

Data for 320^0 Angle of Rotation

Tapping Points	Initial Reading (in of H_2O)	$\alpha = 320^0$ (in of H_2O) (Convex surface)		Initial Reading (in of H_2O)	$\alpha = 320^0$ (in of H_2O) (Concave surface)		Pressure Diff. DP (in of H_2O)
1	1.7	1.5	0.2	1.7	1.9	-0.2	-0.4
2	1.7	1.3	0.4	1.7	1.82	-0.12	-0.52
3	1.7	1.2	0.5	1.7	1.82	-0.12	-0.62
4	1.68	1.15	0.53	1.68	1.8	-0.12	-0.65
5	1.72	1.1	0.62	1.72	1.95	-0.23	-0.85
6	1.7	1.18	0.52	1.7	1.82	-0.12	-0.64
7	1.8	1.3	0.5	1.8	2.03	-0.23	-0.73
8	1.7	1.3	0.4	1.7	1.9	-0.2	-0.6
9	1.75	1.32	0.43	1.75	2	-0.25	-0.68
10	1.7	1.28	0.42	1.7	1.95	-0.25	-0.67
11	1.68	1.22	0.46	1.68	1.9	-0.22	-0.68
12	1.6	1.2	0.4	1.6	1.8	-0.2	-0.6
13	1.78	1.4	0.38	1.78	2	-0.22	-0.6
14	1.5	1.12	0.38	1.5	1.7	-0.2	-0.58
15	1.6	1.18	0.42	1.6	1.85	-0.25	-0.67
16	1.65	1.2	0.45	1.65	1.8	-0.15	-0.6
17	1.68	1.18	0.5	1.68	1.72	-0.04	-0.54

Data for 330^0 Angle of Rotation

Tapping Points	Initial Reading (in of H_2O)	$\alpha = 330^0$ (in of H_2O) (Convex surface)		Initial Reading in of H_2O	$\alpha = 330^0$ (in of H_2O) (Concave surface)		Pressure Diff. DP (in of H_2o)
1	1.7	1.28	0.42	1.7	1.7	0	-0.42
2	1.7	1.15	0.55	1.7	1.68	0.02	-0.53
3	1.7	1.13	0.57	1.7	1.7	0	-0.57
4	1.68	1.18	0.5	1.68	1.62	0.06	-0.44
5	1.72	1.2	0.52	1.72	1.78	-0.06	-0.58
6	1.7	1.35	0.35	1.7	1.68	0.02	-0.33
7	1.8	1.45	0.35	1.8	1.85	-0.05	-0.4
8	1.7	1.38	0.32	1.7	1.75	-0.05	-0.37
9	1.75	1.48	0.27	1.75	1.8	-0.05	-0.32
10	1.7	1.45	0.25	1.7	1.75	-0.05	-0.3
11	1.68	1.28	0.4	1.68	1.72	-0.04	-0.44
12	1.6	1.3	0.3	1.6	1.62	-0.02	-0.32
13	1.78	1.4	0.38	1.78	1.42	0.36	-0.02
14	1.5	1.2	0.3	1.5	1.53	-0.03	-0.33
15	1.6	1.28	0.32	1.6	1.65	-0.05	-0.37
16	1.65	1.3	0.35	1.65	1.65	0	-0.35
17	1.68	1.22	0.46	1.68	1.53	0.15	-0.31

Data for 340^0 Angle of Rotation

Tapping Points	Initial Reading (in of H_2O)	$\alpha = 340^0$ (in of H_2O) (Convex surface)		Initial Reading (in of H_2O)	$\alpha = 340^0$ (in of H_2O) (Concave surface)		Pressure Diff. DP (in of H_2O)
1	1.7	1.1	0.6	1.7	1.52	0.18	-0.42
2	1.7	1.1	0.6	1.7	1.48	0.22	-0.38
3	1.7	1.2	0.5	1.7	1.52	0.18	-0.32
4	1.68	1.3	0.38	1.68	1.48	0.2	-0.18
5	1.72	1.4	0.32	1.72	1.55	0.17	-0.15
6	1.7	1.5	0.2	1.7	1.48	0.22	0.02
7	1.8	1.6	0.2	1.8	1.63	0.17	-0.03
8	1.7	1.48	0.22	1.7	1.56	0.14	-0.08
9	1.75	1.5	0.25	1.75	1.6	0.15	-0.1
10	1.7	1.48	0.22	1.7	1.53	0.17	-0.05
11	1.68	1.4	0.28	1.68	1.5	0.18	-0.1
12	1.6	1.4	0.2	1.6	1.46	0.14	-0.06
13	1.78	1.5	0.28	1.78	1.6	0.18	-0.1
14	1.5	1.3	0.2	1.5	1.35	0.15	-0.05
15	1.6	1.4	0.2	1.6	1.45	0.15	-0.05
16	1.65	1.43	0.22	1.65	1.5	0.15	-0.07
17	1.68	1.35	0.33	1.68	1.4	0.28	-0.05

Data for 350^0 Angle of Rotation

Tapping Points	Initial Reading (in of H_2O)	$\alpha = 350^0$ (in of H_2O) (Convex surface)		Initial Reading in of H_2O	$\alpha = 350^0$ (in of H_2O) (Concave surface)		Pressure Diff. DP (in of H_2o)
1	1.7	1.1	0.6	1.7	1.35	0.35	-0.25
2	1.7	1.15	0.55	1.7	1.35	0.35	-0.2
3	1.7	1.3	0.4	1.7	1.4	0.3	-0.1
4	1.68	1.48	0.2	1.68	1.4	0.28	0.08
5	1.72	1.6	0.12	1.72	1.42	0.3	0.18
6	1.7	1.65	0.05	1.7	1.4	0.3	0.25
7	1.8	1.68	0.12	1.8	1.5	0.3	0.18
8	1.7	1.58	0.12	1.7	1.43	0.27	0.15
9	1.75	1.6	0.15	1.75	1.48	0.27	0.12
10	1.7	1.55	0.15	1.7	1.4	0.3	0.15
11	1.68	1.5	0.18	1.68	1.38	0.3	0.12
12	1.6	1.5	0.1	1.6	1.35	0.25	0.15
13	1.78	1.65	0.13	1.78	1.48	0.3	0.17
14	1.5	1.45	0.05	1.5	1.25	0.25	0.2
15	1.6	1.52	0.08	1.6	1.3	0.3	0.22
16	1.65	1.55	0.1	1.65	1.38	0.27	0.17
17	1.68	1.48	0.2	1.68	1.22	0.46	0.26